

**Dunedin groundwater monitoring, spatial
observations and forecast conditions under
sea-level rise**

SC Cox

LH Easterbrook-Clarke

MHJ Ettema
NI Stevenson

LA Chambers

**GNS Science Report 2023/43
December 2023**



DISCLAIMER

The Institute of Geological and Nuclear Sciences Limited (GNS Science) and its funders give no warranties of any kind concerning the accuracy, completeness, timeliness or fitness for purpose of the contents of this report. GNS Science accepts no responsibility for any actions taken based on, or reliance placed on the contents of this report and GNS Science and its funders exclude to the full extent permitted by law liability for any loss, damage or expense, direct or indirect, and however caused, whether through negligence or otherwise, resulting from any person's or organisation's use of, or reliance on, the contents of this report.

BIBLIOGRAPHIC REFERENCE

Cox SC, Ettema MHJ, Chambers LA, Easterbrook-Clarke LH, Stevenson NI. 2023. Dunedin groundwater monitoring, spatial observations and forecast conditions under sea-level rise. Lower Hutt (NZ): GNS Science. 103 p. (GNS Science report; 2023/43). <https://doi.org/10.21420/5799-N894>

SC Cox, GNS Science, Private Bag 1930, Dunedin 9054, New Zealand

MHJ Ettema, Otago Regional Council, Private Bag 1954, Dunedin 9054, New Zealand

LA Chambers, GNS Science, PO Box 30368, Lower Hutt 5040, New Zealand

LH Easterbrook-Clarke, GNS Science, Private Bag 1930, Dunedin 9054, New Zealand

NI Stevenson, formerly Otago Regional Council

CONTENTS

ABSTRACT	V
KEYWORDS	V
1.0 INTRODUCTION	1
1.1 Context.....	1
1.2 Dunedin.....	4
2.0 DUNEDIN DATA AND REFERENCE DATUM.....	6
2.1 Monitoring Network.....	6
2.2 Groundwater Observations and Reference Datum	6
2.3 Temporal Context of Monitoring Epoch.....	8
2.4 Present Harbour and Sea Level.....	11
2.5 Topographic Elevation	12
2.6 Rainfall	13
2.7 Stormwater and Flooding.....	13
2.8 Sea-Level Rise	15
3.0 PRESENT-DAY GROUNDWATER.....	17
3.1 Interpolation of Statistical Surfaces.....	17
3.2 Groundwater Elevation	18
3.3 Depth to Groundwater	20
3.4 Effect of Tides and Storm Surge.....	22
3.5 Response to Rainfall.....	26
3.6 Subsurface Storage for Rain.....	27
4.0 FORECAST FUTURE STATE OF GROUNDWATER.....	31
4.1 Groundwater Levels.....	31
4.2 Emergent Groundwater	32
4.3 Loss of Subsurface Storage Capacity.....	35
5.0 OTHER RELEVANT DATA AND STUDIES	40
5.1 Numerical Groundwater Model	40
5.2 Stormwater and Wastewater Networks.....	49
5.3 Coastal Inundation.....	53
5.4 Groundwater Chemistry and Saline Intrusion.....	55
6.0 DISCUSSION AND RESULTS	57
6.1 Assumptions and Uncertainties	57
6.2 Application of the Empirical Model.....	58
6.3 Delineating Hazard and Risk	59
6.4 Impact Forecast.....	60
6.5 Data and its Availability.....	62
7.0 SUMMARY AND CONCLUSIONS.....	64
8.0 ACKNOWLEDGMENTS	67
9.0 REFERENCES	68

FIGURES

Figure 1.1	The influence of the coast on shallow unconfined groundwater	3
Figure 2.1	Groundwater monitoring sites in Dunedin.....	7
Figure 2.2	Plots of 2019–2023 groundwater elevation against the numerical day of the year at the four Otago Regional Council sites with longer-term data.....	10
Figure 2.3	Plots of 2019–2023 groundwater elevation against percentiles of the observations in each epoch, compared against the longer-term 2010–2018 data records	11
Figure 2.4	Exemplars of heavy rainfall events experienced in Dunedin, plotted as cumulative hourly rainfall against time since the start of rain.....	14
Figure 3.1	Interpolated median groundwater elevation (<i>GWL_{median}_2023</i>)	18
Figure 3.2	Interpolated depth to median groundwater elevation (<i>DTW_{median}_2023</i>).....	22
Figure 3.3	Areas where Dunedin’s coastal plain is below Mean High Water Springs sit protected from the harbour and ocean behind elevated reclaimed land and sand dunes	23
Figure 3.4	Tidal efficiency at each of the monitoring sites	24
Figure 3.5	Comparison between geometric models of the elevation (in NZVD2016) of the water table at median, mean high water springs and 95% percentile levels based on observations from the 2019–2023 epoch.....	26
Figure 3.6	The RRI ratio as a series of piezometer point observations and an interpolated grid.....	27
Figure 3.7	Calculated grid of <i>RAIN_{storage}_fromGWL_{median}</i> at the present day (0 cm sea-level rise)	28
Figure 3.8	Comparison of maps showing places where the subsurface storage above median, Mean High Water Springs and p95 levels of the water table would be exceeded by a 12-hour ARI10 rainfall of 60.2 mm.	29
Figure 3.9	Comparison of places where subsurface storage above Mean High Water Springs level of the water table would be exceeded by 12-hour rainfall at a 2-, 5-, 10-, 50- and 100-year average recurrence intervals (corresponding to rainfalls $\geq 35.8, 49.3, 60.2, 89.9, 105$ mm, respectively)....	30
Figure 4.1	Forecasts of places where groundwater is expected to become emergent ($DTW \leq 0$) with sea-level rise	34
Figure 4.2	Forecasts of the percentage of the 9.2 km ² area of the Dunedin coastal plain where groundwater will become emergent as sea levels rise	35
Figure 4.3	Forecasts at various levels of sea-level rise, showing places where 12-hour rainfall at ARI 1, 10, 100 and 1000 intervals will exceed the available subsurface storage for infiltration from that rain	38
Figure 4.4	Forecasts of the percentage of the 9.2 km ² area Dunedin coastal plain where groundwater may begin to contribute to pluvial flooding as sea levels rise	39
Figure 5.1	Median groundwater levels of the present-day median level of groundwater, representing a long-term calibrated ‘steady state’ in the numerical groundwater model.....	43
Figure 5.2	Interpolated <i>GWL_{median}_2023</i> and future forecasts at various increments of sea-level rise for comparison with the equivalent colour range and levels from the numerical groundwater model..	44
Figure 5.3	Calculated grids of the difference in elevation between the median levels from the empirical-based geometric groundwater model of this study, minus the median groundwater level (general ‘annual’ solution) from numerical groundwater model of Chambers et al. (2023).....	45
Figure 5.4	Classification of grid models of groundwater elevation defining areas where the water table at median condition is calculated to lie below mean sea level.....	46
Figure 5.5	Graph showing the mean (± 1 standard deviation) of the difference between empirical (geometric) and numerical groundwater median elevations	47
Figure 5.6	Different forecasts of the percentage of a 5.8 km ² area in South Dunedin where groundwater will become emergent as sea levels rise	47

Figure 5.7	Position of stormwater network relative to the median water table in the flat-lying area of Dunedin.....	51
Figure 5.8	Position of wastewater network relative to the median water table in the flat-lying area of Dunedin.....	51
Figure 5.9	Stormwater network position relative to the water table at Mean High Water Springs.....	52
Figure 5.10	Wastewater network position relative to the water table at Mean High Water Springs.....	52
Figure 5.11	Illustration of places where land has potential to be flooded by coastal inundation and how this is forecast to evolve with sea-level rise.....	54
Figure 5.12	Forecasts of the percentage of the 9.2 km ² area of Dunedin’s coastal plain that might become inundated from the harbour as sea levels rise.....	55
Figure 5.13	Electrical conductance of groundwater (µS/cm) as piezometer spot values and an interpolated grid, overlain by modelled %Seawater contours.....	56
Figure 6.1	Summary of thresholds at which groundwater may become a direct hazard or an indirect contribution to another hazard.....	60
Figure 6.2	Summary of forecasts of the percentage of the 9.2 km ² area of Dunedin’s coastal plain exposed to various hazardous or hazard-contributing processes.....	61

TABLES

Table 2.1	Comparison of statistics for longer-term and 2019–2023 epochs of groundwater levels at three long-term Otago Regional Council monitoring sites.....	9
Table 2.2	High tide and storm tide anomalies at Green Island and Dunedin tide gauges.....	12
Table 2.3	Musselburgh rainfall depth-duration-frequency table from HIRDS v4 (NIWA 2023b).....	13
Table 2.4	Time at which various scenarios of sea-level rise will be reached in Dunedin.....	16
Table 3.1	Summary of statistical surfaces and other datasets are developed to represent ‘present day’ Dunedin groundwater elevation during the 2019–2023 epoch.....	19
Table 3.2	Summary of statistical surfaces developed to represent ‘present day’ Dunedin depth to groundwater as defined by the 2019–2023 epoch.....	21
Table 3.3	Summary of statistical surfaces developed to represent ‘present day’ tidal behaviour in groundwater.....	25
Table 3.4	Summary of rainfall-recharge datasets developed for Dunedin groundwater.....	29
Table 6.1	Summary of data that accompanies this report.....	62

APPENDICES

APPENDIX 1	MAP OF PLACE NAMES	77
APPENDIX 2	GROUNDWATER MONITORING SITES	78
APPENDIX 3	DUNEDIN GROUNDWATER FORECAST.....	81
APPENDIX 4	METADATA (CONTENT OF GIS DATASETS)	83
APPENDIX 5	GLOSSARY OF TERMS.....	100

APPENDIX FIGURES

Figure A1.1	Map with key place names that may have been referred to in this study.	77
Figure A3.1	Maps showing areas of zero subsurface storage capacity, emergent groundwater and coastal inundation (from NIWA) for various recurrence intervals and increments of sea-level rise	81

APPENDIX TABLES

Table A2.1	Dunedin groundwater monitoring sites that were operational during 2019–2023.....	78
Table A2.2	Dunedin groundwater level statistics from 2019 to 2023	79
Table A4.1	Detailed description of GIS datasets generated from the 2019–2023 groundwater monitoring and used in this report.....	83
Table A4.2	Detailed description of GIS datasets generated to forecast the potential effects of sea-level rise in this report.....	91
Table A4.3	Detailed description of GIS datasets generated for the Dunedin City Council three waters service network, containing data and observations extracted from interpolated models of groundwater data for Dunedin	96

ABSTRACT

Dunedin City has a large number of assets and critical infrastructure sitting on a low-lying coastal plain that is underlain by a largely unseen and relatively poorly understood hazard. Shallow groundwater in this area limits the unsaturated ground available to store rain and runoff, promotes flooding and creates opportunities for infiltration into stormwater and wastewater networks. Groundwater levels are expected to rise as sea level rises, causing greater frequency of pluvial flooding and/or direct inundation from below once it nears the ground surface.

Monitoring network developments in 2019 and 2021 have significantly improved information on Dunedin's groundwater. Groundwater level, temperature and specific conductance observations at 15 minute intervals have been collated into a time-series database. A wide variety of statistics have been generated for each site, including median, maximum, minimum, 95th and 5th percentiles, mean, standard deviation and range of groundwater levels. Other collated site data include: tidal amplitude, efficiency and phase lag; distance from harbour or sea; groundwater sample pH, electrical conductivity; calculated seawater percentage; and a rainfall response index reflecting the local efficiency of rainfall recharge.

This report updates a previous report, published in 2020, to incorporate monitoring and observations over the period 6 March 2019 to 1 May 2023. It is accompanied by derivative ArcGIS data and spatial analysis of these groundwater observations. A series of statistical surfaces have been generated to represent the present-day (2023) water-table elevation and depth to groundwater, the response to rainfall recharge and tidal forcing and the available subsurface storage of rain infiltration. The level of groundwater is influenced by subsurface flow and runoff from the hills in the west and north but will be further encroached from the south and east by sea-level rise in the harbour and ocean in the future.

Simple geometric models have been developed using the present shape and position of the water table, combined with tidal fluctuations, to forecast the future state of groundwater levels at 10 cm increments of sea-level rise. These geometric models are strongly empirical, with many implicit assumptions and caveats – particularly, that they do not account for groundwater flow and possible changes in water-budget mass balance. Although many variables and controlling processes are simplified into a single parameter, the projected groundwater levels highlight how local variations in the water table shape and slope interact locally with the ground elevation or infrastructure networks. The models depict spatial patterns well, but are relatively conservative and may over-estimate groundwater-related contribution to hazard and how this will evolve over time.

Groundwater spatial datasets, such as water-table elevation and rainfall recharge, provide tools from which inundation or flood-vulnerable areas can be identified and other hazards, such as liquefaction susceptibility, modelled. The spatial exposure to the loss of subsurface storage, emergent groundwater and coastal inundation are combined in a summary of negative impacts from these processes as sea levels rise. Hazards associated with groundwater are likely to be gradual and will precede a step-like increase in exposure to coastal inundation. Likewise, groundwater's contribution to pluvial flooding may well have been experienced in many places prior to the emergence of groundwater. The impact forecast highlights the need for planning to take a holistic multi-hazard long-term view.

KEYWORDS

Groundwater, water table, tides, rain, flooding, sea-level rise, climate change, stormwater, infrastructure, hazard, risk

This page left intentionally blank.

1.0 INTRODUCTION

1.1 Context

Shallow groundwater presents a largely unseen, and poorly-understood, hazard that has potential to become a major problem in low-lying coastal areas as climate changes and sea levels rise (Bell et al. 2017; Bosserelle et al. 2022). Where there are strong hydraulic links with the ocean, sea-level rise is expected to drive concomitant changes in groundwater level (Befus et al. 2020). This slow but chronic threat can flood communities from below. By decreasing the depth (or volume) of unsaturated ground available to store water, groundwater rise can increase the frequency of hazards associated with surface runoff, river flooding and coastal-storm inundation (Rahimi et al. 2020). More directly, it causes instability in building foundations and roads, can infiltrate and overwhelm stormwater and wastewater systems, leads to poor public health through dampness and mould issues in housing, increases liquefaction potential, can redistribute underground contamination and/or can emerge above ground to cause flooding, pollution, salinity stress or other environmental issues (Hummel et al. 2018; Knott et al. 2018; Liu et al. 2018; Habel et al. 2020). Subsurface stormwater and wastewater networks that rely on gravitational flow are particularly vulnerable and potentially prone to damage and system collapse, especially where they are old. Groundwater infiltration and rising base levels at the coast reduce network capacity and can result in sewage overflows, with associated public health and environmental costs.

Understanding the intensity, duration and spatial reach of hazards, and how various hazards interplay, is becoming a standard expectation for planning, mitigation and adaptation. But shallow unconfined groundwater is, for the most part, still poorly quantified/understood, with significant temporal (frequency) and (perhaps more importantly) spatial uncertainty. Different models of varying complexity can be applied, depending on the problem at hand to be solved (Doherty and Moore 2021). There are trade-offs involved in selecting complex or more simple models that are context dependent and require a definition of the decisions the model will be used to inform.

At the simplest end of the modelling spectrum is a commonly adopted 'quick' screening model, identifying relative community exposure to groundwater or coastal inundation hazards. It assumes that groundwater levels will equilibrate locally with sea level and that elevation above sea level (and perhaps distance from the coast) can be used as a proxy for hazard and/or risk (Wu et al. 2002). So-called 'bathtub' models can be generated quickly from digital topography, using Geographic Information System (GIS) techniques to provide first-order approximations of land elevation relative to sea level (e.g. Beca 2014). But, while useful for non-specific, generalised desktop assessments of regional asset exposure, the approach reflects little of the principles of groundwater systems and the dynamics of either subsurface flow or wave inundation. These commonly assume a condition that inundation becomes permanent or 'chronic', whereas locations may well be reached by processes that are initially episodic and/or transient. To translate hazard into risk and/or potential losses, there also needs to be some understanding of fragility functions (vulnerability) and hazard thresholds (e.g. Kreibich and Thielen 2008), which are locally variable and rarely quantified. These are just some of the many significant challenges and problems associated with downscaling from global to regional to local models.

As work progresses and more information comes to hand, there is a natural need to shift from a generalised understanding of exposure to a probabilistic understanding of where and how often the deleterious effects will be felt. Without nuances of local variability and site-

specific hazard, generalised screening studies can quickly cause distress to individual property owners and cannot be reliably used for developing adaptation solutions. Downscaling to quantify hazard at a site-specific level generally requires a holistic understanding of natural systems and the magnitude and frequency of processes that can perturb their present state. Analysis of exposure to groundwater-related hazards then very commonly becomes hampered by a widespread lack of shallow groundwater information within coastal land. Such areas are rarely monitored or studied in detail, principally because shallow coastal groundwater is commonly unsuitable for domestic or agricultural supply. Local (cf. global) processes and impacts of climate change and sea-level rise are, for the most part, still poorly quantified/understood, with significant **temporal** (frequency) and (perhaps more importantly) **spatial** uncertainty in the hazards faced across our communities.

Coastal groundwater systems respond dynamically to a variety of external driving forces. Levels of the water table fluctuate considerably with inter-annual and seasonal shifts in recharge, as well as higher-frequency variations caused by storm events, local river floods or tidal cycles. Tidal fluctuations and influence of sea level commonly diminish exponentially with increasing distance inland (Figure 1.1A). The shallow groundwater system can, alternatively, be perturbed by longer-term changes in climate-related precipitation and the persistent stressor of rising sea level (Figure 1.1B). Such dynamic fluctuations can be used for calibrating groundwater models, and the attenuation in phase and amplitude in high-frequency variations can be tracked laterally and provide information on local ground permeability and potential future effects of sea-level rise (Hsieh et al. 1987; Rotzoll and El-Kadi 2008; Rotzoll and Fletcher 2013). Low-lying areas potentially affected by rising groundwater can extend considerable distances inland from the sea.

Near-surface variations in hydrogeology and subsurface storage appear to be locally important for suburb-scale exposure to groundwater-related flood hazards. Groundwater surfaces tend to be gently sloped, rather than flat, with a hydraulic gradient and humps, ridges and hollows caused by the natural flow system and interplay with urban development, drainage, stormwater systems and other engineering features. Unconfined groundwater and the natural position of the water is locally dependent on subsurface storativity (void space); permeability; potentiometric gradients from surrounding topography; capillary action; the presence of large water bodies, such as lakes or the sea; and recharge/loss from rainwater and surface waterways. Humps reflect local inability to flow quickly from rainfall or hillslope recharge or upwards flow, whereas hollows develop through more porous layers or flow to natural or human-made drainage networks. Urban development commonly disturbs the natural equilibrium through impervious surface changes to infiltration or runoff and bypass in stormwater systems. Fully numerical hydrologic groundwater models are commonly able to capture and quantify such features, as well as budgets of groundwater recharge and flux (e.g. Chambers et al. 2023). These models are useful for predicting the dynamic nature of both groundwater level and flow-rate hazard responses, e.g. the capacity of a drainage system to mitigate a flooding risk. These predictions are important in the design of adaptation and hazard mitigation engineering solutions. However, it is currently rare for these numerical models to have high spatial resolution (e.g. at property scale <100 x 100 m), and their development and calibration is time-intensive. Therefore, investment in fully numerical models is more likely to be used in support of engineering design, while simpler models are available for assessing hazard and risk.

Occupying middle ground, once there is sufficient data, is a compromise between the overly simplistic 'bathtub'-level groundwater modelling approach and more difficult and computationally expensive hydrologic models of groundwater levels and flows. Local empirical

observations can be used to characterise the water table, shallow groundwater and their behaviour under a changing climate or sea-level condition, providing information required for hazard and risk assessment. This approach has been applied here for this study of Dunedin City, in the South Island of New Zealand, where a monitoring network has been installed specifically to fill a knowledge gap on the position and dynamics of shallow coastal groundwater beneath this urban centre. Recent monitoring and mapping of groundwater, together with LiDAR surveying of topography, provides both the spatial and temporal understanding of present condition of shallow coastal groundwater that is then used to forecast future state and associated hazards. Statistical surfaces have been developed to define the present-day geometry of the water table, understand connection with the sea, then forecast the future state under the effects of sea-level rise at a site-specific scale.

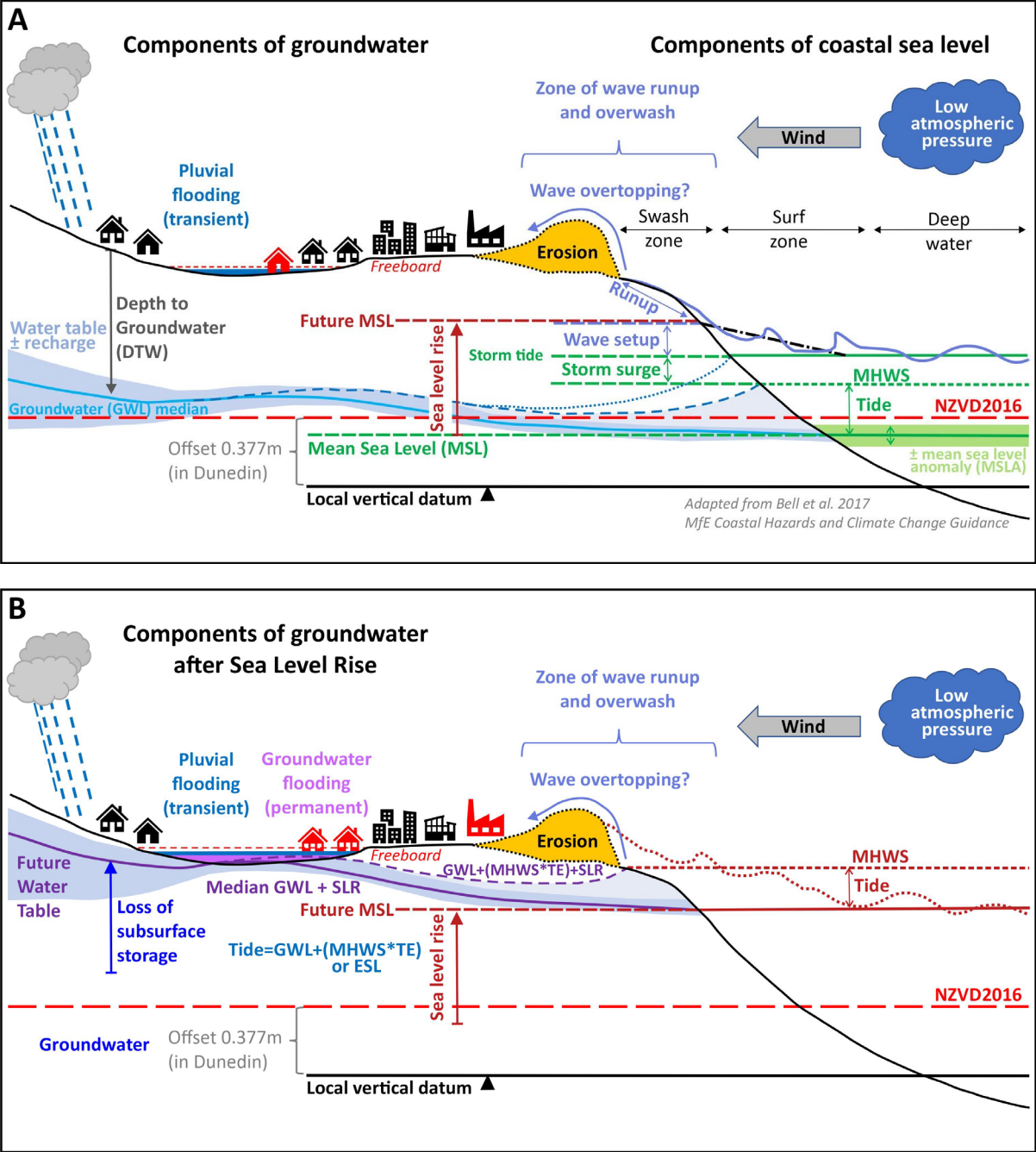


Figure 1.1 The influence of the coast on shallow unconfined groundwater. (A) Components of groundwater and sea level at present state. (B) Changes forced on the groundwater system by sea-level rise. Adapted and developed after Bell et al. (2017) to show groundwater.

The empirical approach accounts for urban influence and local hydrogeologic heterogeneity, such as local variations between silt-dominated estuarine and marine sediments and sand- or gravel-rich onshore facies, which are embedded within local monitoring observations and enable property-scale spatial precision. The empirical approach can also be used to characterise variations in the water table shape and slope caused by subsurface geology, local recharge, urban development and/or interactions with the ground elevation or infrastructure networks. Transient event-based processes and driving forces can also be characterised with the monitoring data and local hazard thresholds identified, while precise mapping of event-related changes can enable fragility to be understood where damage has occurred. From relatively minor investment in shallow groundwater monitoring and data processing, the Dunedin approach has potential to improve both spatial and temporal understanding of the present and future state of shallow coastal groundwater over vulnerable parts of the city.

1.2 Dunedin

The city of Dunedin has a large number of assets and critical infrastructure situated at, or close to, sea level. There are around 2700 Dunedin homes <0.5 m above the spring high tide mark, which is more than double that in any of the other coastal urban centres in the country (PCE 2015). Presently protected by a slightly elevated margin of reclaimed land and fragile sand-dunes, the flat-lying coastal land, particularly in South Dunedin, is crucial to present-day functional operation of the city. However, the flat-lying land in Dunedin is also exposed to a suite of natural hazards of differing importance and potential consequence (Goldsmith and Hornblow 2016; Glassey 2018). There has been particular concern over the potential for the Pacific Ocean to drive a permanent rise in groundwater and emergence in urban areas or even initiation of transient seepage springs (Rekker 2012; Fordyce 2014; Goldsmith and Hornblow 2016; Cox et al. 2020).

Local hills in Dunedin are composed of Caversham Sandstone and/or volcanic rocks of the Dunedin Volcanic Group (Benson 1968; Glassey et al. 2021) which form local bedrock. The hill suburbs locally shed rockfall and landslides, while their catchments deliver runoff onto a coastal isthmus between the Pacific Ocean and Otago Harbour. Quaternary sediments form a veneer on bedrock that is typically <40 m thick but locally seems to reach as much as 70 m (Glassey et al. 2021). Young sedimentary materials are composed of sands and silts deposited under marine to estuarine conditions, inter-layered by sandy and gravelly sediments laid down in fans and river valleys. These amplify seismic shaking and are predicted to have some potential for liquefaction (Barrell et al. 2014), but the city lies within a region of relatively low seismic hazard for New Zealand (Gerstenberger et al. 2022).

Much of the low-lying land was reclaimed from coastal marshes and inter-tidal deposits following European settlement in the late 1800s, levelled with a thin (~1.0 m) veneer and developed. Property and infrastructure are separated from the Pacific Ocean (to the south) by an elevated sand dune barrier >10 m high and from Otago Harbour (in the northeast) by a broad ridge of land >2–5 m high that was reclaimed in the 1960s–1970s, extending the 1850 shoreline to the present wharf and rock wall shoreline. Although the coastal and harbourside land is presently protected from direct inundation by the ocean, there is some hazard and risk from storm surge, coastal erosion, breaches of coastal defences (e.g. marine inundation or tsunami). There were breaches of the dunes last century (Goldsmith and Hornblow 2016), but subsequent engineering, monitoring and active protection have mostly mitigated erosion until now. Maintenance of the dune system will be critical to manage future storm surge and extreme sea-level hazard from the ocean.

Small areas of inundation presently occur on roads and industrial land around the margins of the harbour but are relatively minor and limited by the c.2–5 m elevation of reclaimed land. Modelling of coastal inundation suggests that there needs to be between 60 and 70 cm of sea-level rise before an annual exceedance probability (AEP) 0.1 (annual recurrence interval: 10-year) storm surge and extreme sea level (ESL) will overtop reclaimed land around the harbour margin and enter South Dunedin (NIWA 2023a; Paulik et al. 2023; see Section 5.3 for further analysis). While providing some degree of protection from coastal inundation, the reclamation also caused the unfortunate and compromising effect of removing pathways for natural drainage. Most rainwater runoff must now pass through engineered stormwater systems, much of it through the Portobello Road pump station, on route to the harbour and ocean.

The lack of natural drainage outlets, as well as low elevation and fall across the coastal plain, make parts of Dunedin prone to surface-water ponding after moderate to heavy rain. Large areas were inundated during rainfall on 3–4 June 2015, causing at least \$28M damage (Macfie 2016) in an event that was both heavy (144 mm) and intense (9–12 mm/hr). The flood also affected house prices, which were locally selling for a discount of ~5% before the flood, then tripled in the area that flooded to ~15% after the flood, but recovered within 15 months (Nguyen et al. 2022b).

Similar styles of pluvial flooding and damage occurred in 1923 and 1968 (Goldsmith and Hornblow 2016), as well as nuisance ponding in 2018 (Cox et al. 2020). The design capacity of the stormwater system has only limited ability to cope with present rainfall and is further impinged by increased development of impervious urban surfaces and hillslope runoff. Surface floodwater in 2015 appears to have been exacerbated by poor maintenance of drains and pumps, but there has been debate over the potential role that shallow groundwater levels may have played, especially as there were significant rises caused by antecedent rainfall in the month prior to the flood (Goldsmith et al. 2015; Dunedin City Council 2015, 2016; Cox et al. 2020). As well as limiting the amount of unsaturated ground available to store rain and runoff, shallow groundwater surrounding the network creates opportunities for infiltration into the aging stormwater and wastewater networks, which presently appear to drain at least some groundwater. Increases in precipitation intensity due to climate change, or a rise in groundwater in association with sea-level rise, seem likely to decrease network efficiency and increase pluvial flood hazard in the future.

Concerns over direct hazard from groundwater and sea-level rise in Dunedin were raised after Otago Regional Council installed monitoring bores in 2009, and strong tidal cycles were observed in a monitoring borehole (I44/0007) installed 150 m from the ocean (Rekker 2012; Goldsmith and Hornblow 2016). Amplitudes of >15 cm, with sinusoid cycles that are little delayed from ocean tides or affected by precipitation, suggested strong hydrologic connection with the Pacific Ocean. While installation of a wider network subsequently showed this site to be anomalous, and sediments are generally much less permeable (Cox et al. 2020), for simple geometrical reasons of its geography, Dunedin's challenge with potential groundwater rise is still omnipresent. The narrow coastal isthmus is encroached from both the Pacific Ocean in the south and Otago Harbour in the east. Shallow groundwater can be realistically expected to eventually result in areas of permanent inundation. However, there is potential for groundwater to drive earlier transient periods of tide- or storm-surge-related emergence, or exacerbate episodic pluvial flooding, when median levels might remain below the surface. Impacts on stormwater and wastewater network efficiency and efficacy, or dampness and community health, may well be experienced in advance of groundwater reaching the surface and being seen. Thus, the investment to carefully monitor and assess the spatial and temporal behaviour of groundwater is easily justified.

2.0 DUNEDIN DATA AND REFERENCE DATUM

2.1 Monitoring Network

The Dunedin shallow groundwater monitoring network comprises 35 sites nearly all spaced <1 km apart (Figure 2.1, Appendices 1 and 2). Standpipe piezometers are installed as either: (i) 42 mm diameter PVC pipes around 6 m deep with 3 m slotted screens (0.5 mm slots at 6 mm spacing), cased in graded K2 quartz sand and capped with a bentonite seal, in a 96 mm hole pushed using a CPT (cone penetrometer test) drill rig; or (ii) 80 mm diameter PVC casing, between 14 and 20 m deep with 3 m screens near the bottom of hole, cased in sand and gravel and capped with bentonite, that were installed within 125 mm holes drilled by sonic drilling. The piezometers are finished with a galvanised steel flush-mount lockable well cap on a raised cement cap, or a lockable steel cover with a c.30 cm upstand.

Initially, shallow groundwater monitoring involved four boreholes, 80 mm diameter by 6 m deep, installed by Otago Regional Council in 2009 (Goldsmith and Hornblow 2016). These sites provide ‘long-term’ monitoring and decadal-scale context of observations. They form a transect across the western side of the coastal plain and a strong tidal response is observed in the borehole closest to the Pacific Ocean (I44/0007 Kennedy Street). Widespread occurrence of near-surface groundwater, but limited tidal fluctuation, was confirmed in a short campaign of observations from 10 hand-augured standpipes (50 mm diameter to 3 m depth) (Fordyce 2014). Floods in June 2015 led to widespread speculation on the area’s long-term future and recognition of the need to increase knowledge in subsurface hydrogeology and condition. A consortium of interested parties undertook geotechnical testing and upgraded the groundwater monitoring into a wider network in 2019. Analysis of initial observations showed relatively little tidal variability compared with I44/0007 (Cox et al. 2020). A further eight infill sites were added to the monitoring network in 2021 to decrease areas of uncertainty in groundwater position and behaviour. Further information on drilling methods and network installation can be found in Cox et al. (2020).

2.2 Groundwater Observations and Reference Datum

Water level and temperature data have been recorded across the monitoring network every 15 minutes by automated transducers. Short epochs of conductivity observations have also been made at most sites and calibrated to water samples. There are a range of transducer types used with different manufacturer specifications, and all require a water density assumption (which is temperature and composition dependent) but will be within ± 0.003 m (3 mm) at 95% (2 sigma) confidence. The automated transducers are mostly unvented, downloaded every three months, although four ‘long-term’ sites are vented and telemetered (Cox et al. 2020).

Unvented pressure data have been corrected for atmospheric pressure variations using a barometer at the Otago Regional Council office (Figure A1.1), which is <5 km from the furthest piezometer, then converted into water levels using a 1000 kgm^{-3} freshwater density. Calculated water-column heights above the transducers (approximately ± 0.002 m) were calibrated to manual checks of groundwater levels collected every 6–8 weeks with an electronic water tape meter (± 0.01 m). Testing showed that any spatial variations in air pressure between the office barometer and a piezometer 2.5 km closer to the coast are insignificant compared with other assumptions and uncertainties in conversion from pressure to groundwater elevation (Cox et al. 2020).

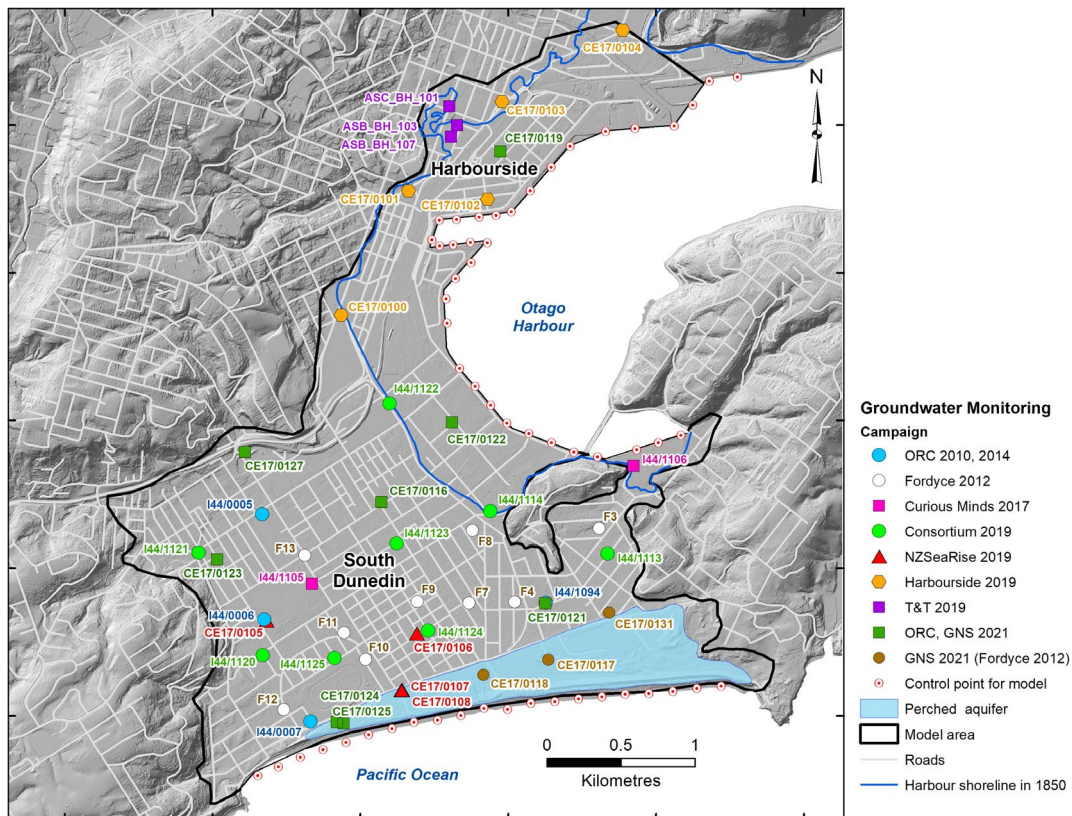


Figure 2.1 Groundwater monitoring sites in Dunedin. Piezometers used in this study (coloured by campaign and labelled with installation date) are shown together with an outline of the flat-lying land and model extent, harbour and coastal control points included in interpolations. Data from most sites are downloaded periodically, but four Otago Regional Council sites are telemetered. The figure also shows the interpreted extent of a perched aquifer in the sand dunes at St Kilda (light blue shade) and the position of the harbour shoreline in 1850 prior to reclamation. A separate map showing place names used in this study is included in the appendices.

To obtain absolute elevations and locations of piezometer and groundwater, a local reference ‘measuring point’ (MP) set at the top of the lining or casing was surveyed by RTK-GPS, which returned average vertical precision ± 0.04 m with maximum uncertainty ± 0.07 m across the network (Appendix 2). A locally measured offset of the MP height above or below ground (GL) enabled depth to groundwater (DTW; negative = above ground, positive = below ground) to be determined from the electronic-tape observations and/or LiDAR surveying. All locations were converted into the standard New Zealand Transverse Mercator 2000 (NZGD2000 EPSG: 2193) coordinate system and Vertical Datum 2016 (NZVD2016 EPSG: 7839). Accounting for all of the assumptions and uncertainties, the groundwater-level precision at each site should be ± 0.005 m (5 mm), whereas absolute accuracy between sites ± 0.05 m (50 mm).

A time-series database hosted by Otago Regional Council is almost entirely complete for the 6 March 2019 – 1 May 2023 epoch presented here, with four ‘long-term’ sites providing decadal-scale context back to 2009. The monitoring data do contain some human-induced data anomalies, such as when slug tests or transducer downloads occurred, or from groundwater sampling drawdown and recovery. Recorded in notes and field sheets, the anomalies have been identified from the time-series at each site and removed for this study. A variety of statistics were then generated from the remaining time-series for each monitoring site, including median, maximum, minimum, 95th and 5th percentiles, mean, standard deviation and range of groundwater levels. Other collated site data include: tidal amplitude, efficiency and phase lag; distance from harbour or sea; sample pH, electrical conductivity and calculated seawater percentage; and a rainfall response index reflecting rainfall recharge efficiency (Cox et al. 2020).

2.3 Temporal Context of Monitoring Epoch

In comparison to observations of rainfall and sea level, which are readily available over many decades, groundwater data are only available over a relatively short period in Dunedin. This report is focused primarily on monitoring observations from 2019 to 2023 (and associated statistical data) that were collated from the period 6 March 2019 – 1 May 2023. While nuisance surface ponding was experienced in February 2020, there were no seriously damaging pluvial flood events during this epoch. To help confidence in the interpretations that arise from these data, the epoch can be examined in context of longer-term variability and the 2015 floods using some sites that have operated for more than a decade.

The longest time-series records for groundwater in Dunedin are from four shallow <6 m piezometers installed by Otago Regional Council – since 2009 at Bathgate Park (I44/0005), Tonga Park (I44/0006) and Kennedy St (I44/0007) and since 2014 at Culling Park (I44/1094) (Figure 2.1). Plots of groundwater level against the numerical day of the year (Julian day) show some tendency toward lower levels during late summer to early autumn (April) but are clearly not sinusoidal over an annual interval – indicating no well-defined or regular seasonal behaviour (Figure 2.2). Kennedy Street (I44/0007) has strong tidal behaviour that is rarely disturbed from expected solar and lunar cycles. Elsewhere, fluctuations are dominated by peaks and recessions over daily to weekly intervals that are coincident with rainfall events. Some cyclicity at a period of 90–100 days may reflect cumulative rainfall and recharge affected by the frequency of storms (Cox et al. 2020). The cyclicity shows good correlation with daily rainfall averaged over the previous 30 days (see Cox et al. [2020]: Figure 2.4).

The piezometer at Culling Park is particularly sensitive to rainfall, but groundwater levels at this site became anomalously low during summer–autumn 2021 and a new replacement piezometer (CE17/0121) was installed nearby in November 2021. Although data from 2019 to 2020 for Culling Park were compared against the 2014–2018 epoch by Cox et al. (2020), it seems that this site has not provided a reliable indication of groundwater conditions since the beginning of 2021 (Figure 2.2). The piezometer is presently being decommissioned from the network.

Statistics for 2019–2023 from the three other long-term piezometers are compared against those from 2010 to 2018¹ (Table 2.1, Figures 2.2 and 2.3). Median groundwater levels during 2019–2023 were within 0.07 m of the 2010–2018 values, and probability distributions are very similar. Although the 2019–2023 groundwater levels appear to be a reasonable proxy (± 0.07 m) for median conditions during the past decade, graphs of percentile distributions (Figure 2.3) show that there were notable extreme values experienced at Tonga Park and Kennedy St that are missing from the more recent 2019–2023 observation period at these sites (Figure 2.3). Here, the maximum groundwater values were those experienced during the June 2015 floods, which were up to 0.6 m higher than the maximum experienced during the 2019–2023 epoch. Upstands installed on the wellheads after the 2015 floods now stop surface flow into the borehole and hydrological connection with any ponded surface water, which may provide an explanation of the lack of extreme values during 2019–2023. At Bathgate Park, the high groundwater level experienced during the 2015 floods was just exceeded by levels during winter 2023 (high groundwater from 27 to 29 July 2023).

¹ Although years have been rounded here as ‘2010–2018’, the actual epoch analysed was 6 March 2010 – 5 March 2019 so as to match the months and any seasonality that may be present in the 2019–2023 epoch.

Table 2.1 Comparison of statistics for longer-term (shaded light grey) and 2019–2023 epochs of groundwater levels at three long-term Otago Regional Council (ORC) monitoring sites. Levels are given in metres NZVD2016. Statistics from other sites are provided in

Table A2.2.

ORC Number	I44/0005		I44/0006		I44/0007	
Name	Bathgate Park		Tonga Park		Kennedy St	
Start Date	6/03/2010	6/03/2019	6/03/2010	6/03/2019	6/03/2010	6/03/2019
End Date	5/03/2019	1/05/2023	5/03/2019	1/05/2023	5/03/2019	1/05/2023
Sample Rate	5–15 min	15 min	5–15 min	15 min	5–15 min	15 min
Mean Level	0.352	0.373	0.159	0.098	0.211	0.214
Standard Deviation	0.079	0.085	0.104	0.096	0.173	0.164
Observation No.	465851	145419	451801	145415	465547	145596
Maximum Level	0.611	0.637	0.989	0.418	1.294	0.857
95th Percentile Level	0.459	0.489	0.313	0.248	0.493	0.487
Median Level	0.364	0.386	0.172	0.104	0.208	0.210
5th Percentile Level	0.205	0.207	-0.02	-0.076	-0.058	-0.040
Minimum Level	0.052	0.131	-0.121	-0.152	-0.349	-0.221
Range	0.559	0.506	1.366	0.570	1.643	1.078
Median Difference	-0.022		-0.068		-0.002	

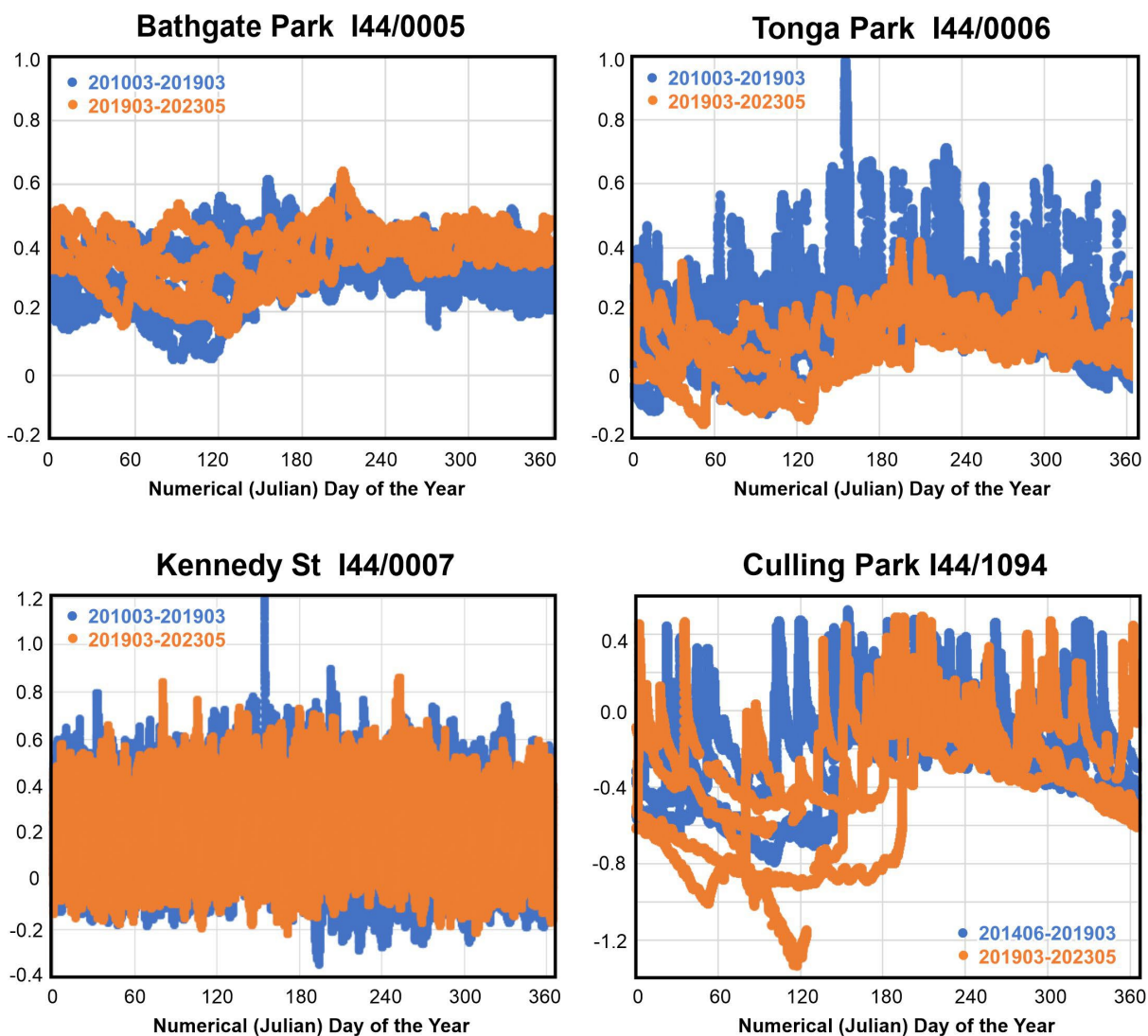


Figure 2.2 Plots of 2019–2023 groundwater elevation (orange) against the numerical day of the year (Julian days as 0–365 values) at the four Otago Regional Council sites with longer-term data (blue). A period of anomalously low groundwater levels at Culling Park, clearly visible in the lower right plot, resulted in the installation of a replacement piezometer CE17/0121 nearby and decommissioning of I44/1094.

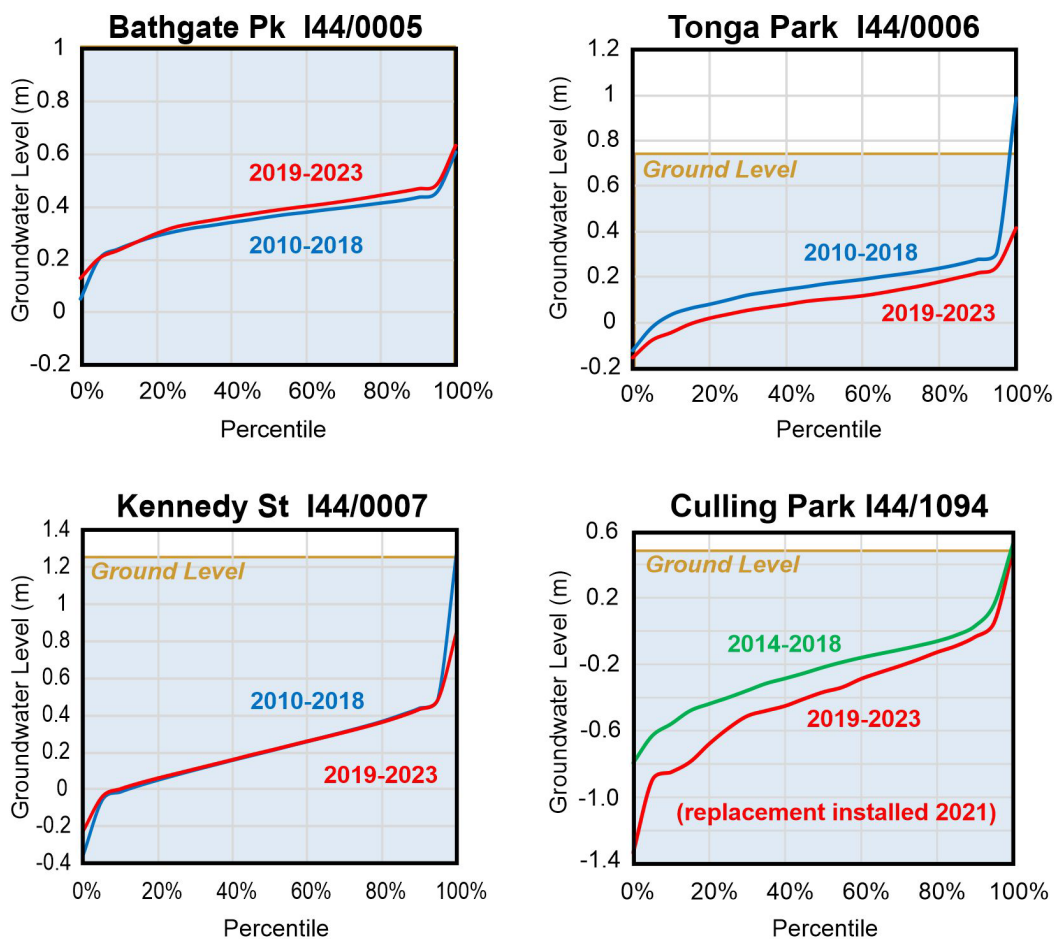


Figure 2.3 Plots of 2019–2023 groundwater elevation (red 2019/03–2023/05) against percentiles of the observations in each epoch, compared against the longer-term 2010–2018 data records (blue 2010/03–2019/02 and green 2014/06–2019/02). Ground level at Bathgate Park (not shown) is 1.15 m (NZVD2016).

Although event rainfall and seasonal variability can be quantified directly from the decadal records, the groundwater-level records are of insufficient length to directly assess whether there are longer-period fluctuations in Dunedin groundwater. Variations in El Niño–Southern Oscillation (ENSO) climate cycles occur at inter-annual two- to four-year cycles, while Inter-decadal Pacific Oscillation (IPO) cycles occur at longer (15- to 30-year) intervals. These have the potential to affect both local precipitation and groundwater levels. It is possible that models could be developed to indirectly assess past climatic effects on groundwater (‘hindcasting’) by extrapolating 2010–2019 groundwater-rainfall co-relationships backward in time, but this was deemed beyond the scope of this report.

2.4 Present Harbour and Sea Level

Observations of local sea level(s) are provided by gauges in both the harbour and ocean. Near-continuous records are available for the DUNT Dunedin tide gauge since 1899, which presently collects data for the upper harbour at 10 minute intervals (Figure A1.1). The offshore Green Island gauge, 9 km southwest of the city, provides ocean data at 1 minute intervals since 2002. Where useful, the acronyms Mean Harbour Level (MHL) and Mean Level of Sea (MLOS) are used to distinguish these observations, whereas Mean Sea level (MSL) is used in a more general context. Although there is a widespread perception that MSL should be zero in NZVD2016, as the datum is based on gravity observations and an approximation of a regional geoid, there are spatial and temporal anomalies of sufficient scale that local offsets need to be applied.

Tidal prediction, standard port tide levels and local MHLs are published regularly in New Zealand (LINZ 2023a). There are also corrections to apply when transferring elevations from the port sites variable distances to other locations. Based on the 2003–2021 standard port observation period, the MHL at DUNT is presently -0.248 m NZVD2016. This has been surveyed relative to both a local benchmark (AFEQ) and cGPS data (Denys et al. 2020). To transfer MLOS from Green Island to the Dunedin shoreline, a spatially dependent conversion is applied that uses AFEQ (LINZ 2023b). A relationship grid produces west–east variation in MLOS -0.277 to -0.287 m (NZVD2016) along the Dunedin Pacific Ocean shoreline (between St Clair and St Kilda). As the difference is not large in the context of other uncertainties (e.g. tides and groundwater), for this study, mean values for 2019–2023 of MHL = -0.22 m and MLOS = -0.07 m (NZVD2016) have been adopted to represent the mean elevation of the harbour and ocean during the associated period of groundwater monitoring.

ESL elevations have been calculated around New Zealand to represent a variety of AEP and average recurrence intervals (ARI) (Stephens et al. 2020; Paulik et al. 2023; Stephens and Paulik 2023). These combine estimates of tide, storm surge, wave set-up and MSL derived from analysis of tide gauges, tide and wave modelling. In Dunedin, the tidal amplitude, wave set-up and storm-surge level all differ in both scale and expected return period when comparing between the open ocean and harbour. Tides in the harbour are amplified by 1.1 times and lag 80 minutes behind the ocean due to the geometry and bathymetry of the harbour. As wave set-up and run-up are relatively short-period, they are unlikely to drive changes in groundwater levels, so have not been considered in this study for groundwater calculations. However astronomical tides and storm-surges are observed to cause episodic rises in groundwater, at least locally near the coast in permeable ground (Cox et al. 2020). Local high tide and storm tide offsets from MHL and MLOS were obtained from Stephens et al. (2020) (Table 2.2) and are used to represent the ESL forcing on groundwater.

Table 2.2 High tide and storm tide anomalies at Green Island and Dunedin tide gauges, used to forecast the annual exceedance probability (AEP) of tides and extreme sea level forcing on groundwater from the ocean and harbour, respectively. Data extracted from Stephens et al. (2020). MHWS7 = Mean High Water Springs water level exceeded by the highest 7% of tides, which occurs approximately every fortnight. The AEP = $1-e^{-1/ARI}$, where ARI is the average recurrence interval (or surrogate 'return period').

AEP	ARI (Year)	Green Island (m above MLOS)	Dunedin Harbour (m above MHL)
1	MHWS7	0.98	1.08
0.633	1	1.35	1.47
0.1	10	1.47	1.60
0.01	100	1.57	1.72
0.001	1000	1.66	1.82

2.5 Topographic Elevation

Definition of the position of land and relative sea level is an important step in any analysis of coastal hazards. The hypsometry relative to the sea level has a strong bearing on the evolution of sea-level-rise-related hazard over time. Land elevation in Dunedin was defined by a LiDAR survey flown for Otago Regional Council by AAM Ltd on 24 June 2021 during low tide (ORC 2022). Laser scanning returned point-cloud density 13.84 points/m². Ground validation using field surveys suggests fundamental vertical accuracy (FVA) within ±0.05 m (2 sigma, 95% confidence level) and accuracy of ±0.21 m horizontally in the Dunedin part of the survey. These data were combined into a digital surface model (DSM) and digital elevation model (DEM) developed at 1 m cell size in NZVD2016 along a wider area of coastal catchments (LINZ 2022) with target accuracies within the specifications of the survey.

2.6 Rainfall

Changes in groundwater level and flood events have been compared and characterised by rainfall observations (daily and hourly) from New Zealand MetService data collected at Musselburgh (Automatic Weather Station 93892). With observations since 1918, this is the longest, most representative, site for rainfall on Dunedin’s coastal plain. Models of high-intensity rainfall events as depth-duration-frequency or intensity-duration-frequency tables are provided by the HIRDS (High Intensity Rainfall Design System) tool created by NIWA (National Institute of Water & Atmospheric Research) (Carey-Smith et al. 2018; NIWA 2023b). Depths of 12-hour rainfall at various AEPs derived from historical data for Musselburgh (Site ID: I50954) are used to represent precipitation in the study area (Table 2.3). Data of 12-hour depths and exceedance probabilities have been used to help calculate subsurface availability of storage for rainfall infiltration within the unsaturated pore-space between the ground surface and the water table (see Section 4.3).

The HIRDS tool also provides an estimation of future depth-duration-frequency and intensity-duration-frequency rainfalls during 2031–2050 and 2081–2100 under RCP 2.6, 4.5, 6.0 and 8.5 climate-change scenarios (NIWA 2023b). These are generalised, based on the Clausius-Clapeyron relation, whereby the amount of precipitable water that the atmosphere can hold increases by ~7% per degree of warming (Carey-Smith et al. 2018). Relative to present day, the 2081–2100 depths for 12-hour rainfall are increased by ~12% under RCP 4.5 and ~20–25% under RCP 8.5. However, given recent cyclones and weather events in New Zealand during 2023, and precipitation from atmospheric river events in particular, there is widespread concern as to whether extreme value analysis using historical data can adequately capture future events (Emmanouil et al. 2022).

Table 2.3 Musselburgh rainfall depth-duration-frequency table from HIRDS v4 (NIWA 2023b). Note: AEP here is derived off a median (p50) rainfall and the relationship with ARI has been simplified to AEP = 1/ARI.

AEP	ARI (Year)	Depth 12-Hour (mm) Historical	Standard Error (mm)
0.633	1.58	32.1	2.5
0.5	2	35.8	2.7
0.2	5	49.3	4.1
0.1	10	60.2	5.8
0.02	50	89.9	13
0.01	100	105	18

2.7 Stormwater and Flooding

Dunedin’s stormwater network on the coastal plain was mostly installed during the 1950s and 1960s. The system was initially designed to be sufficient to keep all stormwater within the piped network for rainfall intensity of 14.3 mm over a 43 minute storm, with some water backing up in the street channels if rain reaches 19.7 mm over the same period (Dunedin City Council 2015, 2016). Planned on a 45.7% runoff coefficient, representing the approximate imperviousness of the catchment at that time, the coverage of buildings, streets, driveways and other impervious surfaces has since increased. The rainfall runoff coefficient may have changed significantly since construction. For example, Mohssen (2017) compared rainfall and pump volumes and calculated 75–80% runoff coefficient for large events. Water that does not get pumped needs to either evaporate, infiltrate to the subsurface (where it is stored in soil pore-space) as groundwater or be stored on the land. Too much of the latter may result in flooding.

Stormwater from catchments on the coastal plain all discharge from South Dunedin into the harbour via the Portobello Road pump station (Figure A1.1). A second pump station, Tainui, is located beside the Musselburgh wastewater pump station and pumps stormwater to Portobello Road from a low-lying area to the southeast of the catchment. The pipe network in South Dunedin can store approximately 20,950 m³ of stormwater, which can be moved through the Portobello Rd pumping station in just under an hour (around 55 minutes) at its maximum capacity (6.3 m³/s) (Dunedin City Council 2015, 2016). Anecdotal evidence suggests that surface-water ponding during past flood events quite commonly starts to accumulate within the first 12 hours of intense rain (see Cox et al. [2020]: Section 6.2). After initial filling of the network, this throughput represents 4.1 mm/hr equivalent rainfall runoff from the stormwater catchments. On this basis, the stormwater system should be able to process up to 56.4 mm of rain during a 12-hour event, which equates to a local 0.1–0.2 AEP based on historical observations at Musselburgh (i.e. ARI of 5–10 years; NIWA 2023b).

This simple theoretical calculation of stormwater network capacity can be tested against the cumulative rainfall totals and during a selection of historical heavy rainfall events experienced in Dunedin (Figure 2.4). Some were sufficiently intense to cause damaging levels of floods (1923, 1968, 2015) or nuisance ponding (2018) (see Cox et al. [2020] for details). Other rainfalls (2017, 2020, 2022 x 2) had large totals, but spread over a longer period, that caused little surface water accumulation but did result in very high, near-surface groundwater levels. The stormwater network capacity curve derived above (shown as a dashed black line in Figure 2.4) appears to be a useful reference to discriminate between those historical heavy rain events that caused flooding, which plot above the line, compared with those that were of insufficient intensity to cause flooding. However, as the subsurface volume to store water in the ground decreases with rising groundwater, the runoff (and coefficient of runoff) will also change. So the pluvial flood risk can be expected to change over time even if the rates and intensity of precipitation is not altered by climate change. Some assessment is provided in Section 4.3, but much more work is warranted to assess this complex and evolving flood hazard and groundwater’s contribution.

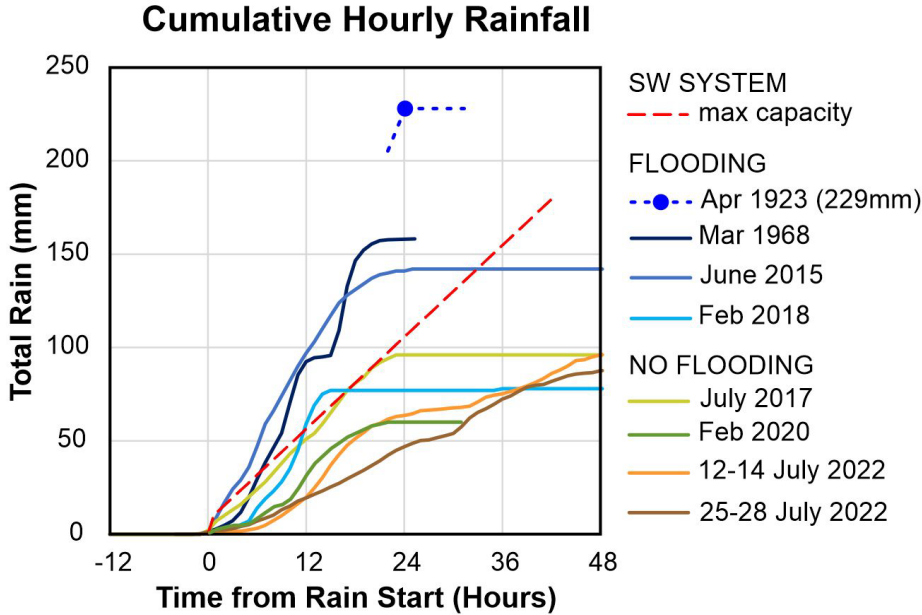


Figure 2.4 Exemplars of heavy rainfall events experienced in Dunedin, plotted as cumulative hourly rainfall against time (in hours) since the start of rain. These data from the Musselburgh weather station show variations in total rainfall and intensity during the storms. Those that resulted in flooding (coloured blue) all sit or reached above the stormwater capacity line (red). Only daily (24 hour) rainfall data were available for the April 1923 event, here plotted as an indicative point marking Dunedin City’s largest recorded daily rainfall (229 mm).

Large parts of Dunedin's wastewater and stormwater networks both lie at or below the water table and are vulnerable to infiltration (see Section 5.2). GIS datasets have been generated to identify places where the network sits relative to (the 2019–2023 position of) the water table, including places where infiltration might switch to exfiltration with groundwater fluctuations. Saltwater intrusion into wastewater pipelines has been an ongoing concern, as the salinity affects secondary treatment efficiency. The likely implications of climate change and sea-level rise (with associated increased rainfall intensity, storm frequency and rising groundwater) is an exacerbation of infiltration and other inflow where infrastructure is not upgraded, which decreases system efficacy.

2.8 Sea-Level Rise

Sea-level rise scenarios have been updated for New Zealand as part of the NZ SeaRise: Te Tai Pari O Aotearoa programme (<https://www.searise.nz>). These are based on the latest climate scenarios from the 2021 IPCC Sixth Assessment Report (AR6), using information on changes in land levels around the coast, known as vertical land movement (VLM) observed by satellite between 2003 and 2011 (Hamling et al. 2022). Estimates have been provided for sites all around the New Zealand coast.

The times at which a particular rise in sea level may be reached are strongly dependent on both climatic and societal futures. These are captured in a series of plausible shared socio-economic pathways (SSPs) introduced by the AR6 report to replace the previous representative concentration pathways (RCPs). Five 'medium confidence' scenarios are now recommended for use in New Zealand (Ministry for the Environment 2022): SSP1-2.6M (sustainability), SSP2-4.5M (middle of the road), SSP3-7.0M (regional rivalry), SSP5-8.5M (fossil-fuel-intensive development) and SSP5-8.5H+ (upper likely range). Additional 'low confidence' scenarios can be used to further stress test long-lived or high-risk infrastructure, subdivision or managed retreat with some of the more uncertain contributors of sea-level rise. As the time at which an amount of sea-level rise can be expected varies greatly between the different scenarios, and between locations, there is considerable uncertainty in time available for action.

In this study, we simply forecast groundwater state at fixed 0.1 m increments of sea-level rise after 2023, instead of trying to predict some uncertain time at which increments of sea-level rise will be attained. Site 4780 (St Clair) is adopted as a reference for Dunedin. The various times at which the sea-level-rise increments might be expected at this site, based on p50 values but without uncertainty, are provided in Table 2.4. Vertical land motion does not appear to have been significant along the Dunedin coast during 2003–2011 (Site 4870 VLM = -0.36 ± 1.02 mm/yr at 1 sigma). Including the local 2003–2011 VLM, p50 subsidence only makes a small difference locally. In this instance of subsidence, a particular increment of sea-level rise would only 'arrive' around five years sooner in Dunedin. There is still some debate as to how representative the contemporary period of satellite-based observations may be, relative to the recurrence interval of earthquakes (10^2 – 10^4 years) and longer-term tectonic motion (10^4 – 10^6 years). For further discussion on VLM, local tectonics and sea-level rise uncertainty see Denys et al. (2020).

Table 2.4 Time at which various scenarios of sea-level rise will be reached in Dunedin, referenced to 2023. These are different scientific forecasts depending on greenhouse gas emissions, mitigation and shared socio-economic pathways (SSP) we may follow. Based on data for Site 4780 (St Clair) using relative sea-level rise data from NZ SeaRise. Note that projections beyond 2170 are not provided in NZ SeaRise estimates (indicated here with dash symbol).

Sea-Level Rise (cm)	10	20	30	40	50	60	70	80	90	100
Medium Confidence										
SSP1-1.9 M	2048	2074	2100	2126	2152	-	-	-	-	-
SSP1-2.6 M	2047	2069	2091	2112	2133	2154	-	-	-	-
SSP2-4.5 M	2043	2061	2078	2093	2108	2121	2134	2147	2158	-
SSP3-7.0 M	2042	2057	2071	2083	2094	2105	2114	2123	2132	2140
SSP5-8.5 H+	2039	2053	2066	2077	2087	2096	2105	2114	2122	2129
Low Confidence										
SSP1-2.6 L	2044	2064	2084	2104	2124	2144	2163	-	-	-
SSP2-4.5 L	2041	2058	2074	2089	2104	2117	2130	2142	2154	2166
SSP5-8.5 L	2052	2066	2077	2086	2094	2101	2108	2115	2120	2126

3.0 PRESENT-DAY GROUNDWATER

3.1 Interpolation of Statistical Surfaces

Site observations of groundwater statistics from 2019 to 2023 (Table A2.1) have been spatially interpolated into grids representing maps of the 'water table surface'. There are many ways to interpolate surfaces, with some testing of resulting uncertainty (e.g. Cooper et al. 2015; Plane et al. 2019) and approaches seem to be hotly debated. While kriging is a geostatistical method commonly adopted for interpolating potentiometric groundwater surfaces, the spatial distribution and small number of monitoring sites in Dunedin does not lend itself particularly well to global statistical approaches. Such methods can also be limited in their ability to extrapolate beyond the outer limit of observation points. Instead, a discretised thin plate technique available through the Topo to Raster function in ArcGIS was adopted for this study. This function is based on the ANUDEM programme (Hutchinson 1989; Hutchinson and Dowling 1991) and was designed for the creation of hydrologically correct digital elevation models. It recognises that topographic landscapes have many ridges (local maximums) and few sinks (local minimums) and uses this information to impose constraints on the interpolation. Similarly, we contend shallow groundwater surfaces can be expected to have numerous maxima (recharge points) and fewer or smoothed minima. The method provides hydrologically informed surfaces that are fitted through the observation points and can be extrapolated beyond data points.

The Otago Harbour and Pacific Ocean are water bodies that both have some influence on the behaviour of groundwater beneath the city and have important potential to impinge on the groundwater in future. Observations of tidal variation, groundwater chemistry and specific electrical conductance can be used as a proxy for saltwater/freshwater mixing and show the degree of saline incursion into the groundwater system (Cox et al. 2020). Interpolated surfaces in this study have been constrained at the harbour and coast using a series of boundary 'control points', where values have been assigned to help rationalise the physics and improve extrapolation beyond the monitoring sites. Essentially, it has been assumed that there is some degree of hydraulic connection, or unconnected loading effect, between groundwater and the harbour or sea. Harbour and coastal points are assigned statistics, such as MHL and MLOS derived from tide gauges at Fryatt St (Dunedin) and Green Island, then included in the interpolation.

Statistical values derived for each groundwater monitoring site have been interpolated with the harbour and ocean control points into a series of raster grids with 8 m cells. A test of differences between observed and interpolated groundwater elevations at piezometer sites yielded mean = 0.0076 m, standard deviation = -0.053, n = 29, maximum = 0.1943 m, minimum = -0.1426 m. Any mathematical interpolation error of the statistical surfaces is therefore expected to be within ± 0.1 m at 95% confidence levels.

'Statistical surfaces' of groundwater elevation are quite distinct from 'static surfaces' or 'event-related surfaces', in that the latter represents the state of groundwater at a particular point in time or are associated with a short change during an event. In contrast, statistics from the monitoring represent a range of states during a longer period – in this case, up to four years from 2019 to 2023. In such data, the maximum level of groundwater, for example, can potentially occur at different times at various sites. Therefore, an interpolated grid of maximum values may not necessarily represent the highest groundwater level reached during a single storm or rainfall event. There is an important caveat that, while statistical interpolations may approximate the potentiometric pressure of groundwater over extended periods, such as

long-term hydraulic gradients, caution is required when they are used to interpret short-term behaviour such as directions of flow. Interpolation of discrete data points on a surface also does not necessarily mean that there is hydraulic connection to other points nearby. However, the statistical surfaces are particularly useful for engineering models and solutions, such as incorporating maximum to minimum ranges in foundation design or distributions in the probabilistic assessment of liquefaction vulnerability (e.g. van Ballegooy et al. 2014, 2015).

3.2 Groundwater Elevation

Groundwater throughout South Dunedin is unconfined, but there is a perched aquifer locally in dune-sand at St Kilda and some semi-confined horizons in the Harbourside area. Levels are dominated by rainfall-related peaks and recessions, are slightly lower during late summer to early autumn and contain subtle tidal-related cycles (Cox et al. 2020). Data from the four longer-term Otago Regional Council monitoring sites suggests that observations from 2019 to 2023 are a reasonable proxy for average conditions during the previous decade (Section 2.3). Although some of the extreme flood-related levels have not been experienced since 2015, low groundwater levels in summer 2022 and high levels during winter 2022 meant that the 2019–2023 epoch contains a wide range of groundwater conditions.

A series of statistical surfaces representing the groundwater elevation (GWL), being the height of the water table (in vertical datum NZVD2016), have been developed to represent the overall state of groundwater between 2019 and 2023 from monitoring observations between 6 March 2019 and 1 May 2023. A summary of these data, and how they were derived, is provided in Table 3.1. These are provided in an accompanying ArcGIS10.8 geodatabase named 'sthDunedin_water_table_model2023.gdb' that accompanies this report.

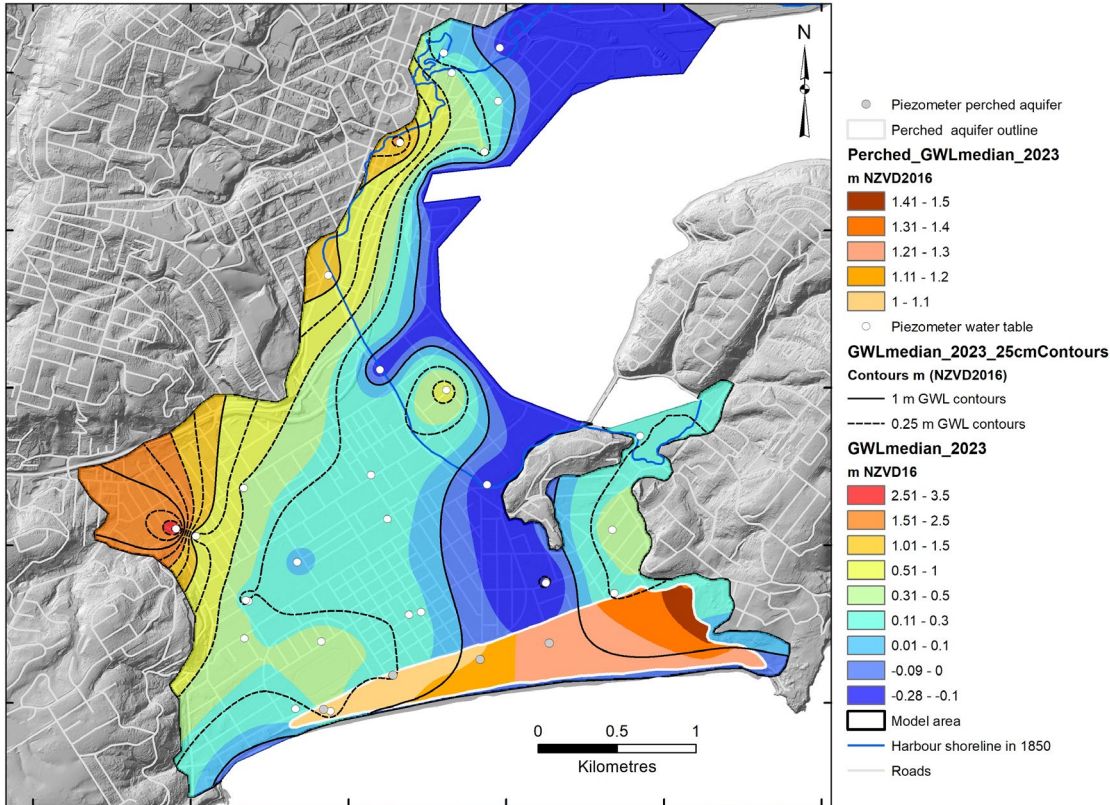


Figure 3.1 Interpolated median groundwater elevation (GWL_{median_2023}), with elevation ranges and gradients highlighted by contours at 25 cm and 1 m intervals. Monitoring sites used in the interpolation are indicated by white dots. An area of perched groundwater, with head approximately 1–1.5 m above sea level, occurs beside the Pacific Ocean in the St Kilda sand dunes. The interpreted extent, monitoring sites (grey dots) and its potentiometric surface of the perched aquifer is also shown.

Table 3.1 Summary of statistical surfaces and other datasets are developed to represent 'present day' Dunedin groundwater elevation (GWL) during the 2019–2023 epoch. These are found in the geodatabase *sthDunedin_water_table_model2023.gdb*.

File Name	Summary
<i>GWLmedian_2023</i>	An interpolated grid surface (8 m cells) mapping the MEDIAN elevation (metres NZVD2016) of groundwater monitored in the period 2019/03/06–2023/05/01. Surface generated using boundary points for the Harbour (set at -0.234 m), Anderson Bay inlet (0.25 m RL) and coast (-0.075 m RL). Excludes shallow wells in perched aquifer (CE17/0108, 0117, 0118, 0124) and artesian/semi-confined sites (CE17/0127, ASB_BH_107). Although 2019–2023 had some extended dry periods, the epoch appears to be reasonably representative of the long-term groundwater condition (checked against 2010–2018).
<i>GWLmedian_2023_25cm Contours</i>	Contour lines (at 25 cm intervals) of median level of groundwater (metres NZVD2016) interpolated for 2019–2023.
<i>GWLmax_2023</i>	Maximum level of groundwater (metres NZVD2016) interpolated from measurements between 2019 and 2023. Surface generated using boundary points for the harbour (set at 1.245 m), Anderson Bay inlet (1.182 m RL) and coast (1.300 m RL).
<i>GWLmin_2023</i>	Minimum level of groundwater (metres NZVD2016) interpolated as above from measurements between 2019 and 2023. Surface generated using boundary points for the harbour (-1.546 m), Anderson Bay inlet (0.19) and coast (-1.473 m).
<i>GWLp5_2023</i>	5 th percentile groundwater level (metres NZVD2016) interpolated as above from measurements between 2019 and 2023
<i>GWLp95_2023</i>	95 th percentile groundwater level (metres NZVD2016) interpolated as above from measurements between 2019 and 2023.
<i>GWLrange_2023</i>	Range (maximum to minimum) of groundwater levels (m) interpolated from measurements between 2019 and 2023.
<i>GWLmean_2023</i>	Mean level of groundwater (metres NZVD2016) interpolated from measurements between 2019 and 2023.
<i>GWLstdev_2023</i>	Standard deviation of groundwater level (m) interpolated from measurements between 2019 and 2023.
<i>GWLmhws_median_2023</i>	An interpolated grid surface (8 m cells) mapping the groundwater elevation at MHWS. A tidal offset to <i>GWLmedian_2023</i> based on the present-day difference between MHWS and MSL (0.98 m MHWS7 in ocean at Green Island), multiplied by the tidal efficiency grid of groundwater fluctuations (Note: need to divide tidal efficiency [TE] values in % to a proportion). $GWLmhws_median2023 = GWLmedian_2023 + (0.98 \times TE)$.
<i>GWLmhws_mean_2023</i>	An interpolated grid surface (8 m cells) mapping the groundwater elevation at MHWS. A tidal offset to <i>GWLmean_2023</i> based on the present-day difference between MHWS and MSL (0.98 m MHWS7 in ocean at Green Island), multiplied by the tidal efficiency grid of groundwater fluctuations (Note: need to divide tidal efficiency [TE] values in % to a proportion). $GWLmhws_mean2023 = GWLmean_2023 + (0.98 \times TE)$.
<i>perched_GWLmedian_2023</i>	An interpolated grid surface (8 m cells) mapping the elevation (metres NZVD2016) of perched groundwater in dune sand at St Kilda to St Clair. Median data derived from monitoring at CE17/0108, 0117, 0118, 0124. Surface generated using piezometer data and <i>perched_aquifer_modelpts</i> .

The median level of groundwater during the 2019–2023 epoch (Figure 3.1) was elevated above the median and mean levels of the sea in the harbour and open ocean during the same period (MHL= -0.22 m and MLOS= -0.07 m [NZVD2016]) but lies below harbour and ocean levels during their high tides. Highest median groundwater values are those adjacent to the hill suburbs, with slopes suggestive of flow out through the flat-lying South Dunedin and Harbourside land, where most groundwater appears to sit slightly elevated at between 0.25 and 0.1 m. The interpolation shows steep gradients in the Forbury area that are largely a function of observations at Fitzroy St (I44/1121) and Surrey St (CE17/0123), but with overall gradients ~0.005 m/m in nearby Caversham that are not unreasonable for hydraulic gradients expected in young, unconsolidated fine-grained sediments recharged from nearby hills (e.g. see Freeze and Cherry [1979]). A piezometer installed through reclaimed land near the Harbour at Turakina Road (CE17/0122) seems slightly anomalous, with groundwater median relatively high at 0.815 m but with behaviour and depth relative to ground that matches neighbouring piezometers.

There is also a zone of perched groundwater in the sand dunes at St Kilda beside the Pacific Ocean (Fordyce 2014; Cox et al. 2020; Figure 3.1). Here the groundwater is elevated at least one metre above MSL, has relatively low electrical conductivity and fresh composition, is recharged by rainfall, contains little tidal signal and is more subdued in its fluctuations compared with groundwater elsewhere across the rest of South Dunedin. Vertical gradients locally suggest that the perched water is downwards percolating and isolated from water in estuarine sediment below. The perched aquifer sites have been treated separately in this report. Grid surfaces were interpolated using a series of modelling points around the mapped outline to provide the minimum possible elevation of the freshwater lens. Files in the accompanying geodatabase are distinguished by the prefix 'perched_' (e.g. *perched_GWLmean_2023*, *perched_DTWmedian_2023*).

3.3 Depth to Groundwater

A series of depth to groundwater (DTW) surfaces (Table 3.2) were derived by subtracting the groundwater elevation grids from the digital elevation model generated from the 2021 LiDAR survey. The grid surfaces (8 m cells) map the depth (metres relative to ground level) based on the 2019–2023 groundwater elevation grids interpolated from monitoring during 6 March 2019 – 1 May 2023. Depth to water grids define the position of the water table relative to ground. The lowest-lying suburbs do not necessarily co-incide with shallowest groundwater, highlighting that vulnerability to shallow groundwater-related hazards does not necessarily reflect topographic elevation. Instead, the water table has elevation and gradient that is variable at kilometre-scales, with important differences from suburb to suburb. The DTW grids provide an indication as to potential groundwater inundation and remaining storage space available for rainfall infiltration.

Negative DTW values potentially indicate places where groundwater might rise above ground and cause inundation. Alternatively, they may simply occur where the model may be limited by differences in the nature and spatial precision of topographic and groundwater datasets. The magnitude of any negative values is certainly unlikely to reflect the actual magnitude of any artesian pressure nor indicate potential ponding depth – if only because these are statistical rather than static surfaces or event-related surfaces. To remove potential confusion, some DTW grids with the suffix 'ag0' have been generated where grid cells with negative 'above ground' values were reset manually to zero.

Table 3.2 Summary of statistical surfaces developed to represent 'present day' Dunedin depth to groundwater (DTW) as defined by the 2019–2023 epoch. These are found in the geodatabase *sthDunedin_water_table_model2023.gdb*.

File Name	Summary
<i>DTWmax_2023</i>	Depth (below ground) of the maximum level of groundwater interpolated for 2019–2023. Values in metres below ground level. Note that <i>DTWmax</i> will have larger values than <i>DTWmin</i> .
<i>DTWmedian_2023</i>	Depth (below ground) of the median level of groundwater interpolated for 2019–2023. Values in metres below ground level.
<i>DTWmedian_2023ag0</i>	Depth (below ground) of the median level of groundwater interpolated for 2019–2023. Values in metres below ground level. Grid cells with negative 'above ground' values were reset manually to zero.
<i>DTWmin_2023</i>	Depth (below ground) of the minimum level of groundwater interpolated for 2019–2023. Values in metres below ground level. Note that <i>DTWmin</i> will have larger values than <i>DTWmax</i> .
<i>DTWp5_2023</i>	Depth (below ground) of the 5 th percentile of groundwater level interpolated for 2019–2023. Values in metres below ground level.
<i>DTWp95_2023</i>	Depth (below ground) of the 95 th percentile of groundwater level interpolated for 2019–2023. Values in metres below ground level.
<i>DTWmean_2023</i>	Depth (below ground) of the average level of groundwater interpolated for 2019–2023. Values in metres below ground level.
<i>DTWmhws_mean2023</i>	A calculated depth (below ground) MHWS level of groundwater based on the mean value from <i>GWLmedian_2023</i> (see Section 3.4)
<i>DTWmhws_median2023</i>	A calculated depth (below ground) MHWS level of groundwater based on the median value from <i>GWLmedian_2023</i> (see Section 3.4).

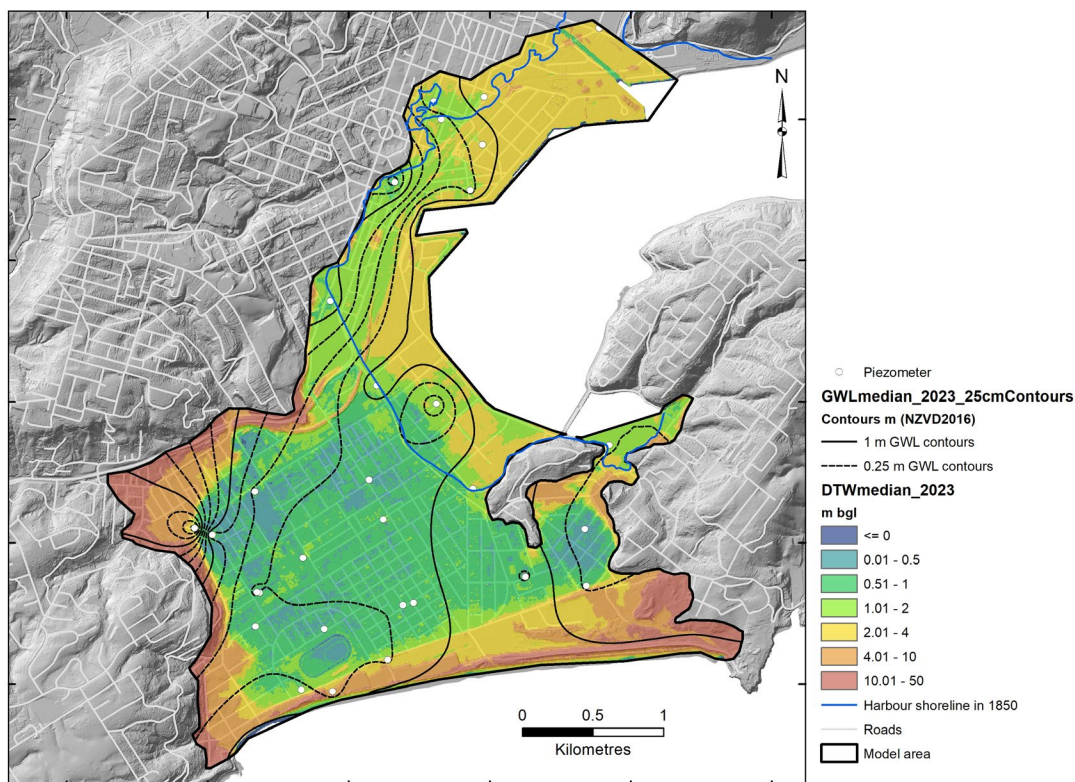


Figure 3.2 Interpolated depth to median groundwater elevation (*DTWmedian_2023*) overlain with the *GWLmedian_2023* level contours at 25 cm and 1 m intervals. Monitoring sites used in the interpolation are indicated by white dots.

3.4 Effect of Tides and Storm Surge

Much of Dunedin City's coastal plain lies at an elevation below MHWS (Figure 3.3). Yet, each successive high tide does not come flooding across the land because it is protected from the Pacific Ocean by a (fragile) dune barrier, or from the harbour by a lip of slightly elevated reclaimed land. The situation highlights that elevation alone cannot always be used as a direct proxy for coastal inundation. However, just like coastal aquifers worldwide (e.g. Ferris 1952; Erskine 1991), the tides and storm surges do cause Dunedin groundwater levels to rise and fall. This tidal response is important as it can be used to help forecast the sensitivity of groundwater and how it may respond to changing sea levels in the future.

Fluctuations in coastal aquifers result from at least two different causes (Hsieh et al. 1987; Erskine 1991; Masterson and Garabedian 2007; Rotzoll and El-Kadi 2008; Yang et al. 2013). In confined aquifers, the additional weight of the water on the surface at high tide increases the pressure on the water at depth, which causes an increase in water levels in piezometers and/or observation wells located near the coast. In this case, no movement of water between the ocean and the aquifer need have occurred. However, in unconfined aquifers, the loading effect does not occur. Instead, saltwater that has moved directly through the pores within the aquifer causes a groundwater level increase.

There are places in Dunedin, such as the Kennedy St (I44/0007) and Tewsley St (CE17/0102) piezometers (Figure 2.1), where there is a very strong, sinusoidal tidal effect on shallow groundwater levels that dominates over other fluctuations (Cox et al. 2020). Comparison of tidal responses with groundwater chemistry (and electrical conductivity in particular) indicated that both types of mixing and loading processes generate the tidal responses (Cox et al. 2020): Tewsley St (CE17/0102) has relatively fresh groundwater that is loaded/unloaded elastically by harbour tides (at ~34% of the tidal range) without flow of saline water

in and out of the piezometer; whereas Kennedy St (144/0007) has a similarly strong tidal response (at ~30% of the tidal range) but instead is brine-rich (~80% sea water, yet variable), reflecting direct mixing of groundwater with inland flow from the ocean.

Regardless of the mechanism, the tidal variability is important in terms of the potential for higher groundwater to contribute to flooding. The tidal effect can be described by measuring phase lag (in minutes) or delay between the tidal peak and groundwater-level response peak, and by the tidal efficiency (TE) amplitude ratio between the magnitudes of the tidal range of groundwater (ΔW) and the tidal range (ΔT).

$$TE = \Delta W / \Delta T \tag{Equation 3.1}$$

The dimensionless tidal efficiency ratio is presented as a percentage in this report. We also found it useful to distinguish the full tidal range (which occurs between high and low tide over 12.42 hours) from the tidal amplitude (between mid- and high tide over 6.2 hours). The tidal amplitude is half of the tidal range.

The upper harbour at Dunedin lags 80 minutes behind tides at Green Island, with a tidal range that is amplified (~110% tidal efficiency) due to the harbour geometry (and bathymetry in particular). Tidal efficiency and phase lag were determined at each groundwater monitoring site relative to the tidal range of the spatially nearest (harbour or ocean) tidal source. A series of interpolated grids (8 m cell size) representing the tidal efficiency, range and amplitude of groundwater tidal changes were developed from these data (Table 3.3). Maps of tidal efficiency (Figure 3.4) show general consistency regarding distance from the tidal source and/or values of nearby data points.

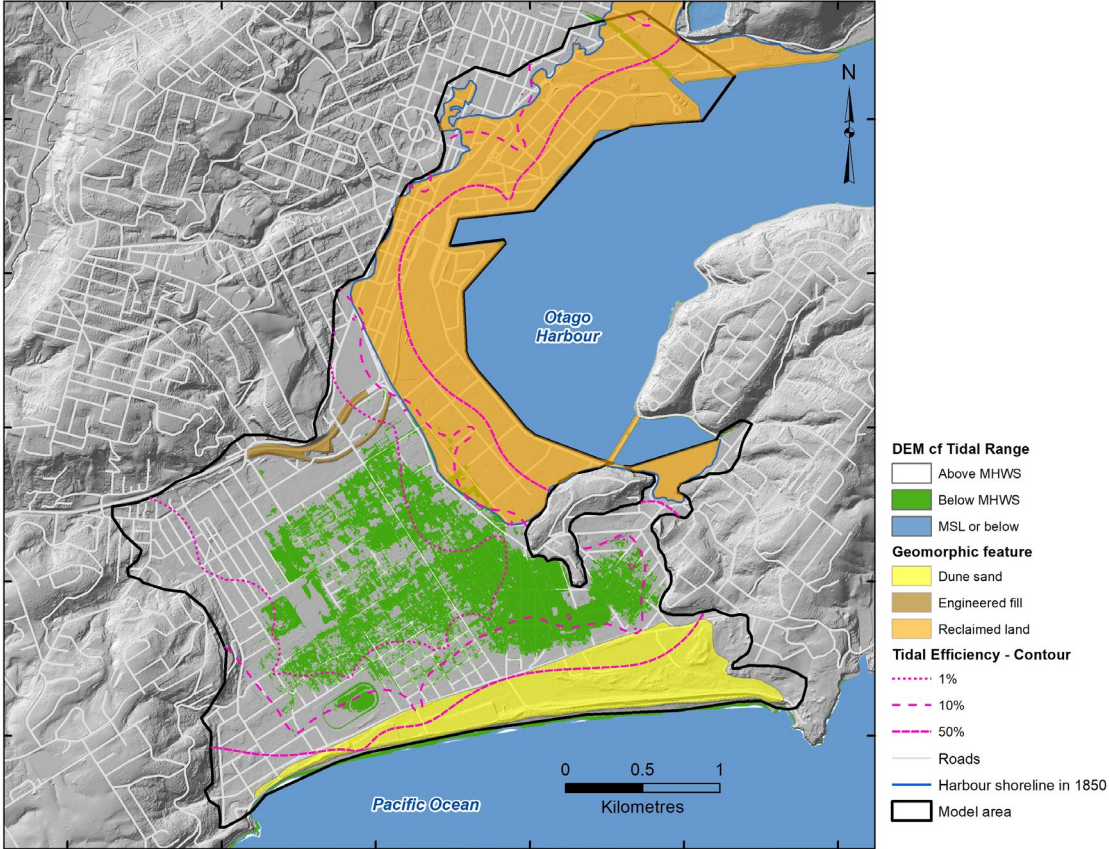


Figure 3.3 Areas where Dunedin’s coastal plain is below Mean High Water Springs (MHWS; green) sit protected from the harbour and ocean behind elevated reclaimed land (orange) and sand dunes (yellow). Contours (pink lines) of tidal efficiency show the percentage (at 1, 10, 50%) of the tidal range transferred into cycles in groundwater level.

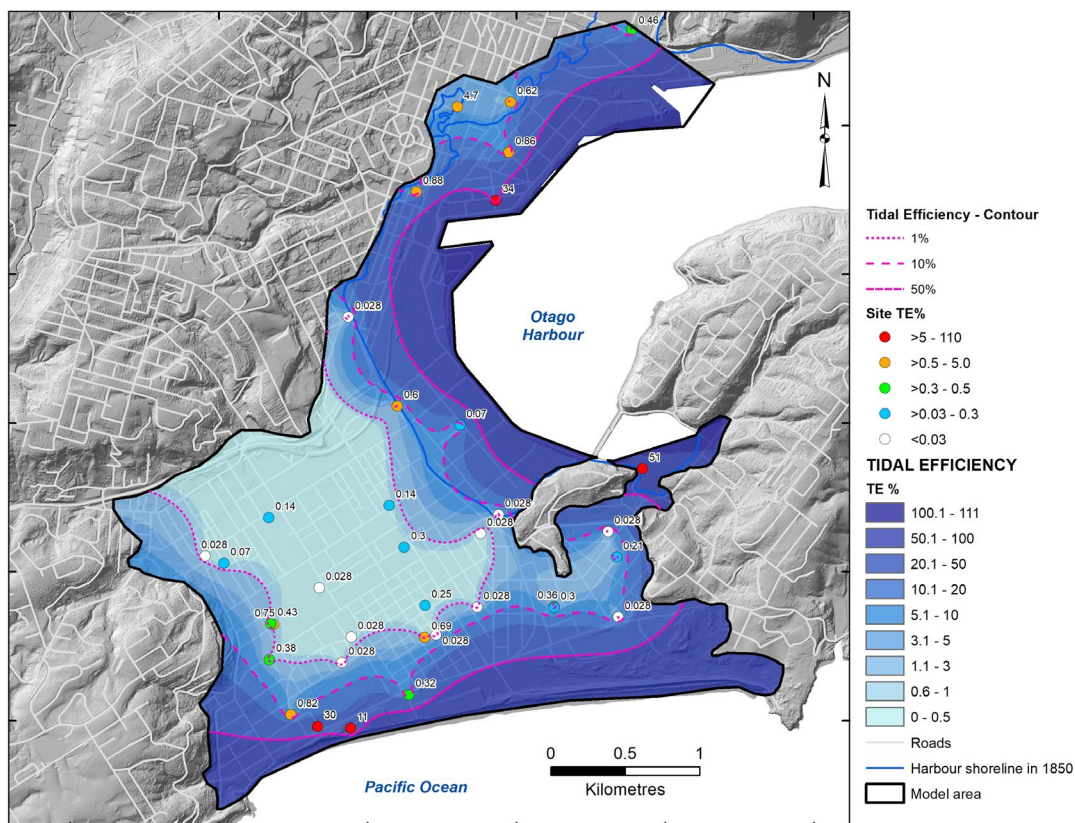


Figure 3.4 Tidal efficiency at each of the monitoring sites, including those from Fordyce (2014), as a percentage of the groundwater tidal range in the nearby ocean or harbour. The blue shading is an interpolated grid surface from the site tidal efficiencies, set with the harbour at 110% due to tidal amplification.

Tidal efficiency decays almost exponentially with distance from the harbour or sea (Cox et al. 2020). Strongly tidal piezometers (e.g. >10% TE) are all within 250 m of the harbour or ocean. At these sites, the amplitude of tidal shifts is generally much larger than those produced by rain, so the tides locally obscure all but the largest (>30 mm) rainfall events. As well as semi-diurnal cycles, these have clear high (spring tide) cycles every two weeks that can be directly correlated to levels in the harbour and ocean tide gauges. However, the presence of spring (3–4 times per year with moon at its perigean) and king (seven-month when moon is at its perigean, is full or is new) tides in the groundwater has yet to be quantified with confidence. To do so requires careful time-series filtering and processing to remove effects of rainfall at these sites (see also Yang et al. [2013]).

Sites positioned along the old 1850s harbour shoreline, now separated from the harbour by around 0.5 km of reclaimed land, have tidal efficiencies of 0.6–4.7% and phase lags from 3 to 6 hours relative to the harbour. Elsewhere on Dunedin’s coastal plain, the tidal responses are very weak and commonly obscured by shifts in groundwater elevation associated with rainfall recharge. For many sites, the tidal signals can only be observed at periods of particularly stable groundwater levels between rainfall events, and a number are at or below the ± 0.003 m (3 mm) lower limit of resolution of the transducers generally suggested by manufacturers.

Graphs of tidal efficiency or phase lag versus distance can theoretically be used to estimate aquifer hydraulic properties, such as the bulk diffusivity and storage (e.g. Erskine 1991; Rekker 2012). However, Cox et al. (2020) found application of theory locally in Dunedin appears nuanced with influencing factors, such as piezometer depth, diameter of the piezometer or style of construction/completion. Scatter on these graphs (and local absence of responses) in part appears to reflect variations in subsurface geology of the local site, in addition to hydraulic conductivity between the piezometer and the ocean or harbour.

For the purpose of this study, we simply use the site observations to characterise the amplitude and spatial reach of tides and assume it will be similar for storm-surge. The tidal efficiency grid has been used in association with high-tide (MHWS7) and storm-tide anomalies in the ocean and harbour (Table 2.2) to calculate the maximum influence they have on groundwater during episodic events. An equation, and nomenclature, for groundwater elevation at MHWS follows the form:

$$[GWL_{xxxx_median_2023}] = [GWL_{median_2023}] + ((XXXX-MSL) \times [TE_%]/100) \quad \text{Equation 3.2}$$

MHWS7 or ESL storm-tide anomaly (in m) above MSL from Stephens et al. (2020) (Table 2.2). In this example, the equation estimates a high-tide / high storm-tide position of groundwater that is referenced to the median level of groundwater during the period 2019–2023. Depth to water surfaces have then been calculated by subtracting groundwater elevation grid from the 2023 LiDAR DEM. Interpolated grid surfaces of the water table at MHWS are compared with median and 95th percentile (p95) levels in Figure 3.5.

Table 3.3 Summary of statistical surfaces developed to represent ‘present day’ tidal behaviour in groundwater (DTW), found in the geodatabase *sthDunedin_water_table_model2023.gdb*.

File Name	Summary
<i>TE_percent</i>	Tidal efficiency (in %) ratio interpolated from site observations of groundwater tidal changes in response to the nearest tidal influence (either the harbour or ocean).
<i>TIDE_amplitude</i>	Amplitude (in metres) of 6.2-hour tidal change in groundwater, interpolated from piezometers, sea and harbour. Tidal amplitude = 0.5 x tidal range measurements.
<i>TIDE_range</i>	Amplitude (in metres) of 12.42-hour tidal change in groundwater, interpolated from piezometers, sea and harbour.
<i>TE_contours</i>	Contours of the dimensionless tidal efficiency (as a percentage) in intervals of 1, 5, 10, 50%. Based on <i>TE_percent</i> grid.

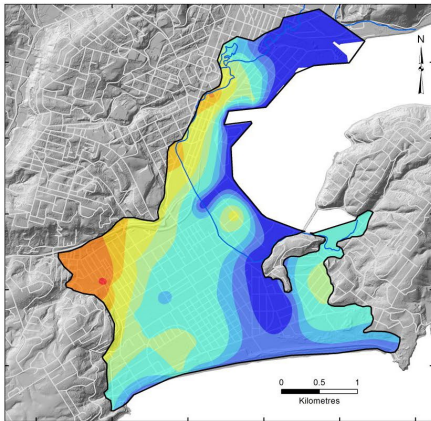
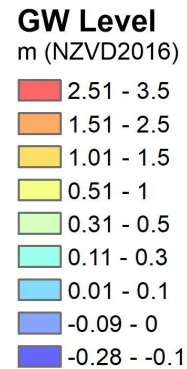
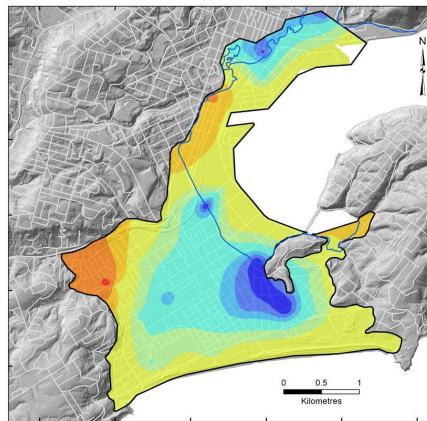
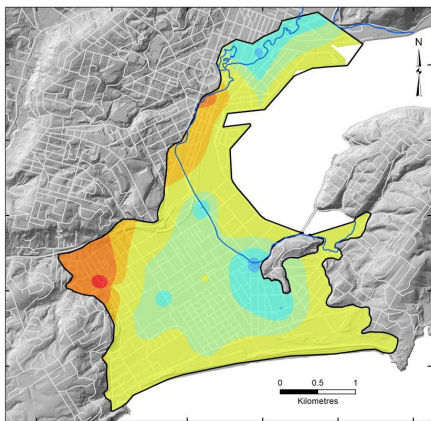
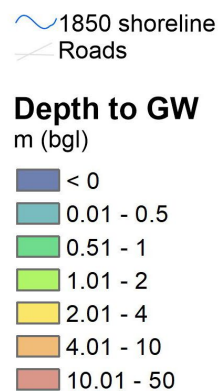
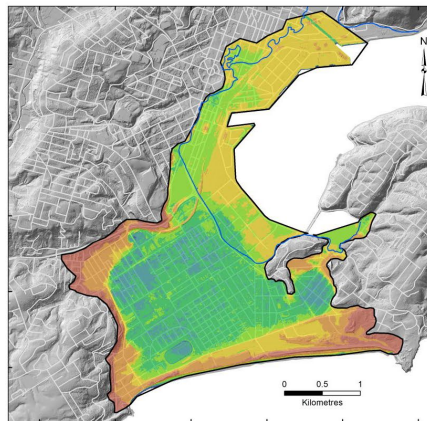
A. GWL median**B. GWL median at MHWS****C. GWL p95****D. DTW median at MHWS**

Figure 3.5 Comparison between geometric models of the elevation (in NZVD2016) of the water table (GWL) at median, mean high water springs (MHWS) and 95% percentile levels based on observations from the 2019–2023 epoch: (A) median groundwater level, (B) calculated level at MHWS, (C) 95th percentile groundwater level (D) and the depth to water below ground at MHWS.

3.5 Response to Rainfall

Groundwater response to rainfall recharge has been characterised at each site using a dimensionless Rainfall Recharge Index (RRI), representing the ratio of the groundwater level change to a measured amount of rainfall:

$$RRI = \Delta W / ER$$

Equation 3.3

where ΔW is the total change in piezometer groundwater level (converted to millimetres) divided by ER , the nearby measured total event rainfall (in millimetres).

Sites can be expected to have variable responses depending on local stormwater drainage, extent of ‘hard’ urban surfaces (i.e. ground imperviousness), piezometer construction method (or ‘well completion’, including piezometer protection to surface water runoff and screen size and type) and subsurface sediment storativity and permeability.

RRI values were initially calculated for each monitoring piezometer site using rainfall events that exceeded about 30 mm in 24 hours, following methodology outlined in Cox et al. (2020). Changes in groundwater level were normalised against rainfall measured at the Musselburgh weather station, which effectively assumes that any spatial differences in total rainfall across the low-lying parts of the city were negligible. A grid of RRI was interpolated by selecting response site values from both 2019–2023 and 2012 observations (Fordyce 2014) (Figure 3.6).

At the harbour and the coast, around the margins of the interpolation, an RRI value of 1 was applied under the assumption that, on average, the response rise of the harbour and sea will equal the total event rainfall and may drive some groundwater rise inland. The RRI grid should be a reasonable representation of recharge during rainfall of 10–50 mm over periods of 12–48 hours, but may not necessarily be applicable for the most-extreme events.

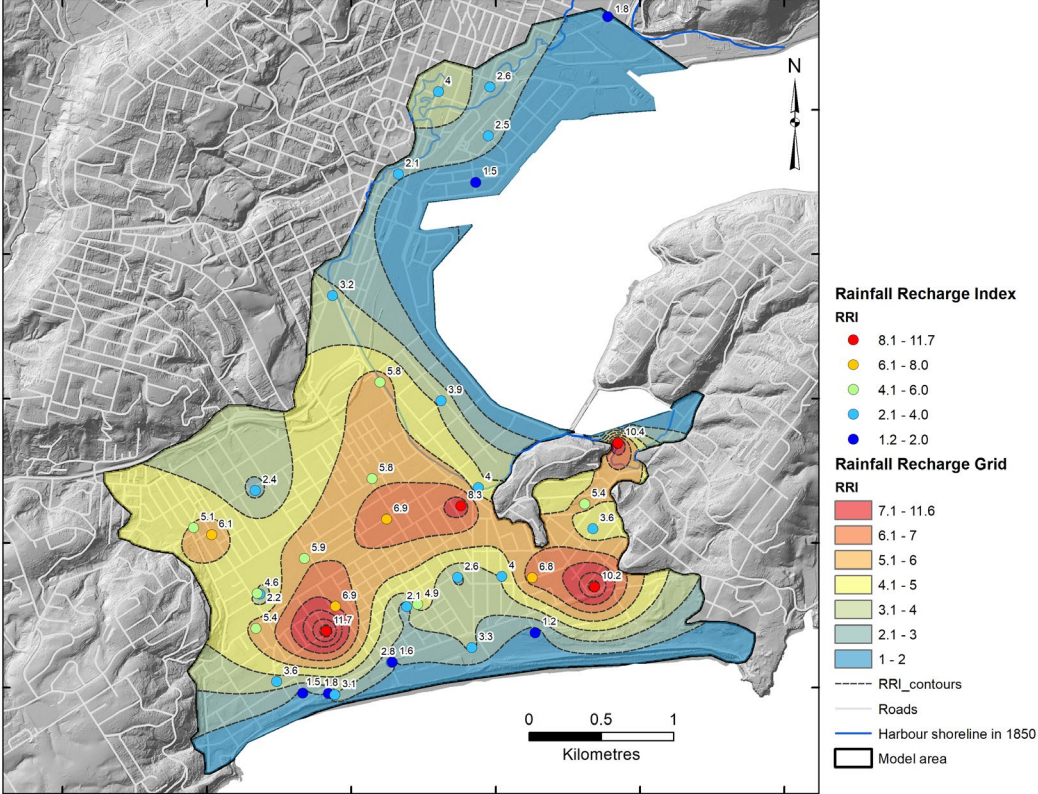


Figure 3.6 The RRI ratio as a series of piezometer point observations and an interpolated grid, which characterises the local rise of groundwater for rain events of around 10–50 mm over a 12–48 hour period.

3.6 Subsurface Storage for Rain

As there appears to be a reasonable degree of spatial consistency in the groundwater responses to rain across the city (Figure 3.6), it makes sense to examine how the elevation of the water table might affect the volume for the storage of rainfall infiltration below ground. Here, we develop a metric using the ratio of the DTW divided by the RRI.

$$[RAINstorage_fromGWLmedian_2023] = [DTWmedian_2023] / [RRI] \quad \text{Equation 3.4}$$

Grids of the rainfall storage (in mm) provide an approximation for the amount of infiltration that can occur before all of the void space is saturated and groundwater becomes emergent. In the accompanying geodatabases (Appendix 4), there are a variety of grid datasets referenced to different statistical states of the water table, such as at median (Figure 3.7), 95th percentile (p95) and MHWS levels.

Ratios of DTW (e.g. *DTWmedian_2023*) divided by RRI were re-calculated into units of millimetres (x 1000) to reflect units in which rainfall is most commonly reported. Amounts required to lift groundwater to the surface mostly range from 10 to 5000 mm and are greater around the raised margins of South Dunedin, where the interpolated groundwater surfaces are deep. Precipitation over 300 mm in a 12–48 hour period are unprecedented for the city (Carey-Smith et al. 2018; NIWA 2023b). Under this simplistic calculation, subsurface storage in these places is unlikely to ever be exceeded by rainfall.

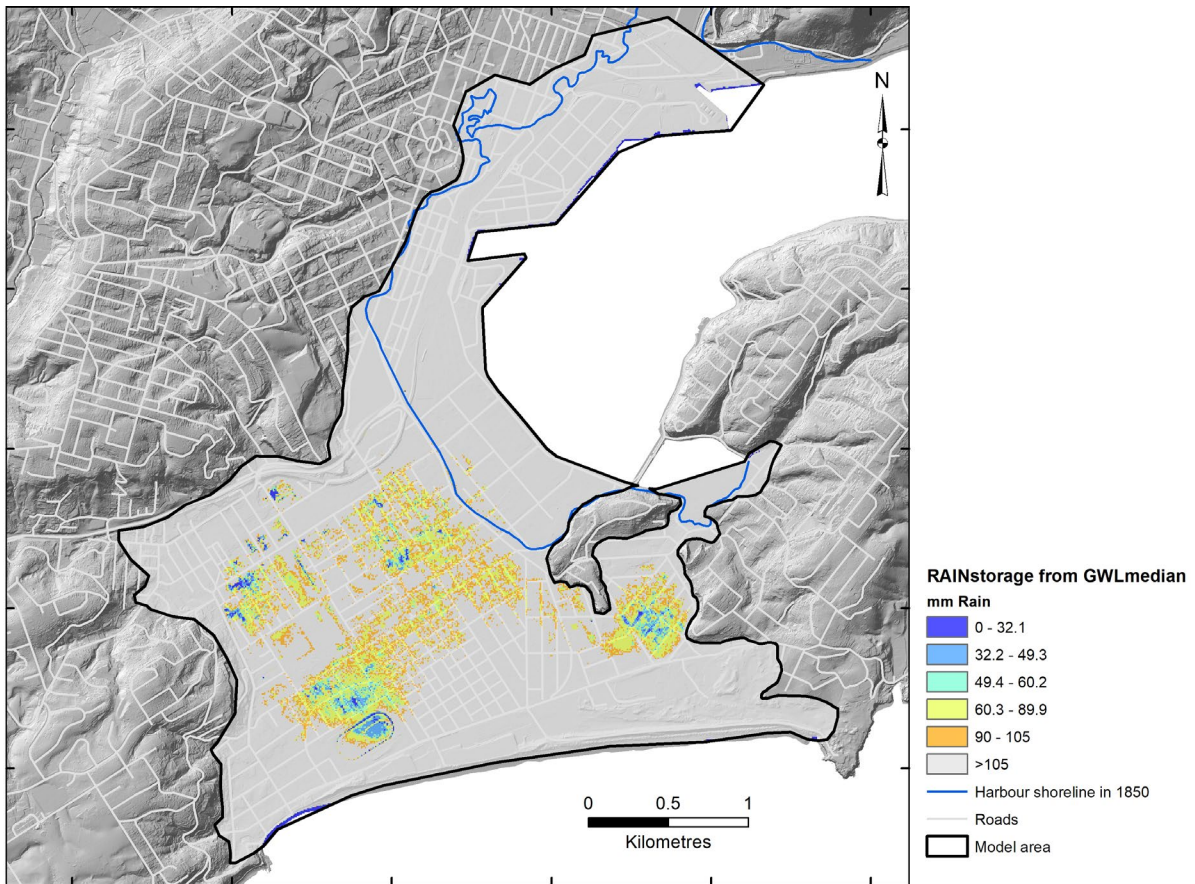


Figure 3.7 Calculated grid of *RAINstorage_fromGWLmedian* at the present day (0 cm sea-level rise), being a measure of void space between the LiDAR ground surface and water table at median elevation, here converted into a millimetres of rainfall equivalent required to lift groundwater to the ground surface based on the RRI. Boundaries between the colour divisions relate to local 12-hour rainfall recurrence intervals.

The grids of *RAINstorage* have also been compared directly with 12-hour rainfall depth-duration-frequency tables using HIRDS v4 data (NIWA 2023b) for Musselburgh (Table 2.3). Places have been distinguished where 12-hour rainfall at a particular recurrence interval (ARI) exceeds the available subsurface *RAINstorage*. A series of 8 m grid files and vector polygons, which contain the text 'RAINstor_12hrEXC', are provided for a range of present-day and future-forecast water table conditions (see Section 4.3 below).

Locations where subsurface storage is exceeded by a 12-hour rainfall of ≥ 60.2 mm, which has a 10-year ARI (0.1 AEP) locally, depend on the elevation of groundwater at the time. There is a significantly greater area of Dunedin where the subsurface storage for this rain would be exceeded at high groundwater levels, such as p95 or MHWS, than at median levels of the water table (Figure 3.8). Alternatively, places where a 12-hour rainfall at various ARIs (from Table 2.3) can exceed available subsurface storage are shown in Figure 3.9.

These maps do not necessarily assume all of the precipitation will infiltrate to groundwater, only that the amounts of infiltration and groundwater rise will be the same as that observed during 2019–2023. They are simply indicators of places where the ground can no longer 'act like a sponge' and absorb any more rainfall, or where groundwater can become emergent in the event of sufficient rain. Since this effectively changes the local area into a place of 100% imperviousness, it affects the runoff coefficient and requirements being called on the stormwater system. As such, it maps where groundwater may begin contributing to pluvial flood hazard. The need for stormwater management is potentially greater where the subsurface storage is lowest.

Table 3.4 Summary of rainfall-recharge datasets developed for Dunedin groundwater, found in the geodatabase *sthDunedin_water_table_model2023.gdb*.

File Name	Summary
<i>RRI_2023</i>	Interpolated grid (8 m cells) of the dimensionless RRI, based on selected site values from event observations of change in groundwater level divided by the rainfall amount (dGWL/TotalRain). Re-calculated in 2023 to replace earlier versions.
<i>RRI_contours</i>	Contours of the dimensionless RRI in intervals of one. Based on <i>RRI_2023</i> grid.
<i>RAINstorage_fromGWLmedian_2023</i>	Calculated grid to provide an estimate of the rainfall limit (in millimetres) and/or available storage before groundwater can be expected to reach the ground surface, based on the median position of groundwater (<i>GWLmedian_2023</i>) and the RRI grid of response site values observed to c.30 mm rainfall events in 2019–2023 and 2012 (using Fordyce [2014] data).

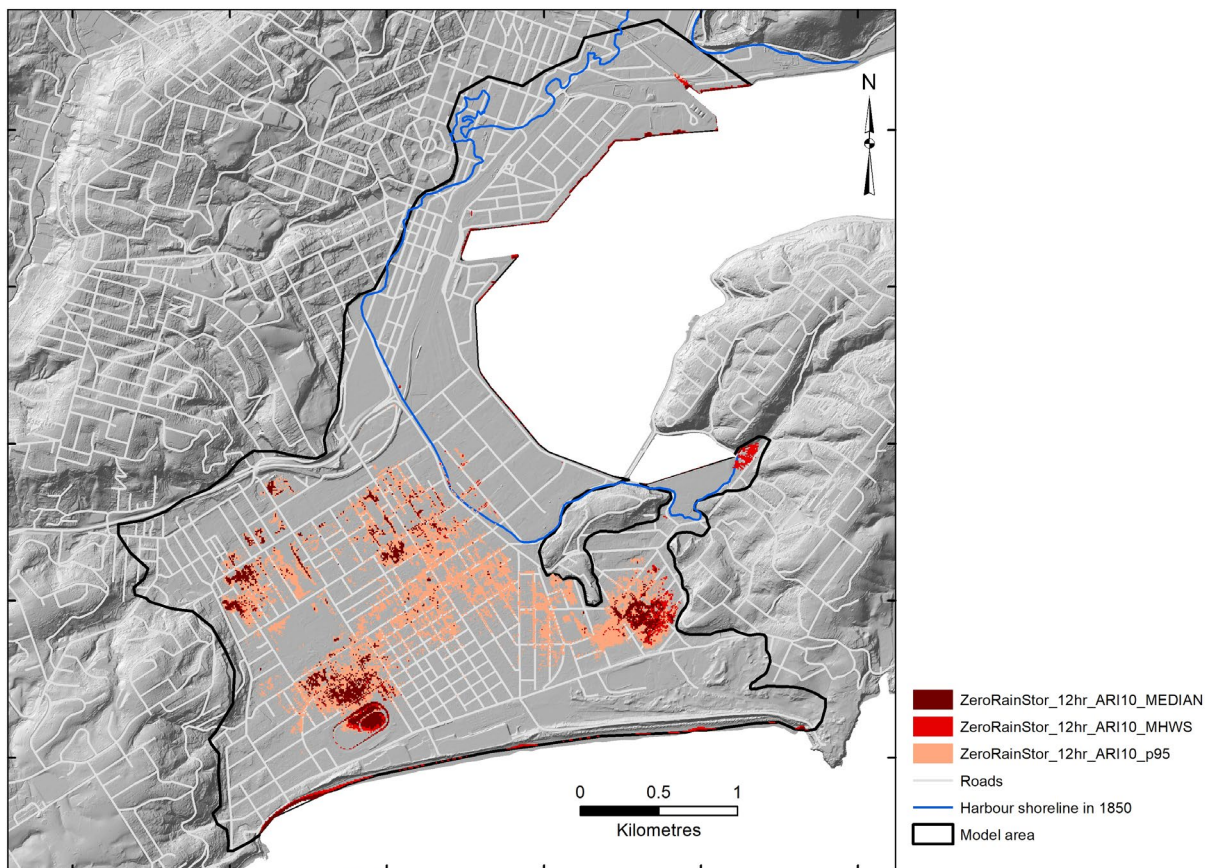


Figure 3.8 Comparison of maps showing places where the subsurface storage above median, Mean High Water Springs (MHWS) and p95 levels of the water table would be exceeded by a 12-hour ARI10 rainfall of 60.2 mm.

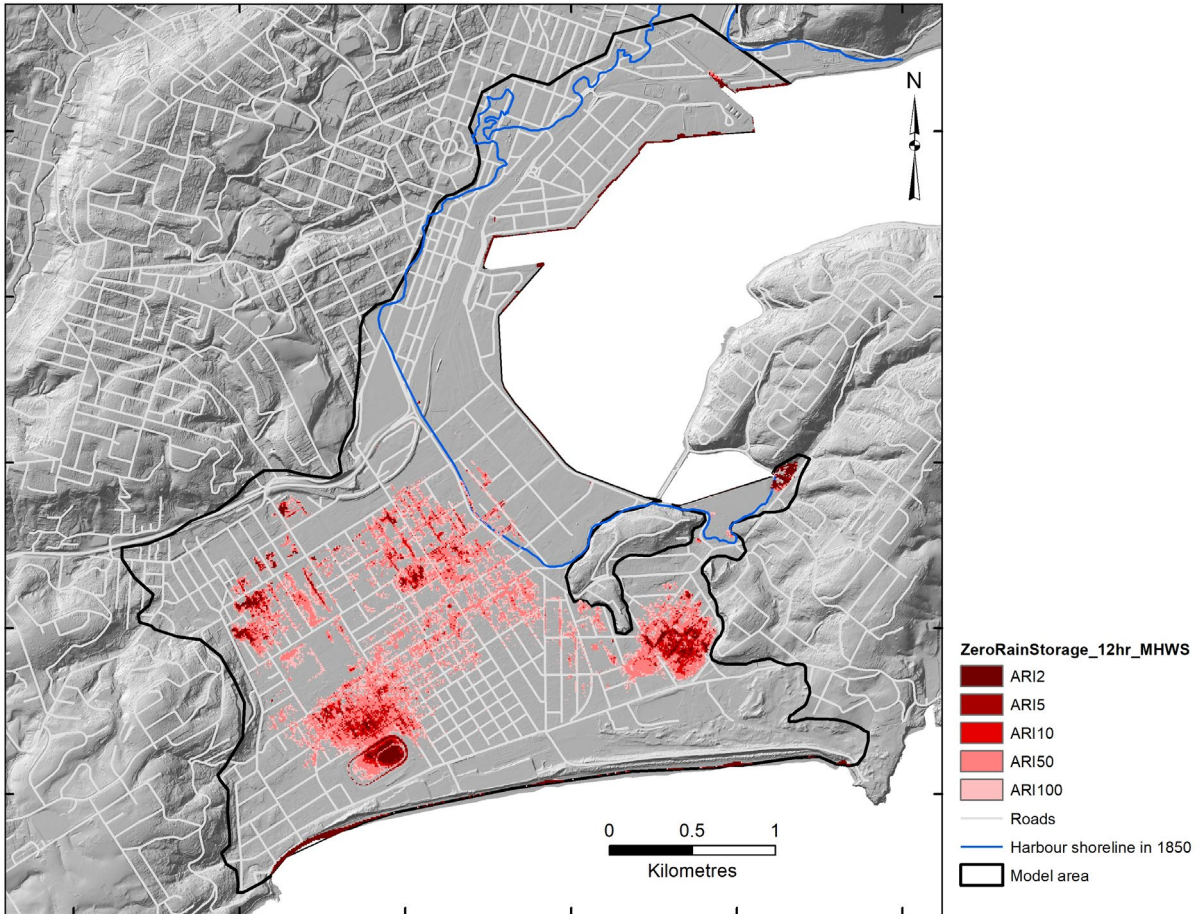


Figure 3.9 Comparison of places where subsurface storage above Mean High Water Springs (MHWS) level of the water table would be exceeded by 12-hour rainfall at a 2-, 5-, 10-, 50- and 100-year average recurrence intervals (corresponding to rainfalls $\geq 35.8, 49.3, 60.2, 89.9, 105$ mm, respectively).

4.0 FORECAST FUTURE STATE OF GROUNDWATER

The future state of groundwater has been forecast in this study relative to fixed 10 cm increments of sea-level rise from 2023, rather than years in the future or to a particular time (see Section 2.7). By focusing on a change in physical state (i.e. the elevation of sea level), it removes one of the major present-day uncertainties (time) relating to societal behaviour. Table 2.4 provides the present indication of possible times at which these increments might occur based on NZ SeaRise data for St Clair (Site 4780) from 2023. MHL has been taken as -0.248 m (NZVD2016) for present day, based on the average from the Dunedin tide gauge (LINZ 2023a).

The digital elevation model is an important present-day reference frame. Importantly, the 2021 LiDAR survey has ± 0.05 m (2 sigma) uncertainty that is within the realm of the sea-level changes being modelled. Calculated groundwater elevations do not account for possible changes in land elevation (subsidence or uplift) but these, for the most part, should be accounted for in the 10 cm sea-level rise increments.

4.1 Groundwater Levels

Basic forecasts of how rising sea level will affect groundwater have been developed based on the present-day groundwater observations and statistical surfaces. At their simplest, it has been assumed that the absolute position of mean (or median) groundwater levels will also rise and that the shape of the water table and tidal response in the future will be, on average, the same as at present – i.e. sitting slightly elevated above MSL in the coastal plain sediments.

The workflow based on Plane et al. (2019) is based on changes to the elevation of the median groundwater surface derived from 2019–2023 observations (e.g. *GWL_median_2023*), with constant offsets of 10 cm (0.1 m) increments added for sea-level rise, to produce a new long-term equilibrated statistical position of the water table (e.g. *SLR010cm_GWLMedian*). We assume a ‘flux-controlled’ system, in which groundwater discharge to the sea persists despite changes in sea level, and that hydraulic gradients are maintained as the water table rises (Werner and Simmons 2009; Gleeson et al. 2011; Michael et al. 2013). There are a number of recent studies taking a flux-controlled approach to modelling saline incursion and shoaling groundwater (e.g. Rotzoll and Fletcher 2013; Hoover et al. 2017; Hummel et al. 2018). We refer to our approach as a ‘geometric model’ to distinguish it from other analytical or fully numerical groundwater models that compute the groundwater flow equation(s).

To incorporate the influence of tides or storm surge, and the decay with distance away from the harbour and coast, a tidal component is then added. This is derived by multiplying the present-day tide or storm-tide anomalies (from Table 2.2) by the local tidal efficiency grid.

The geometric model equation, and nomenclature, follows the form:

$$[SLR0Y0cm_GWLmedian_xxxx] = ([GWLmedian_2023] + 0.Ym) + ((XXXX-MSL) * [TE_%]/100) \quad \text{Equation 4.1}$$

where [] indicates an interpolated statistical surface grid (raster dataset), *0Y0* is an integer to represent a 0.1 m increment of sea-level rise, and *XXXX* is either the MHWs7 or storm-tide anomaly in metres at 1-, 10-, 100- or 1000-year ARI ESL above MSL (Figure 1.1; Table 2.2).

Forecasts using this approach contain a number of implicit assumptions:

1. Future median and mean positions of the water table will equilibrate with the harbour and ocean, as they do with MSL along the coast at present (a 'flux controlled' end-member groundwater system).
2. Tides will continue to influence groundwater levels to the same extent they do now, depending on the permeability of the sediment, and decaying inland with distance from the coast.
3. Processes controlling the present hydraulic gradients will not change sufficiently to alter the water table shape, with slopes continuing to be maintained by rainfall recharge, flow of water from the hill suburbs and with potential to be locally affected by urban infrastructure.
4. In areas away from the coast, the water table will continue to sit at an elevated position above sea level, and any drainage will be no more, or no less, efficient than at present.
5. Future tidal ranges will be similar to those at present, as well as the present-day 0.98 m difference between MHWS and MSL, and tidal amplification in the Dunedin harbour will remain the same in the future.

By taking the observed and mapped position of groundwater into account this empirical-based 'geometric model' approach is quite distinct from elevation-based 'bathtub groundwater models' in which the water table is assumed to be horizontal and everywhere equilibrated with MSL (e.g. Beca 2014). The geometric models attempt to account for subsurface heterogeneity and highlight spatial variations in the water table height and ground elevation, and can also incorporate the influence of tides. Being empirical, there are many variables and controlling processes simplified into a single parameter, but these are based on statistical surfaces from present-day observations, which do not account for groundwater flow and possible changes in water-budget mass balance. This is where they are perhaps most distinct from computationally more difficult numerical groundwater models (Chambers et al. 2023; see also Section 5.1). Assuming a flux-controlled water table is also known to be conservative, with potential for over-estimation of hazard if models do not account for groundwater discharge to topographic lows and drains (Befus et al. 2020).

A series of depth to groundwater (DTW) grids have been generated to represent the shallowing of groundwater as sea levels rise by subtracting groundwater elevation grids from the 2021 LiDAR DEM, using the equation:

$$[DTW0X0cm_GWLMedian_MHWS] = [DEM] - [SLR0X0cm_GWLmhws] \quad \text{Equation 4.2}$$

Seven different grids have been generated for each of the 10 cm increments of sea-level rise, resulting in 77 datasets from 0 to 100 cm of sea-level rise. These forecast groundwater conditions at: median, MHWS, p95, ESL1, ESL10, ESL100 or ESL1000 levels (where the 1–1000 represent storm tides' various ARI recurrence intervals). These grids are supplied in the accompanying ArcGIS10.8 geodatabase named '*sthDunedin_water_table_forecasts.gdb*'.

4.2 Emergent Groundwater

Groundwater is calculated to be emergent at the ground surface where $DTW \leq 0$, so this discriminant was used to convert grid files into a series of 'emergent groundwater' polygons, which are more easily manageable for diagrams and calculations. These polygons represent a range of possibilities, from relatively 'permanent' inundation that might be expected on an average annual or daily basis, through to shorter-term reach of groundwater-related effects during episodic and rare events.

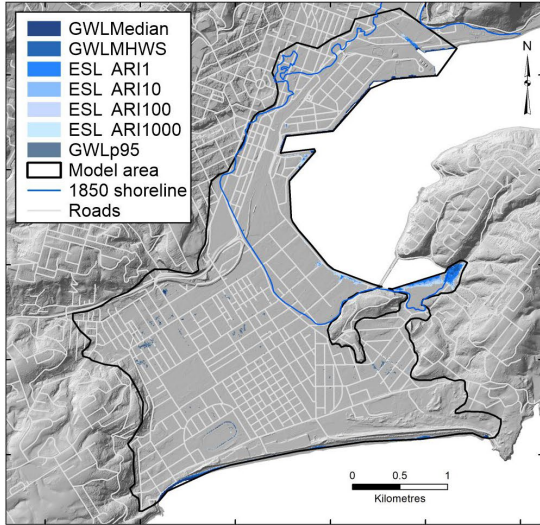
The forecast emergence of groundwater on the Dunedin coastal plain is illustrated in Figure 4.1. The figure was generated using files named with the prefix *poly_DTW0X0cm_GWL** in the *sthDunedin_water_table_forecasts.gdb* geodatabase but showing only six of the 11 sea-level rise increments calculated. It illustrates that, by the time sea-level rise reaches 40 cm, there is quite a large area in South Dunedin where 'high' groundwater, at p95 levels, is calculated to intersect with the topographic surface and become emergent. Stated simply, this is because the present-day 95th percentile groundwater level is in many places already at depths less than 40 cm. By the time sea level reaches 60 cm above its present-day elevation, the geometric models forecast widespread emergence of groundwater in South Dunedin even when groundwater is at median levels, let alone at more elevated p95 or MHWs condition. In Harbourside at 60 cm sea-level rise, only the highest storm-surge-related conditions (ARI100, 1000) appear sufficient to result in emergent groundwater. By the time sea-level rise is 80 cm, the geometric models forecast that emergent groundwater will be ubiquitous in South Dunedin and also starting to reach the ground surface in Harbourside during high-tide and extreme storm-tide events. But at 80 cm sea-level rise, flooding issues may well have developed already from harbour storm surge and coastal inundation flowing directly across the land (see Section 5.3 below).

When considering the forecast emergence of groundwater from these geometric models, it is important to highlight their simplification. Further work may be needed before using maps and datasets as a direct proxy for hazard. For example:

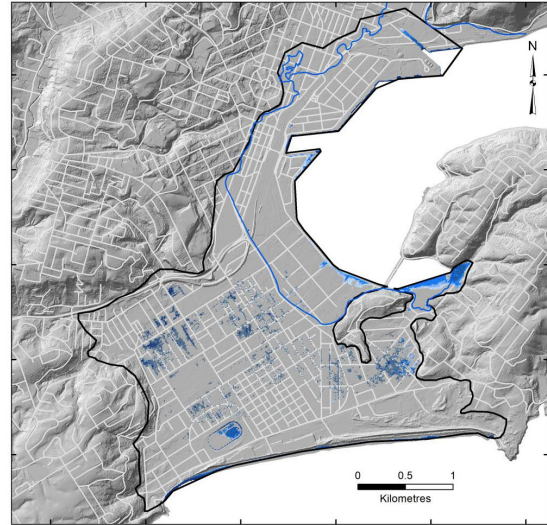
1. Once groundwater becomes emergent at one site, a spring may form. This may be sufficient to lower potentiometric head nearby ('relieve pressure') and change the shape of the water table locally. These models are unable to account for changes in water table geometry once groundwater becomes emergent nor for any accumulation and depth of water on the land surface.
2. The geometric models assume that any present-day drainage will continue to perform in much the same way in future. Drains will be neither overwhelmed, such that the groundwater table radically changes its elevation and rises, nor will they become more efficient, for example, with greater ingress into drains as the water table rises. The future performance of the stormwater system, and its role in controlling groundwater, is a significant unknown in these future forecasts. The geometric models also cannot account for changes in climate and/or precipitation.
3. Groundwater emerging at the surface may not necessarily represent the greatest hazard/issue locally. There may have been detrimental effects to infrastructure performance, bearing capacity for buildings or public health at much deeper levels of groundwater (e.g. at 1–0.5 m depths). Once it reaches the ground surface, emergent water may initially be a relatively minor nuisance, requiring more substantial flows and ponding to flood levels before they are damaging. There are also many solutions (bigger drains, pumps, etc.) for mitigating relatively small amounts of emergent groundwater.

Emergent Groundwater: Permanent & Episodic

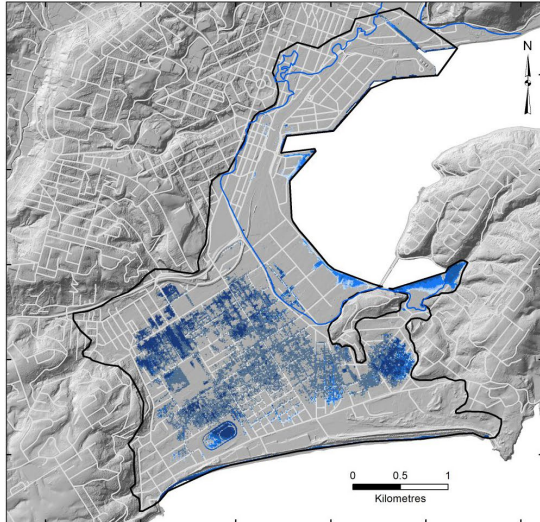
SLR 0 cm



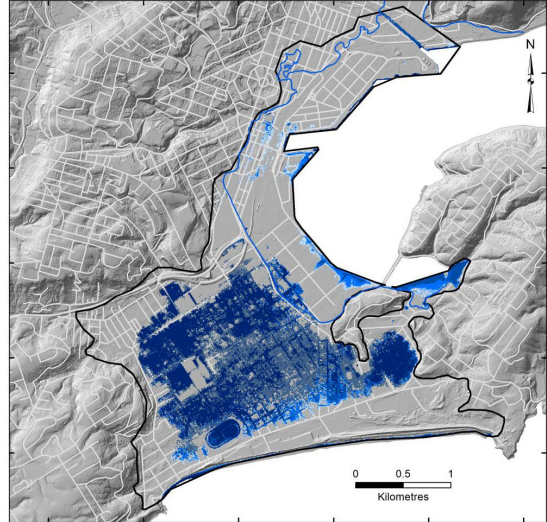
SLR 20 cm



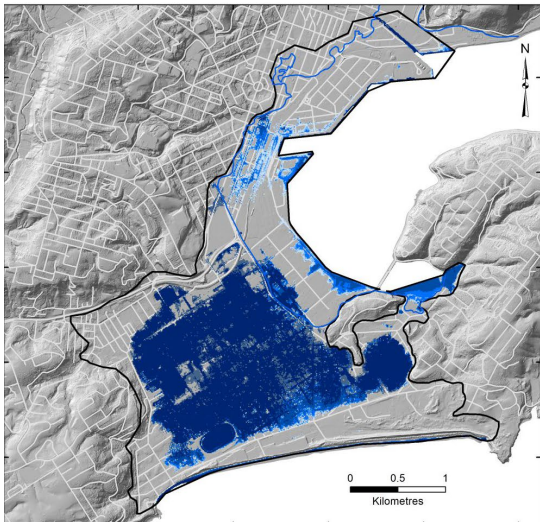
SLR 40 cm



SLR 60 cm



SLR 80 cm



SLR 100 cm

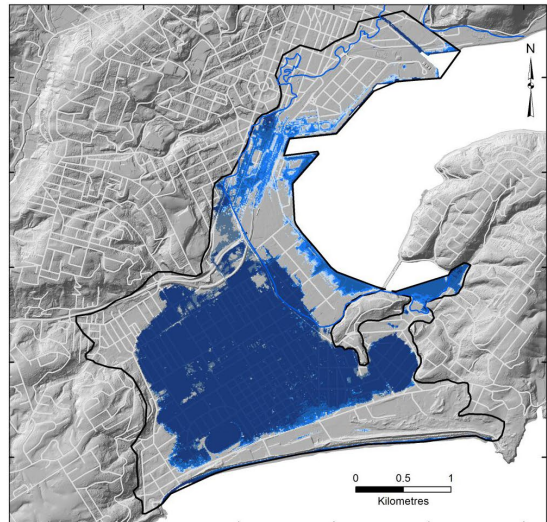


Figure 4.1 Forecasts of places where groundwater is expected to become emergent (DTW ≤ 0) with sea-level rise. Each panel has seven shades of blue representing emergence when groundwater is at median, MHWS, p95 and ESL at 1-, 10-, 100-, 1000-year ARI levels (see also Appendix 3).

Emergent groundwater: permanent & episodic

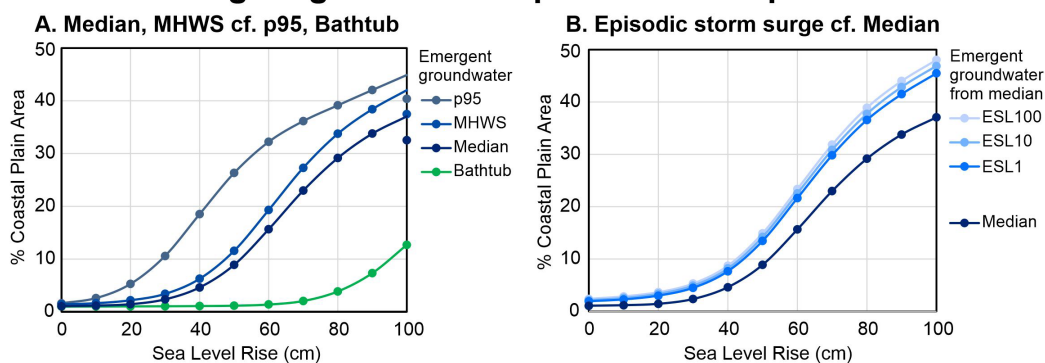


Figure 4.2 Forecasts of the percentage of the 9.2 km² area of the Dunedin coastal plain where groundwater will become emergent as sea levels rise. (A) Comparison of the percentage area of emergence under median, MHWS and 95th percentile levels. A ‘bathtub model’ (green line) where groundwater level is assumed to equal mean sea level (GWL = MSL) is shown for reference. (B) The areas affected by episodic storm surge and ESL forcing and raising of groundwater at 1-, 10- and 100-year ARI levels, compared with a median level reference.

The emergent groundwater datasets may not be suited for ‘hazard mapping’ per se. Instead, it may be more appropriate for them to be used to indicate relative contributions of groundwater to a complex hazard, rather than a hazard itself, then forecast the evolution of that contribution over time. For example, within the 9.2 km² model area across the South Dunedin – Harbourside coastal plain (see black polygon in Figure 4.1), the relative spatial importance of groundwater at high percentiles (p95) is compared with median conditions by calculating the proportion of land where emergent groundwater is expected (Figure 4.2A). Difference between the 95th percentile and median levels has a spatial contribution to hazard that is equivalent to about 20–30 cm worth of sea-level rise. The difference between the median and MHWS, or median and ESL forcing during storms (Figure 4.2B), is not nearly as significant during the first 50 cm of sea-level rise. Additional contribution of tides or storms to hazard exposure, above the median groundwater-related exposure, is limited spatially by the tidal efficiency of the ground and exponential decay of the sea’s influence on groundwater inland from the coast. Additional tide or storm contribution only becomes important once sea-level rise reaches 60–70 cm, by which time other processes such as coastal inundation may well be dominant (see Section 5.3 below).

4.3 Loss of Subsurface Storage Capacity

A series of geometric models have been calculated to show places where 12-hour rainfall, at various recurrence intervals, will exceed the available capacity to store infiltration from that rain in the subsurface, depending on whether the groundwater is sitting at the median, MHWS or 95th percentile (p95) level prior to the rainstorm. The 12-hour period was chosen, rather than 24 hours, because flood events are quite commonly developing and surface waters starting to accumulate within the first 12 hours of intense rain (e.g. Figure 2.4). Calculations have been based on present-day observations of rainfall recharge, using monitored changes in groundwater level during rainfall events (Figure 3.6). To do this, it is assumed that the present ratio of infiltration/runoff and porosity of the ground will not change in future, so that the ability for the ground to absorb water will decrease as depth to groundwater (DTW) gets shallower because of sea-level rise. Grids of DTW at different sea-level rise increments were divided by the present-day RRI grid (combining Equation 4.2 with Equation 3.4). In the geodatabase *sthDunedin_water_table_forecasts.gdb* that accompanies this report, these grids are labelled with the prefix *RAINstor_mm_SLR0X0cm_****, where *X* is an integer for sea-level rise in centimetres and ***** represents either MED (median), MHWS (mean high water springs) or p95 (95th percentile) conditions of groundwater.

Clearly the underlying assumption of constant rainfall recharge will be incorrect or oversimplified if, for example, urban development results in a significant change to asphalt, roofs or other impervious surfaces, or if the stormwater network loses efficiency due to the rising sea. However, the intention is to provide a proxy for situations where and when groundwater levels might contribute locally to pluvial flooding, assuming that all other factors remain the same. Note that these calculations **do not** provide a measure of pluvial flood hazard per se, which also depends on local topography and other factors such as runoff and ability to pond, as well as the extent of impervious surfaces. But, as the groundwater is likely to rise with sea levels in future, whereas local topography is not, the aim is to provide some general insight of how pluvial flood hazard may evolve both spatially and temporally under the influence of rising groundwater.

A rainfall of 60.2 mm in 12 hours is expected to have an AEP of 0.1 at Musselburgh in South Dunedin, or an ARI of 10 years (NIWA 2023b). For each 10 cm increment of sea-level rise, the rain storage grids *RAINstor_mm_SLROX0cm_**** have been discriminated to show where they are ≤ 60.2 mm rainfall, or other equivalent depth discriminant, for events at 1-, 100- or 1000-year ARI (Table 2.3). Grid files were then converted into a series of polygons, each labelled *poly_RAINstor_12hrEXC_SLROX0_ARI#* in the geodatabase *sthDunedin_water_table_forecasts.gdb* where **X** is an integer for sea-level rise and **#** is an integer for the recurrence interval in years. The polygons are more manageable for calculations and GIS processing.

The forecast change in subsurface storage capacity across the Dunedin coastal plain is illustrated in Figure 4.3 but shows only six of the 11 sea-level rise increments calculated. Here, the polygons have been used to depict places where available storage is exceeded by rainfall infiltration when groundwater is at MHWS level. Using a reference level of MHWS may be more relevant cf. median or p95 conditions, as a high tide should be experienced at least once by groundwater within a 12-hour rainstorm. Figure 4.3 highlights that, at present (sea-level rise = 0 cm), there is only a relatively small area of land with insufficient storage for a 12-hour rainstorm at ARI of 1, 10 or 100 at MHWS (see also Figure 3.8). Subsurface porosity presumably alleviates at least some flood hazard, even if the rise in groundwater is delayed during rainfall. However, the situation on the coastal plain changes dramatically with sea-level rise, such that, by 40 cm sea-level rise, there appears to be limited capacity for land in South Dunedin to absorb even 12-hour rainfall at annual recurrence (< 30.8 mm). In comparison to South Dunedin, the Harbourside area appears to be much less problematic. By 60 cm sea-level rise, there appears to be no capacity for the ground to store any infiltration in South Dunedin, presumably requiring total reliance on the stormwater network or other engineered storage solutions to limit pluvial flooding. In stark contrast to South Dunedin, subsurface storage in Harbourside does not appear to be exceeded at all until at least 80 cm sea-level rise – by which time groundwater may have already become emergent during episodic storm surge (Figure 4.1), or there may be inundation directly from the harbour (see Section 5.3).

The influence that different groundwater conditions have in controlling the available subsurface storage, compared with various ARIs of 12-hour rainfall totals, is shown in Figure 4.4. These data show similarities to the emergence of groundwater, in that natural variability of groundwater levels between, for example, median and p95 is clearly very important to both subsurface storage and emergent groundwater across the coastal plain (Figure 4.4A). At high groundwater (e.g. 95th percentile), there can be as much as 15% more area of the coastal plain that would no longer have storage available for a 12-hour ARI10 rainfall of 60.2 mm than at median groundwater.

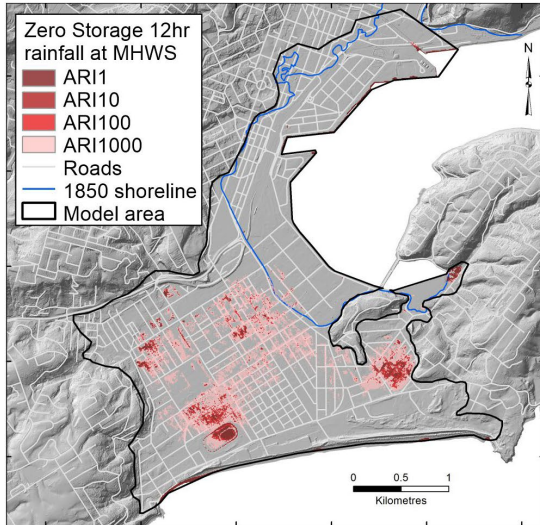
When rainfalls at different ARIs are compared (Figure 4.4B), these calculations highlight the need for careful stormwater and flood modelling. These data suggest that, while 15% of the coastal plain has insufficient storage capacity for a 12-hour ARI100 rainfall of 105 mm at present day, by the time 40 cm of sea-level rise has occurred an equivalent area of land would have its storage potential exceeded by a much smaller 12-hour ARI2 rainfall of 35.8 mm. This may be the equivalent of increasing impervious surfaces across the city and increasing catchment runoff.

The present stormwater system is suggested to remove between 60 and 80% of rainfall on South Dunedin and near environs, carrying it northeast by gravity and discharging it to the Harbour through a pumping station (Goldsmith and Hornblow 2016; Mohssen 2017). The flux of surface water to groundwater, and the changing level of groundwater, involves smaller volumes than surface runoff and so is unlikely to play a dominant role in pluvial flooding. Instead, groundwater is probably a secondary contributor to the present flood hazard that may increase if the stormwater system efficiency goes down (for example, due to sea-level rise). Careful modelling will be required to fully understand the implications for flood hazard and the serviceability of stormwater upgrades versus lifespan of infrastructure investment.

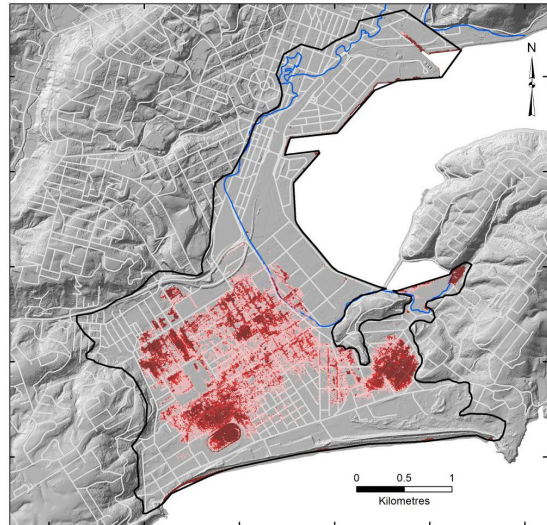
Variation between median and p95 condition (based on 2019–2023 observations) results in a large difference in land ‘exposed’ to a loss of storage capacity, equivalent to the difference in area caused by 20–30 cm of sea-level rise. This also highlights the importance that antecedent groundwater conditions might play. It has been shown that levels of Dunedin groundwater can be reasonably modelled by taking the average total rainfall during the past 30 days (Cox et al. 2020). If the recurrence interval between rainstorms is short and the frequency of heavy precipitation events is low, there can be insufficient time for groundwater to recede. It is rational to suggest that having multiple moderate-sized events at intermediate AEPs could lead to a loss of storage capacity that would contribute to a pluvial flood hazard that is greater than a single very large rain event. Inter-relationships of multiple events have yet to be quantified and remain a worthwhile avenue for future work.

No subsurface storage for 12hr rain at MHWS

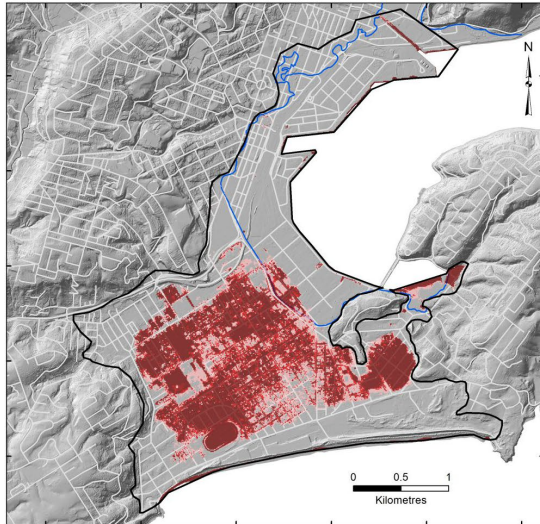
SLR 0 cm



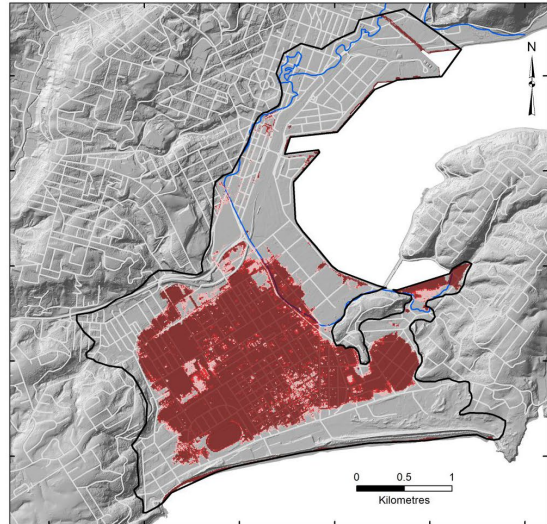
SLR 20 cm



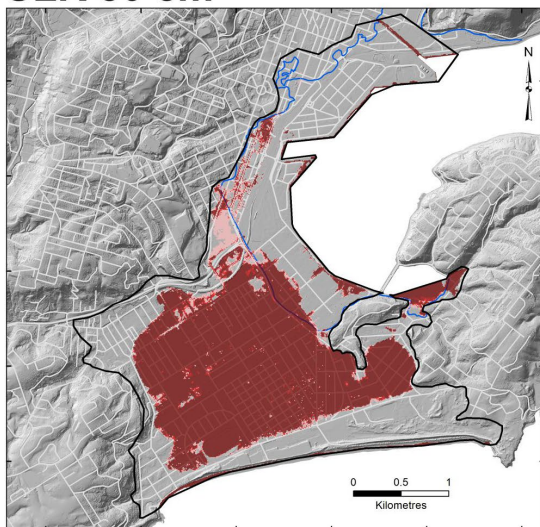
SLR 40 cm



SLR 60 cm



SLR 80 cm



SLR 100 cm

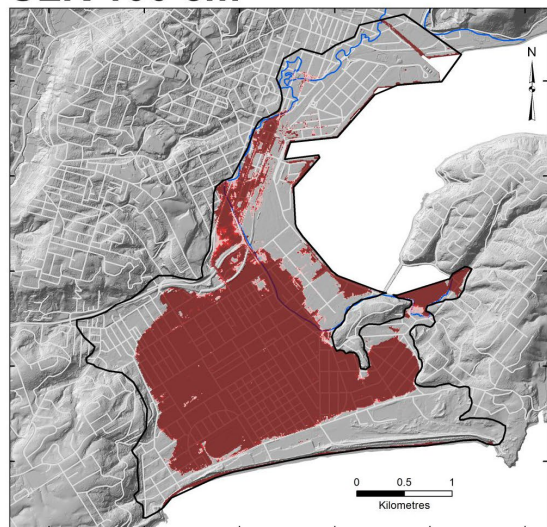


Figure 4.3 Forecasts at various levels of sea-level rise, showing places where 12-hour rainfall at ARI 1, 10, 100 and 1000 intervals (shades of brown-red-pink), will exceed the available subsurface storage for infiltration from that rain (see also Appendix 3).

Subsurface storage exceeded by 12 hr rainfall

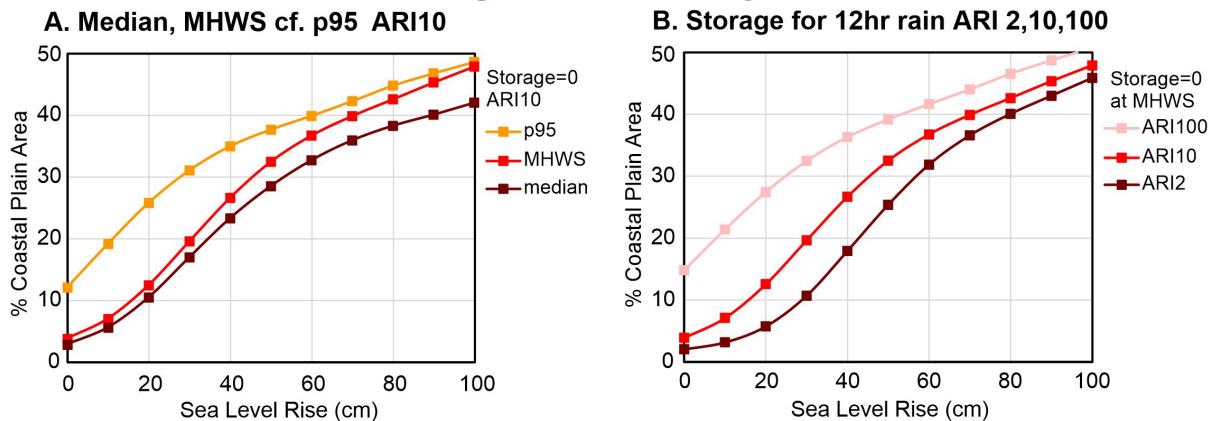


Figure 4.4 Forecasts of the percentage of the 9.2 km² area Dunedin coastal plain where groundwater may begin to contribute to pluvial flooding as sea levels rise. (A) Comparison of the percentage area where storage would be exceeded by a ARI10 (60.2 mm) 12-hour rain when groundwater is at median, MHWS and 95th percentile levels. (B) Proportions of the coastal plain where 12-hour rain at 2-, 10- and 100-year ARI (at 35.8, 60.2 and 105 mm respectively) are calculated to exceed the available subsurface storage when groundwater is at MHWS level.

The values presented here represent 12-hour rainfall using the historical observations of rainfall for ARI and AEP. Given that there is uncertainty around whether future rainfall recharge will be affected by changing drain performance or urban development, and that simple application of the Clausius-Clapeyron relation to historical data (e.g. for HIRDS, Carey-Smith 2018) might under-estimate future events, it was deemed untenable to apply a different future depth-duration-frequency relationship to the calculations of available subsurface storage capacity. Instead, it is perhaps better to simply consider the subsurface storage loss (e.g. Figure 4.4) as a minimum contribution of groundwater state to evolving flood hazard.

5.0 OTHER RELEVANT DATA AND STUDIES

5.1 Numerical Groundwater Model

The first numerical model of groundwater in South Dunedin was constructed by Rekker (2012) using MODFLOW, attempting to compute the long-term equilibrium (steady-state) flow of groundwater in the shallow aquifer and the influence of Dunedin City Council's current network of stormwater pipes. The model is a single layer finite-difference grid of 40 x 40 m cells in 90 rows and 80 columns. A series of maps were produced from the calibrated model showing the influence of rising sea level and extent of ponding above ground. These were later reproduced to highlight possible environmental changes and the importance of rising groundwater (Goldsmith and Hornblow 2016). A key aspect of the model and interpretation was a reliance on observations from only three long-term monitoring bores, the southern-most closest to the ocean (I44/0007 Kennedy Street) being strongly tidal (Figure 2.2). Hydraulic conductivity of the aquifer was estimated from variation in tidal response with distance from the sea (Rekker 2012). The tidal response and high degree of hydraulic communication with the Pacific Ocean observed at Kennedy Street has since been shown to be relatively anomalous (Cox et al. 2020).

More recently the same steady-state model set-up was re-developed, and a different modelling approach was adopted that incorporates observations from the new (much larger) groundwater monitoring network, stormwater pumping outflows and a wider range of possible aquifer properties and their spatial variability (Chambers et al. 2023). Specifically, in this approach, the predictions of interest were a description of (i) the transient progression of annual groundwater levels as sea levels rise and (ii) the sea-level-rise-driven increase in total groundwater flux to the surface/wastewater drainage networks.

A highly parameterised (>1000 parameters) Bayesian framework (or workflow) was applied by Chambers et al. (2023) to estimate the spatial and temporal probability of groundwater levels (head) in relation to specified model top elevations, informed by LiDAR data. The workflow employs a Monte Carlo-type ensemble evaluation (Chen and Oliver 2013; White 2018), where predictions are made using hundreds of history-matched models across thousands of parameters (that is, a parameter ensemble).

The term 'history matching' is used deliberately here to convey the notion that the model can explain the historical behaviour of the simulated system using many different parameter fields, and that no single model parameter field in the ensemble (of model parameter field realisations) is unique in this regard. Hence, uncertainty estimates accompany these predictions, enabling the spatial mapping of the average annual probability of groundwater emergence at the land surface in response to long-term sea rise (groundwater inundation), supporting decision-making in South Dunedin.

The 'model-top' land surface elevation for each 40 x 40 m cell was estimated from a mean aggregation of the metre-scale 2021 LiDAR survey. At present, the modelling approach is unable to account for small-scale topographic features and carries an inherent uncertainty associated with scaling that has yet to be assessed. Simulations were generated for a steady-state history-matching period, with stresses represented by long-term average conditions for the period 2010–2020 and a transient 'projection' period to simulate system response to future sea-level rise on an annual average basis.

Median groundwater levels have been extracted from both the steady-state 'present-day' solution and future conditions under sea-level rise (Figure 5.1). For comparison, the equivalent interpolated surface and empirical geometric models calculated in this study (see Section 3.2) are shown in Figure 5.2 using the same colour range. Differences in forecast groundwater elevations from the empirically based geometric model and numerical model (Chambers et al. 2023, here converted to an 8 m equivalent grid) are further illustrated in Figure 5.3. The numerical model does not discriminate the perched aquifer in the coastal sand dunes and has down-weighted the history-matching contribution of data from CE17/0122 (Turakina Road) near the Harbour (see Chambers et al. 2023). At present day (i.e. steady-state, history-matched), sea-level rise = 0 cm condition the differences are relatively subtle, but they increase progressively with sea-level rise. This is presumably either a consequence of assuming the water table geometry is constant and consistently equilibrated with rising sea level in the geometric model and/or assumptions about the efficiency of the drainage function in the numerical model.

In the numerical model, the projected sea-level-rise-driven probability of groundwater reaching the model top, and spatial extent of inundation, is mitigated by the interaction between rising groundwater and the waste/stormwater drainage networks. An abstract numerical representation tries to account for what is likely a very complex interaction. It generates a condition towards the end-member 'head-controlled' system (using terminology of Gleeson et al. [2011] or Werner and Simmons [2009]). Subsurface infiltration into the wastewater and stormwater network appears to already be suppressing groundwater elevations locally (Cox et al. 2020), so may be embedded already as an integral part of empirical observations and monitoring data. The numerical model predicts that the total flux of groundwater discharging to drainage networks will increase substantially as groundwater levels increase. In the SSP5-8.5 medium confidence example given by Chambers et al. (2023), drain flux in 2100 is calculated to have increased by 32%. But Chambers et al. (2023) acknowledge that there is significant uncertainty in predictions that rely on drainage being able to offset the effects of sea-level rise, and the tenuous (linear) assumption may significantly over-estimate the hydraulic response of the waste/stormwater networks in the future.

There has been relatively little specific examination of the relationship between groundwater levels and actual infiltration, for either stormwater or wastewater networks in Dunedin. Peaks in wastewater flow were shown to coincide more closely with the water-table elevation than rainfall during short periods of monitoring by Fordyce (2014). Losses to the stormwater network are a significant component in the groundwater flow model, and there is a baseflow volume in the stormwater network in the absence of rainfall, which discharges around 430 m³/day at the Portobello pumping station outlet (Rekker 2012) that appears to be sourced, at least in part, from groundwater. Additional monitoring and spatial collection of data from the drainage network will be needed before uncertainty in the predictions of groundwater fluxes to the waste/stormwater networks can be reduced further in the modelling approach (Chambers et al. 2023).

The importance of the influence of drainage in relation to hazard forecasts is perhaps highlighted by Figure 5.4, where areas in the numerical model predicted to be below MSL are shown with different shades of blue for progressive increments of sea-level rise. There are substantial areas where the numerical model predicts groundwater to be below MSL, which would require overly efficient drains, pumping drawdown or perhaps discharge offshore. Such areas are not matched by present-day observations in the monitoring network where

groundwater is nearly everywhere at sea level or some elevation above sea level.² A better understanding of future stormwater system performance is needed before it can be argued that the numerical model results are physically realistic in terms of groundwater elevation.

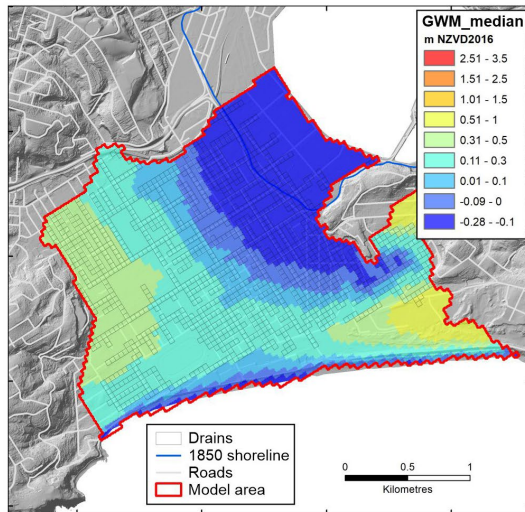
The mean difference (± 1 standard deviation) between the geometric and numerical models increases linearly with sea-level rise (Figure 5.5), such that, by 100 cm of sea-level rise, the numerical groundwater model is, on average, approximately 0.6 m lower than the geometric model. As a result, there is a major difference between the emergent groundwater and hazard predicted by geometric models (pessimistic/over-predicted) compared with numerical models (likely optimistic/under-predicted).

The numerical model provides a probability that groundwater will reach model top and be emergent within each 40 x 40 m cell on an annual time step. There are few cells in the numerical models where there is 100% chance of groundwater emergence. For this study, the total area of cells in the 5.8 km² numerical modelling area of South Dunedin where there is either 10% and 50% probability of emergence were extracted, to compare the evolution of this probability with the emergent cells predicted from median and 95th percentile levels in the geometric models (Figure 5.6). The numerical model at 50% probability of emergence is close to a bathtub model in which groundwater levels are set to equilibrate with MSL.

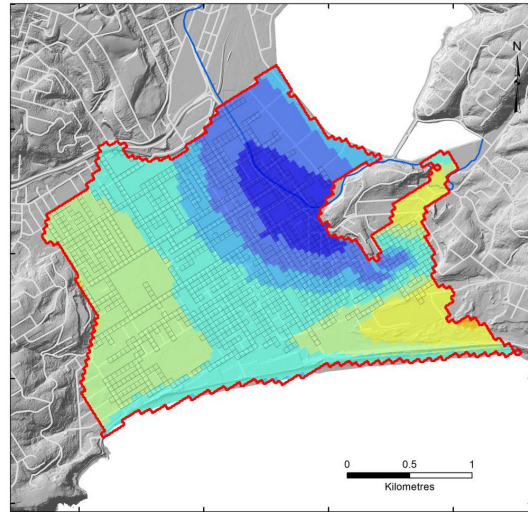
2 Mean sea level is -0.25 m in NZVD2016. The lowest mean groundwater levels for 2019–2023 were at CE17/0212 Culling Park (new) (-0.248 m), I44/1114 Timaru St (-0.237 m) and I44/1022 Anderson's Bay Rd (-0.236 m). The now decommissioned I44/1094 Culling Park (old) piezometer had a GWL mean of -0.394 m, which was spurious (see Figure 2.2).

Numerical Model: Median Groundwater Elevation

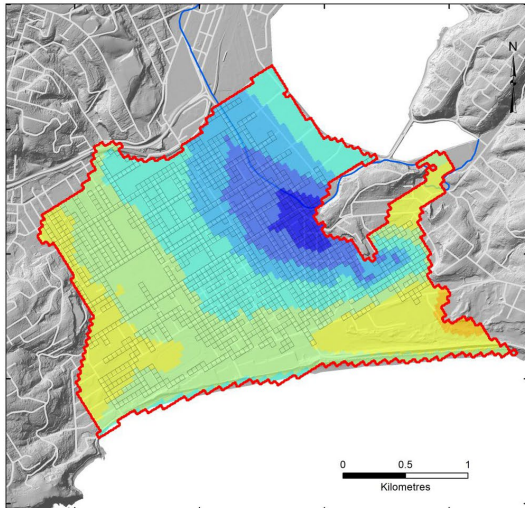
SLR 0 cm



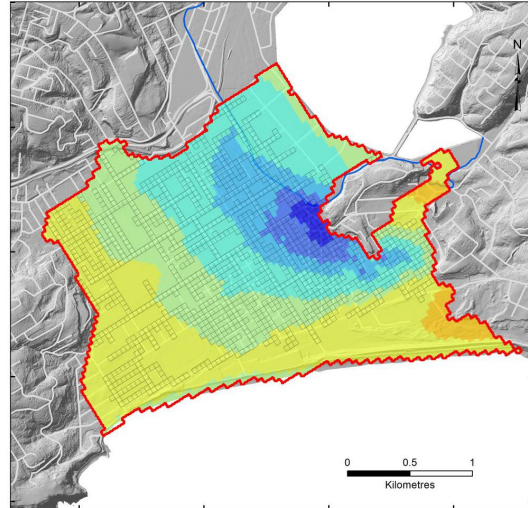
SLR 20 cm



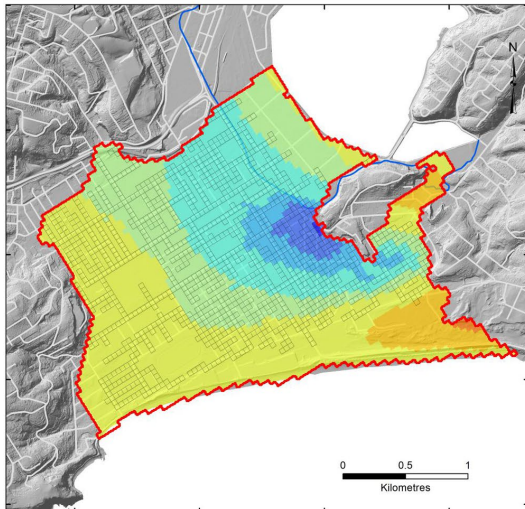
SLR 40 cm



SLR 60 cm



SLR 80 cm



SLR 100 cm

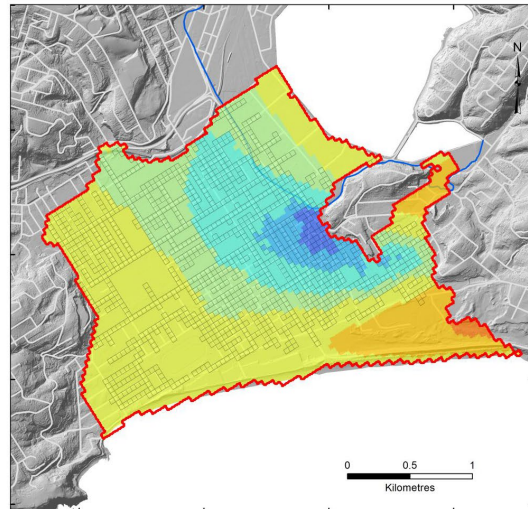
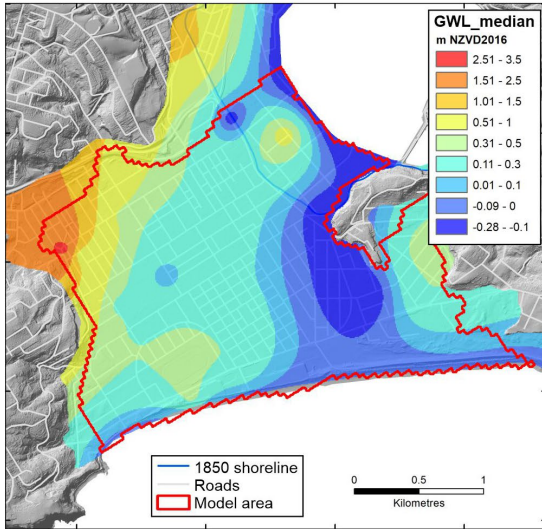


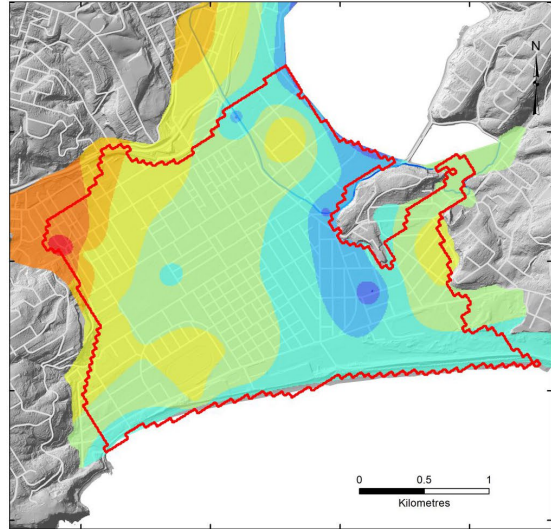
Figure 5.1 Median groundwater levels of the present-day median level of groundwater (top left), representing a long-term calibrated 'steady state' in the numerical groundwater model, and a series of future forecast median levels at various increments of sea-level rise. Coloured elevations are in metres (NZVD2016). The red polygon indicates the 5.8 km² area of the numerical groundwater models. Cells where a drainage function is applied have a grey outline.

Geometric Model: Median Groundwater Elevation

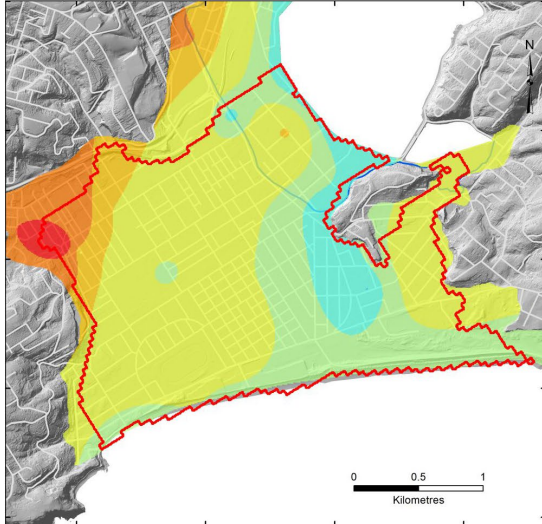
SLR 0 cm



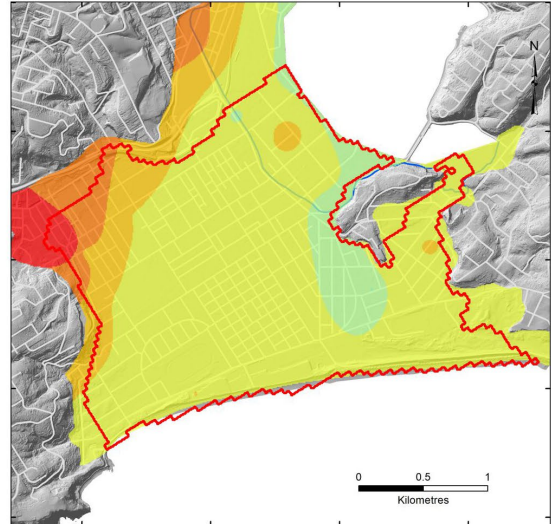
SLR 20 cm



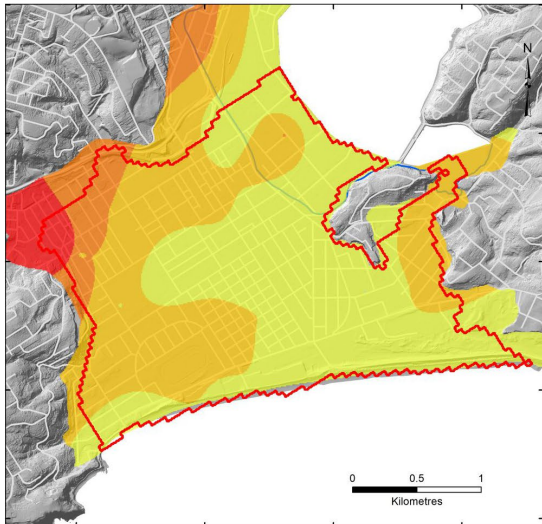
SLR 40 cm



SLR 60 cm



SLR 80 cm



SLR 100 cm

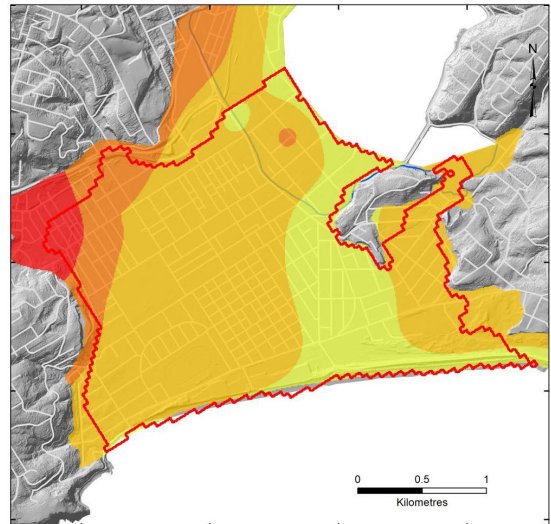
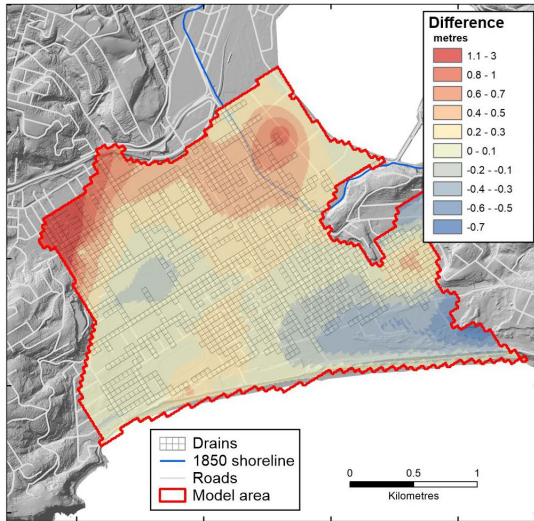


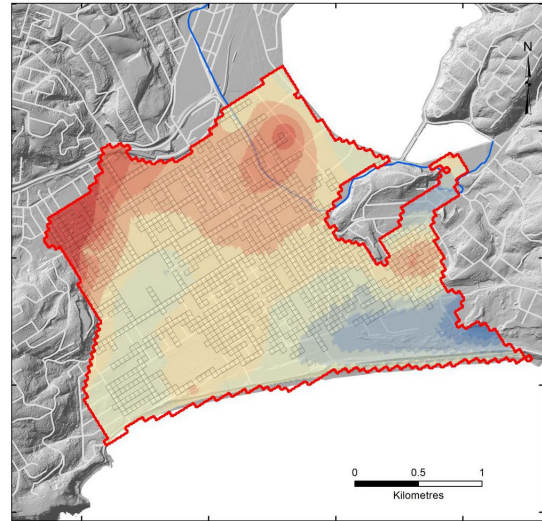
Figure 5.2 Interpolated *GWL_median* 2023 (top left) and future forecasts at various increments of sea-level rise for comparison with the equivalent colour range and levels from the numerical groundwater model. Present day (2023) sea level is approximately -0.25 m in NZVD2016.

Geometric-Numerical Model Difference GWL Median

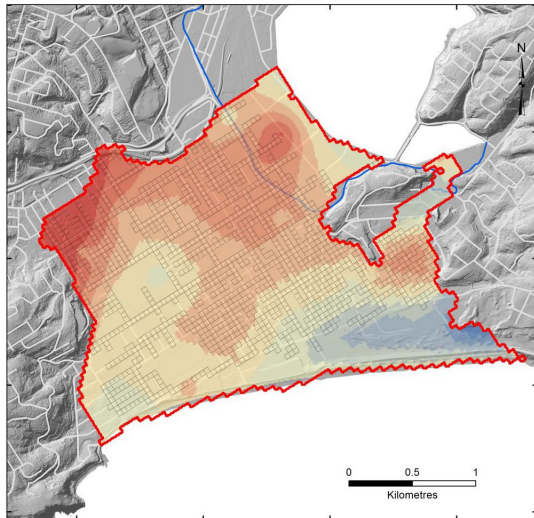
SLR 0 cm



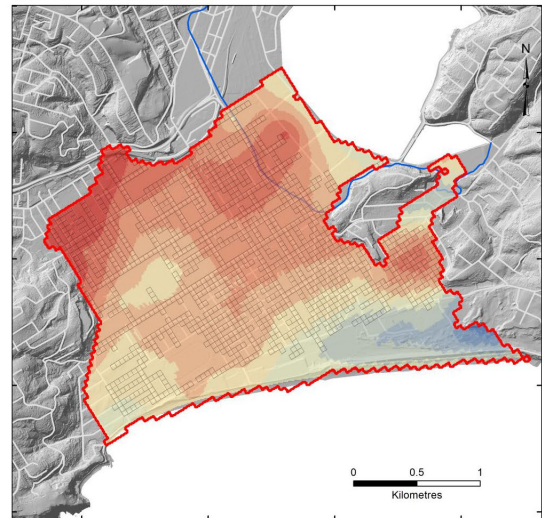
SLR 20 cm



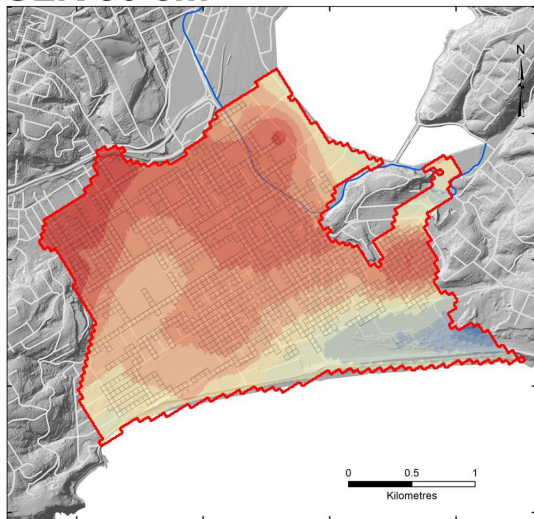
SLR 40 cm



SLR 60 cm



SLR 80 cm



SLR 100 cm

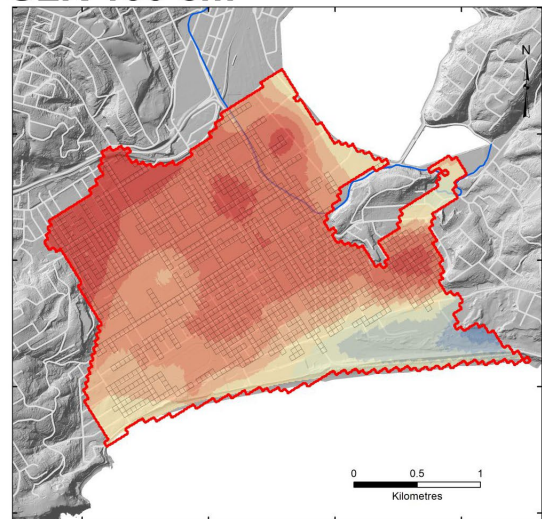
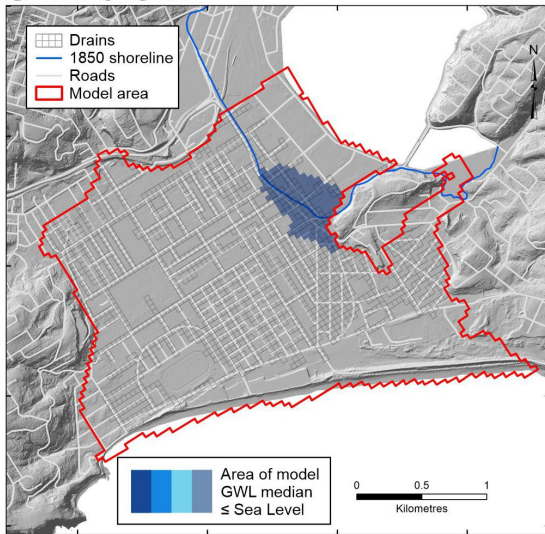


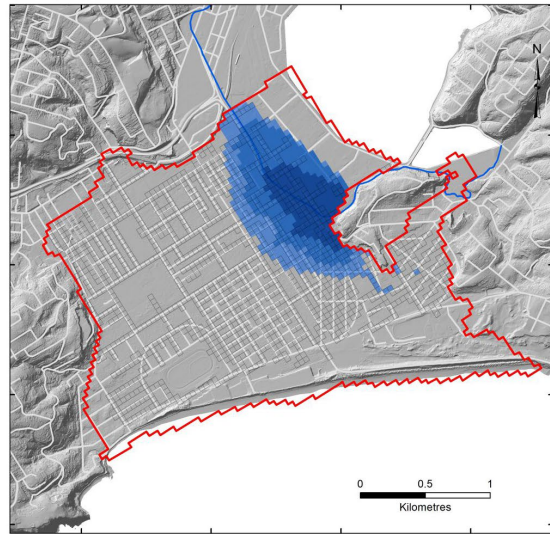
Figure 5.3 Calculated grids of the difference in elevation between the median levels from the empirical-based geometric groundwater model of this study, minus the median groundwater level (general 'annual' solution) from numerical groundwater model of Chambers et al. (2023). Red shades represent a positive difference, whereas blue shades a negative difference.

GWL Median below Sea Level(s)

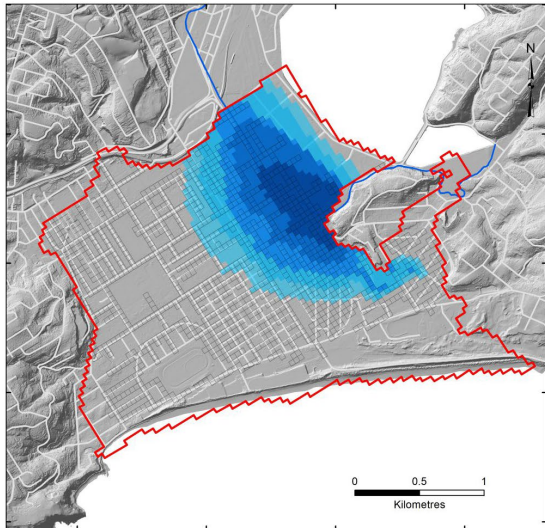
SLR 0 cm



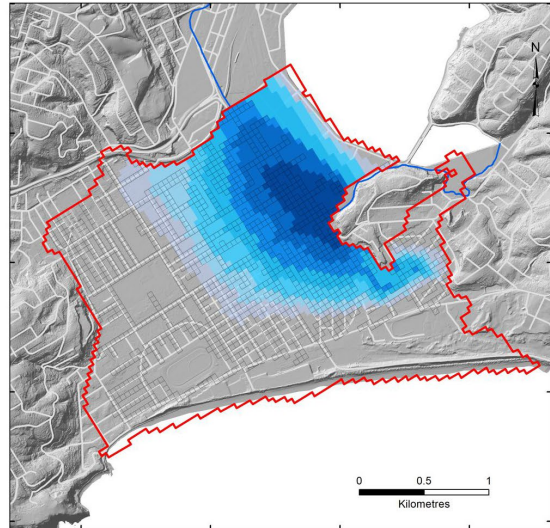
SLR 20 cm



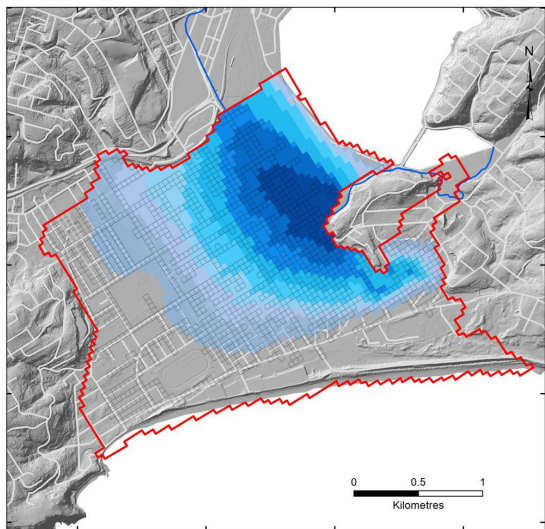
SLR 40 cm



SLR 60 cm



SLR 80 cm



SLR 100 cm

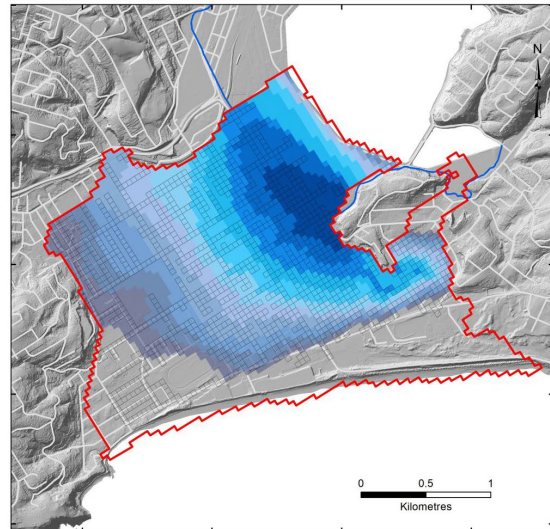


Figure 5.4 Classification of grid models of groundwater elevation (see Figure 5.1) defining areas where the water table at median condition is calculated to lie below mean sea level. Each blue shade represents the area below each 10 cm sea-level rise increment.

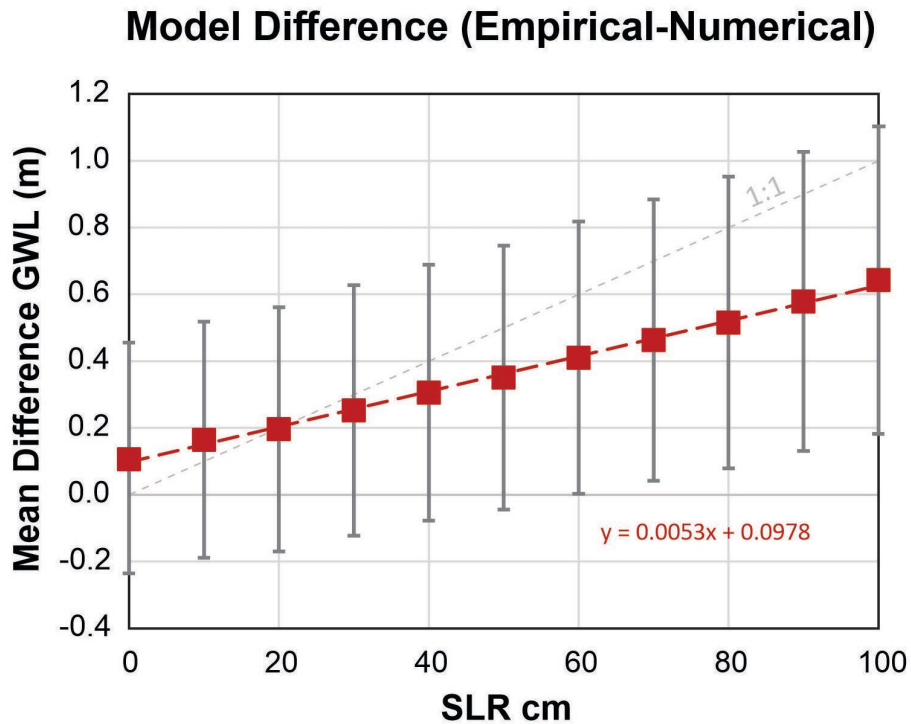


Figure 5.5 Graph showing the mean (± 1 standard deviation) of the difference between empirical (geometric) and numerical groundwater median elevations (see Figure 5.3), generated by subtracting the numerical groundwater model from the geometric model and determining the mean of the model area cell difference. The mean difference increases consistently with sea-level rise, but at a rate that is not equivalent to the increments in sea level.

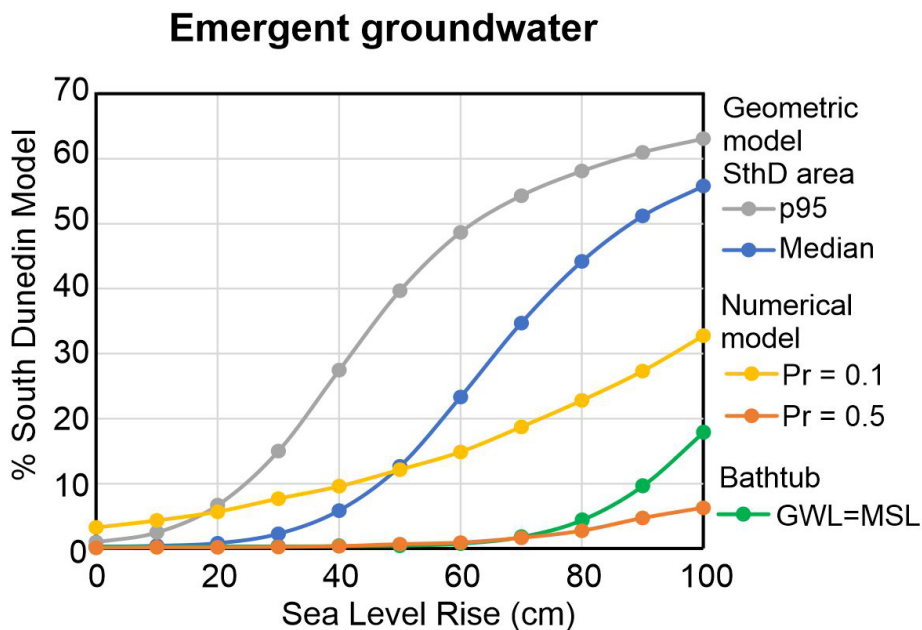


Figure 5.6 Different forecasts of the percentage of a 5.8 km² area in South Dunedin where groundwater will become emergent as sea levels rise. The percentage area of groundwater emergence from geometric models under median and 95th percentile (p95) conditions (similar to Figure 4.2) has been re-calculated for comparison with the 10% and 50% probability of emergence from the numerical groundwater model. A simplistic 'bathtub model', where groundwater level is assumed to everywhere be equal sea level, is also shown for reference.

The comparison of models and modelling approach reinforces concerns from a number of recent studies around the importance yet difficulty of incorporating drainage flux and drainage efficiency into the numerical models of sea-level rise (Habel et al. 2017, 2019; Befus et al. 2020; Chambers et al. 2023). Coastal groundwater systems tend to sit between two possible end-member situations (see Werner and Simmons [2009], Gleeson et al. [2011] and Michael et al. [2013]): (1) flux-controlled (or recharge-limited) systems, in which groundwater discharge to the sea is persistent despite changes in sea level, but the water table will rise by the same amount as sea level; and (2) head-controlled (or topographic limited) systems, whereby ground water abstractions, engineered drainage or surface features maintain the head condition in the aquifer despite sea-level changes. Human intervention can shift the groundwater response to sea-level rise towards either end member (Befus et al. 2020).

It seems that the present groundwater system in Dunedin's coastal plain, beneath the urban development, has some characteristics of a 'head-controlled' (topography limited) system, in that it seems to be partially controlled by the storm-water drainage. There is only minor saline intrusion (see Cox et al. 2020), a baseflow in the drains and discharge, and many places where the elevation of the water table coincide with the stormwater and wastewater networks (see below, Figures 5.9 and 5.10). Whether the effect of engineering is able to maintain this 'efficiency' into the future is unclear, however.

The limited data available from the stormwater and wastewater networks results in some epistemic uncertainty in groundwater-related hazard impact forecasting for Dunedin. On one hand, geometric models, like other 'flux-controlled' models, appear to provide site-specific scenarios that may over-estimate (conservatism) the potential for sea-level-rise-driven groundwater emergence. The presented geometric models incorporate shorter-term (events-based) groundwater-level fluctuations to estimate statistical distributions of groundwater levels, which are then interpolated to estimate an average depth (e.g. median) and potential extremes (e.g. p95) based on the available data (currently only four years' worth of data). These surfaces are then 'lifted' via sea-level rise increments to estimate the sea-level-rise-driven groundwater hazard, while not accounting for physical processes that may change as sea levels rise (e.g. increase in groundwater fluxes to drainage networks, reducing rises in groundwater levels).

On the other hand, the more recent physically based numerical modelling approach does not explore system response to shorter-term extreme events, but rather estimates long-term average changes in the probability of heads and fluxes in response to sea-level rise (Chambers et al. 2023). The estimated groundwater-related hazard must be framed in this extreme event context to fully realise the decision-support potential of this modelling approach. Future numerical modelling endeavours should explore the adequacy of steady-state-only history matching in the context of reducing uncertainty in the prediction of extreme groundwater levels, e.g. through the development of an events-based transient groundwater flow model (see Moore and Doherty [2021]). In addition, the impact of LiDAR-estimated elevation uncertainty should also be addressed in future work. For example, small-scale low-lying topographic features at the scale of the model cell (40 x 40 m) may lead to higher probabilities of groundwater emergence than those currently predicted (non-conservatism).

As discussed, the numerical models do provide information on subsurface flow volumes and drainage flux, which will be particularly important for exploring engineering solutions and developing mitigation options. Perhaps the numerical model's greatest advantage may be in the ability to easily alter future rates of precipitation as a boundary condition, or runoff/infiltration and drainage (which may be non-linear with sea-level rise), which is simply not possible in the

empirical-based geometric modelling. But further work is needed on the drainage 'function' and expectations of stormwater-system performance in the future. Collection of data from stormwater and wastewater networks, and collaborative work to understand interactions between the natural groundwater system (traditionally the role of geoscience) and the human-built system of urban infrastructure (traditionally the role of engineers), is clearly warranted and must be seen as a priority for understanding Dunedin's future.

As an alternative, there are also 'hybrid' data-driven and physically based numerical modelling approaches that incorporate the empirical model statistical groundwater surfaces as underpinning observations into machine learning (Koch et al. 2019). There is evidence that pre-processing of empirical information, e.g. the statistical groundwater surfaces, can improve the predictive performance of numerical models, particularly for transient groundwater flow or episodic conditions.

5.2 Stormwater and Wastewater Networks

High groundwater levels commonly limit the available drainage space and create opportunities for infiltration into both stormwater and wastewater networks (Hummel et al. 2018; Habel et al. 2020; Bosserelle et al. 2022). Infiltration into the Dunedin wastewater network has previously been experienced in the low-lying parts of the city and attributed to wastewater pipes being below the water table such that groundwater enters through leaking joints or cracks (Opus 2011). Infiltration and inflow of groundwater and stormwater occur in any wastewater system to some degree, but locally caused problems in Dunedin (Opus 2011). The three main issues are that: (i) overflows or flooding can be triggered where the system lacks capacity, (ii) diluted wastewater can cause problems for biological treatment and (iii) energy may be wasted in pumping unnecessary additional volumes. Intrusion of saltwater into wastewater pipelines has been of concern for the Dunedin City Council due to its effect on pipe condition and, more importantly, the wastewater treatment plant processes. Increased salinity at the Tahuna Wastewater Treatment Plant kills the bacteria used to treat the wastewater to a secondary level (Opus 2011). Reducing this infiltration has already been a target for at least some previous capital works (Cox et al. 2020).

Saltwater intrusion also occurs regularly into the stormwater system via the outfall pipes, but there is also some degree of groundwater infiltration into pipelines, particularly during high tides, that reduces network capacity (Osborne and Sinclair 2011). There is a baseflow volume in the stormwater network in the absence of rainfall, which discharges around 430 m³/day at the Portobello pumping station outlet (Rekker 2012) and appears to be sourced, at least in part, from groundwater. Aging pipes seem particularly vulnerable to infiltration and leakage (Opus 2011; URS 2011). Infiltration to the stormwater network is a significant component in the 'calibration' (history matching) of groundwater flow models (e.g. Rekker 2012; Chambers et al. 2023), but losses (exfiltration to groundwater) could also be occurring locally. The likely implications of climate change and sea-level rise, with associated rising groundwater and of subsurface storage loss, is an exacerbation of infiltration and increased runoff. Reduced capacities of both stormwater and wastewater systems appears likely to become an issue to overcome both in Dunedin (see also Opus [2011] and URS [2011]) and other low-lying coastal cities (Bosserelle et al. 2022).

A key aspect of Dunedin City's management of stormwater and wastewater involves understanding the system capacities and areas for improvement. The installation of a wider groundwater monitoring network, and the detailed mapping of groundwater levels and electrical conductivity (e.g. Cox et al. 2020), was a significant new knowledge step that enables

places to be identified where the stormwater and wastewater networks sit above or below the water table. A network GIS layer provided by the Dunedin City Council has elevations for a large number of network nodes, being sumps, manholes, network joins, etc. Node invert levels and pipe lowest 'down elevations' were supplied in Dunedin Drainage Datum and converted to NZVD2016 by subtracting 100.377 m. Each node or pipe was assigned a value for the local position of the water table from median (*GWLmedian_2023*), maximum (*GWLmax_2023*), MHWS (*GWLmhwsmmedian2023*) and minimum (*GWLmin_2023*) groundwater grids. A series of layers have been generated in a geodatabase *DCC_Services_2023.gdb* that accompanies this report (see Appendix 4).

Stormwater and wastewater node and pipe low points have been coloured according to their elevation (in metres) above or below the water table in Figures 5.7 and 5.8, respectively. Comparison of the figures highlights that the wastewater network is deliberately constructed at a level deeper than the stormwater, so is more commonly situated below the water table. Interpolated models of network elevations were also derived by interpolation of the stormwater and wastewater node heights (background shading Figures 5.7 and 5.8). At the first order, the networks follow topography, deviating locally with design slopes to enable gravitational flow where possible.

Grids of difference between the network elevations and groundwater levels were derived by subtracting the water table grid from the stormwater or wastewater elevation grids. The situation at MHWS (Figures 5.9 and 5.10) highlights places (blue) where the networks are substantially below the water table and likely to be most vulnerable to infiltration. They can be combined with electrical conductivity data and models of %Seawater (see Figure 5.3 in Cox et al. 2020) to examine potential for saline incursion and/or models of inundation associated with sea-level rise (e.g. Section 4). These models can also be used to identify places where infiltration might switch to exfiltration (leakage and losses) at times when groundwater levels fall. Stormwater and wastewater monitoring can potentially be targeted at places that may enable thresholds for groundwater-network exchanges to be defined in relation to network flows, age and construction material and methods. In turn, this may enable critical tipping points for system collapse to be foreseen. Concurrent monitoring of network flows and groundwater fluctuations at a wider number of sites is the next logical step to fully understand the groundwater infiltration and rationalise long-term investments in infrastructure.

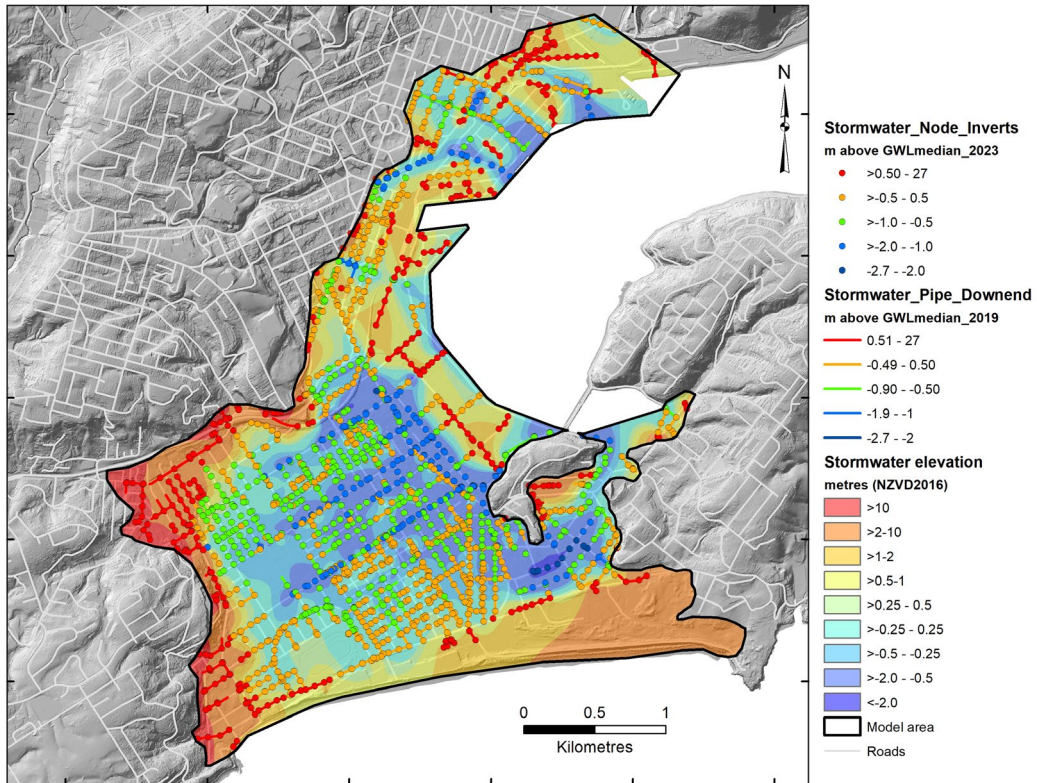


Figure 5.7 Position of stormwater network relative to the median water table in the flat-lying area of Dunedin, with nodes and pipes coloured according to their position (in metres) above or below the median groundwater model GWL_{median_2023} . Red nodes and pipes are >0.5 m above the median water table and orange ± 0.5 m above, whereas blue nodes are below the water table and are potential sites for infiltration. Background transparent shading is a surface elevation model of the stormwater network in metres NZVD2016.

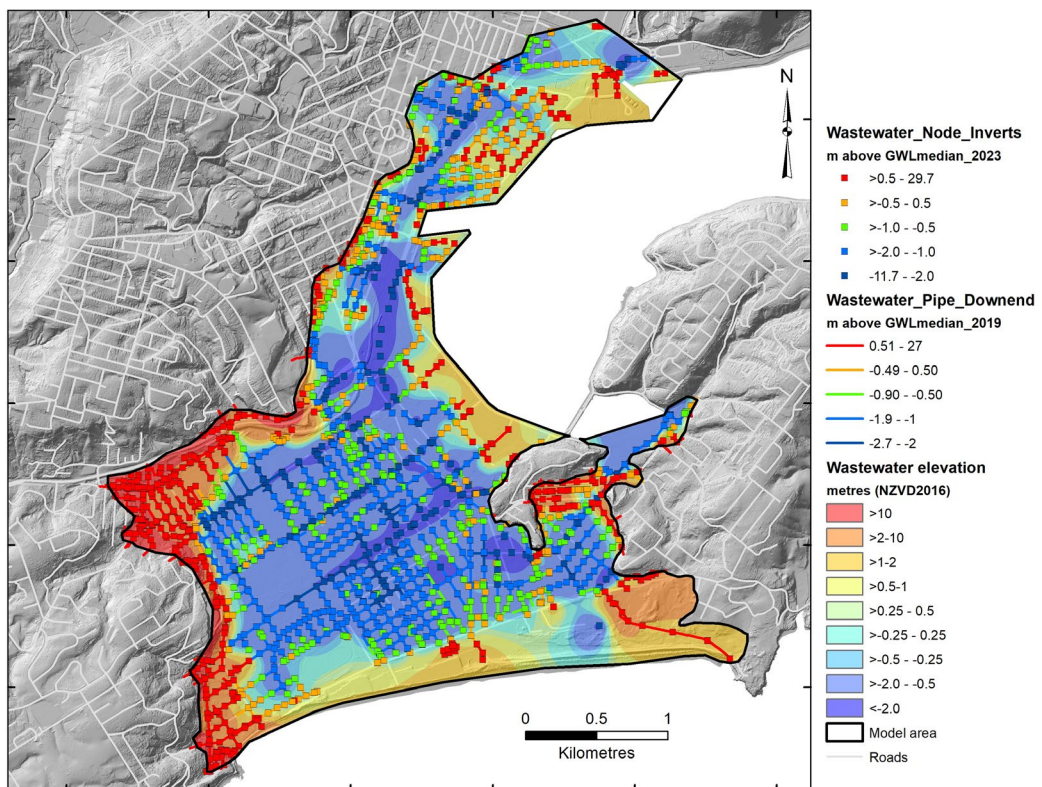


Figure 5.8 Position of wastewater network relative to the median water table in the flat-lying area of Dunedin, with nodes and pipes coloured according to their position (in metres) above or below the median groundwater model GWL_{median_2023} . Colours follow the same class ranges as the stormwater network.

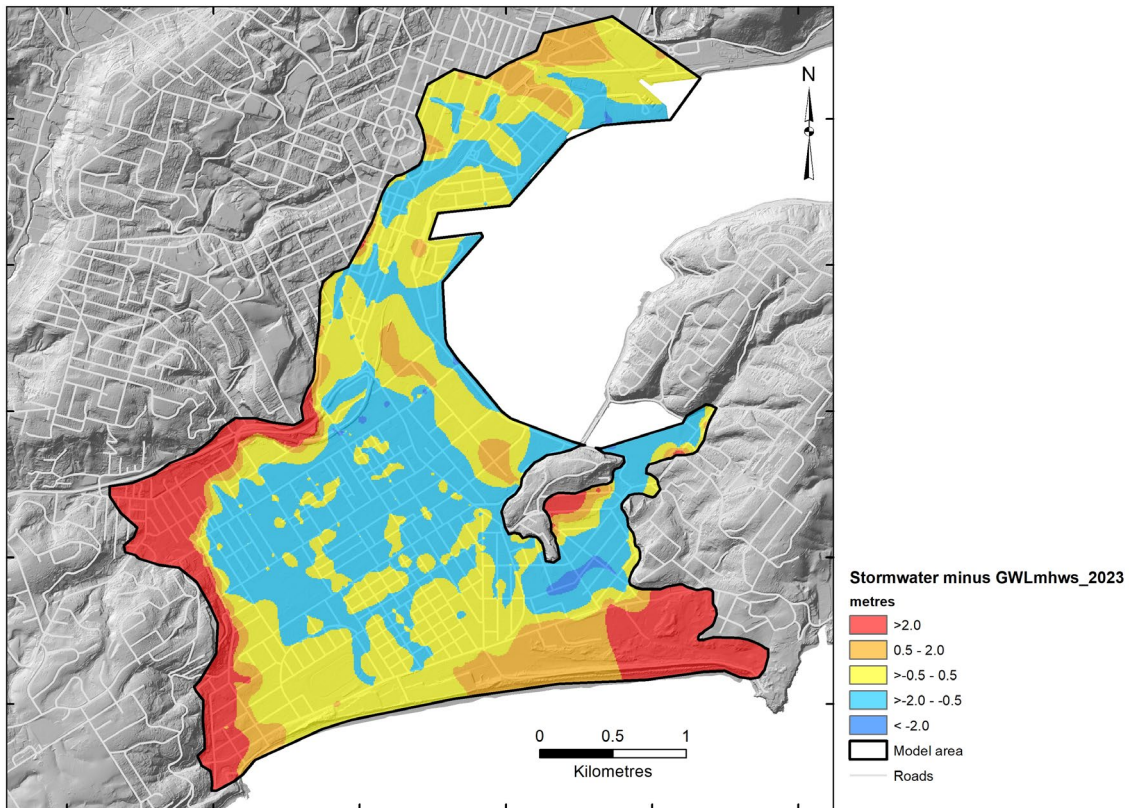


Figure 5.9 Stormwater network position relative to the water table at Mean High Water Springs (MHWS), derived by subtracting the *GWLm_{hws}_median2023* model from an elevation model derived from the stormwater network nodes. Blue areas are significantly below the water table and are potential places for infiltration.

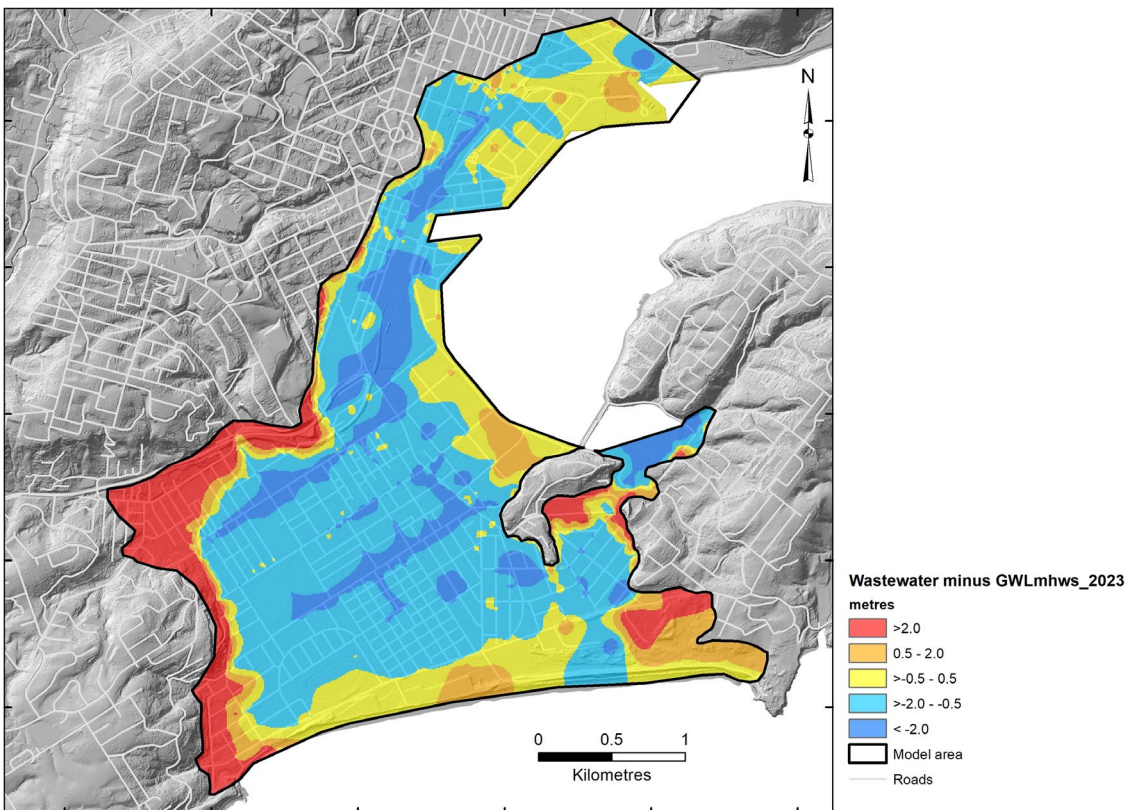


Figure 5.10 Wastewater network position relative to the water table at Mean High Water Springs (MHWS), derived by subtracting the *GWLm_{hws}_median2023* model from an elevation model derived from the sewer network nodes. Blue areas are significantly below the water table and are potential places for infiltration.

5.3 Coastal Inundation

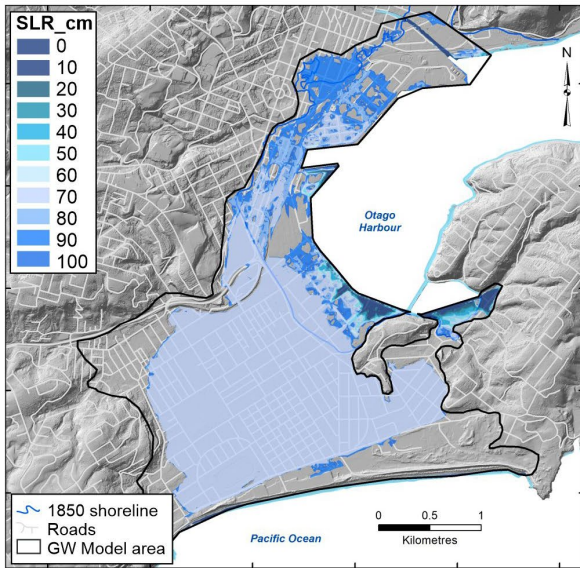
An extreme coastal flood map dataset has been computed for New Zealand by NIWA (Stephens and Paulik 2023) using analysis of sea-level measurements and numerical models from analysis of tide gauges, with tide and wave modelling (Stephens et al. 2020). Potential inundation is mapped onto digital elevation models using a static (cf. hydrodynamic) methodology in which cells must be hydraulically connected to the coastline, as well as having topographic elevation below ESL, to become inundated (Breilh et al. 2013; Yunus et al. 2016). This is of particular relevance to Dunedin, which has much land lying below MHWS and ESL levels (Figure 3.3) but is protected from the overland flow of water by a raised margin of coastal land. Maps of inundation at 1% AEP are available online (NIWA 2023a), but a range of scenarios have been calculated at AEP of 39, 18, 10, 5, 2, 1, 0.5, 0.2 and 0.1% (Paulik et al. 2023). These nine AEP scenarios have equivalent ARI, or return periods, of: 2, 5, 10, 20, 50, 100, 200, 500 and 1000 years.

Locally, maps have been generated by combining estimates of tide, storm surge, wave set-up and MSL and comparing against the 2021 LiDAR data at 10 cm increments of sea-level rise. A dataset has been provided under contract to Otago Regional Council, with a selection reproduced here with permission from NIWA for illustrative purposes (Figure 5.11). The figure highlights the combined effect of sea-level rise and ESL AEP, as well as the importance of the sand dune barrier and reclaimed land providing a degree of protection from both Otago Harbour and the Pacific Ocean. There is a major change where inundation is suddenly predicted across the low-lying parts of South Dunedin, which could occur from a 1-in-100-year ARI ESL once sea-level rise has reached 60 cm, or from a smaller 1-in-10-year ESL once sea-level rise reaches 70 cm. These scenarios assume that the level of protection is maintained, which depends strongly on whether recent erosion of the dunes slows or can be managed (e.g. Goldsmith and Hornblow 2016; Nguyen et al. 2022a). Coastal erosion, whether gradual or in more extreme events like storms and tsunamis, has not been factored at all into this study but none-the-less will be absolutely critical to the future of South Dunedin.

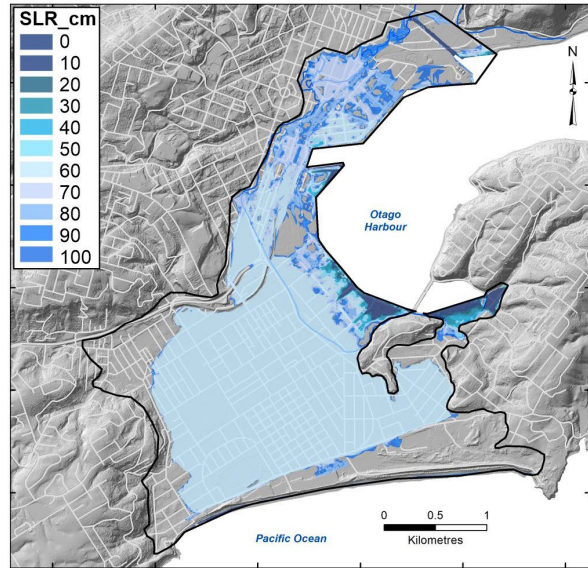
The percentage of the coastal plain (9.6 km² model area) exposed to inundation under various ARI scenarios has been calculated for comparison with the land affected by groundwater emergence determined by geometric modelling (Figure 5.12). The forecast exposure curves highlight the sharp change (jump) in the amount of land exposed to inundation hazard once ESL begins to overtop the c.2 m elevated topographic 'ridge' of reclaimed land along the margin of the harbour. But although this change appears dramatic and clearly critical to hazard and risk, it comes after a gradual increase in exposure to emergent groundwater (and change in subsurface storage) that may well have affected a substantial portion of the same land prior to this coastal inundation.

Coastal Inundation

ARI 10

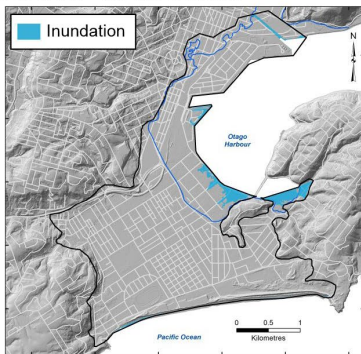


ARI 100

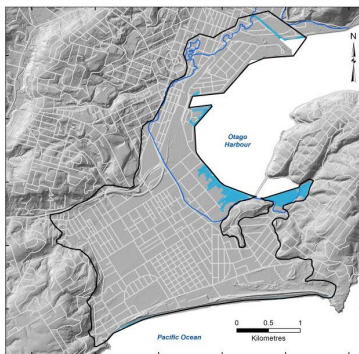


NB: Based on static model by NIWA (see Stephens et al. 2023) and assumes protective dune system remains intact.

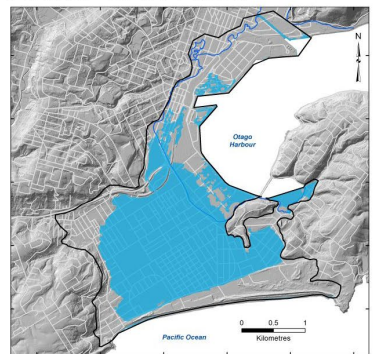
ARI10 SLR 50cm



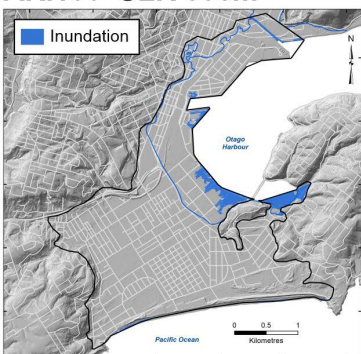
ARI10 SLR 60cm



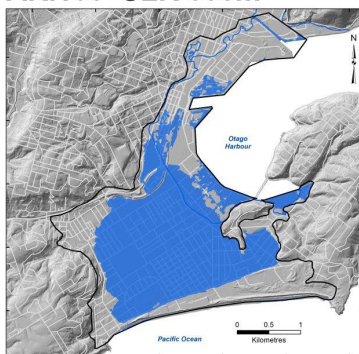
ARI10 SLR 70cm



ARI100 SLR 50cm



ARI100 SLR 60cm



ARI100 SLR 70cm

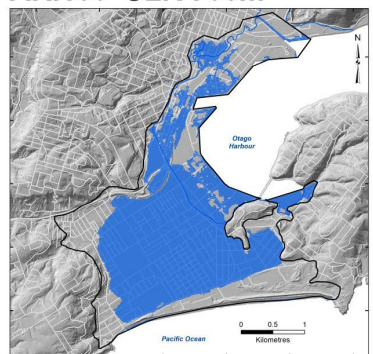


Figure 5.11 Illustration of places where land has potential to be flooded by coastal inundation and how this is forecast to evolve with sea-level rise. The top two panels show the difference between 10- and 100-year ARI, shaded differently for 10 cm increments of sea-level rise. The lower six panels separate out the areas of potential inundation at 50, 60 and 70 cm of sea-level rise from ESL at 10- and 100-year ARI. The models are based on static inundation and assume that protection by the sand dune barrier remains intact so that inundation is from the harbour. Based on data from NIWA. See also Appendix 3.

Coastal inundation from ESL

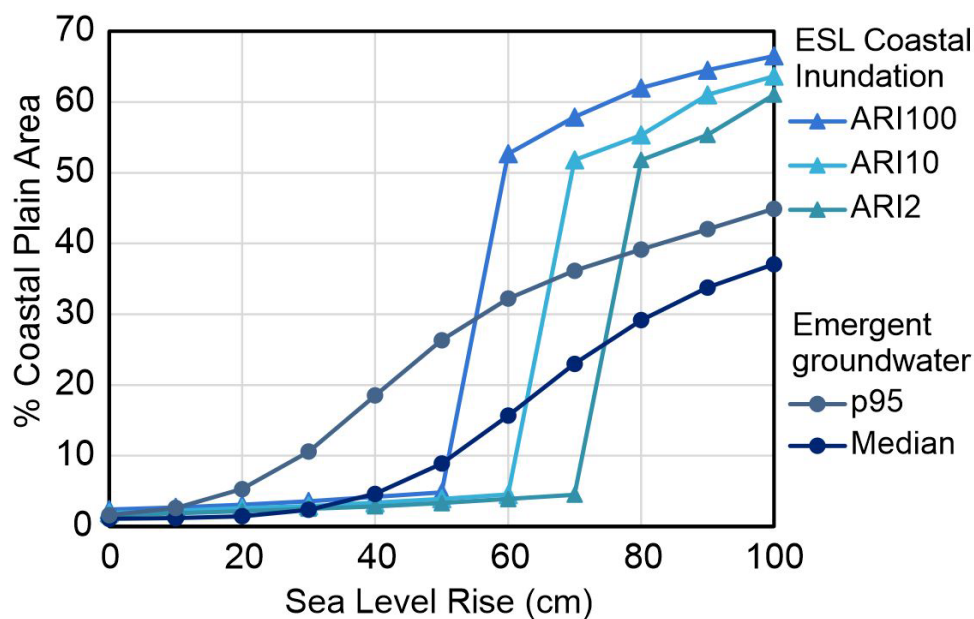


Figure 5.12 Forecasts of the percentage of the 9.2 km² area of Dunedin's coastal plain that might become inundated from the harbour as sea levels rise. Here, the 'static' models of ESL inundation are plotted for ARI 100-, 20- and 2-year scenarios corresponding to 1%, 10% and 39% AEP. The percentage area of emergence under median and 95th percentile levels (from Figure 4.2A) are shown for comparison.

5.4 Groundwater Chemistry and Saline Intrusion

All of the groundwater monitoring network sites have been sampled and tested for electrical conductance and pH in the field. The majority have also had samples analysed in the laboratory for hydrochemistry and stable isotopes. Approximately one half of the monitoring sites have also had short epochs where time-series conductivity data have been collected using electronic conductivity meters. Groundwater chemistry and the degree of saline incursion has been described in detail in Fordyce (2014), Cox et al. (2020) and Yeo (2021), so has not been specifically studied nor updated for this report. Hydrochemistry and isotopic analyses suggest that the shallow groundwater is composed of water from three distinct sources: freshwater, marine and of mixed origin. Only one monitoring site (I44/0007 Kennedy Street) has groundwater that is predominantly marine water in origin. Rainfall is the predominant contributing source of recharge (Yeo 2021). A map of conductivity and a model of %Seawater³ mixed in the groundwater, from Cox et al. (2020: Figure 3.4), is reproduced here (Figure 5.13) for general reference.

3 The model from Cox et al. (2020) assumed a freshwater end member with specific conductance of 100 $\mu\text{S}/\text{cm}$ mixes with seawater at 50,860 $\mu\text{S}/\text{cm}$.

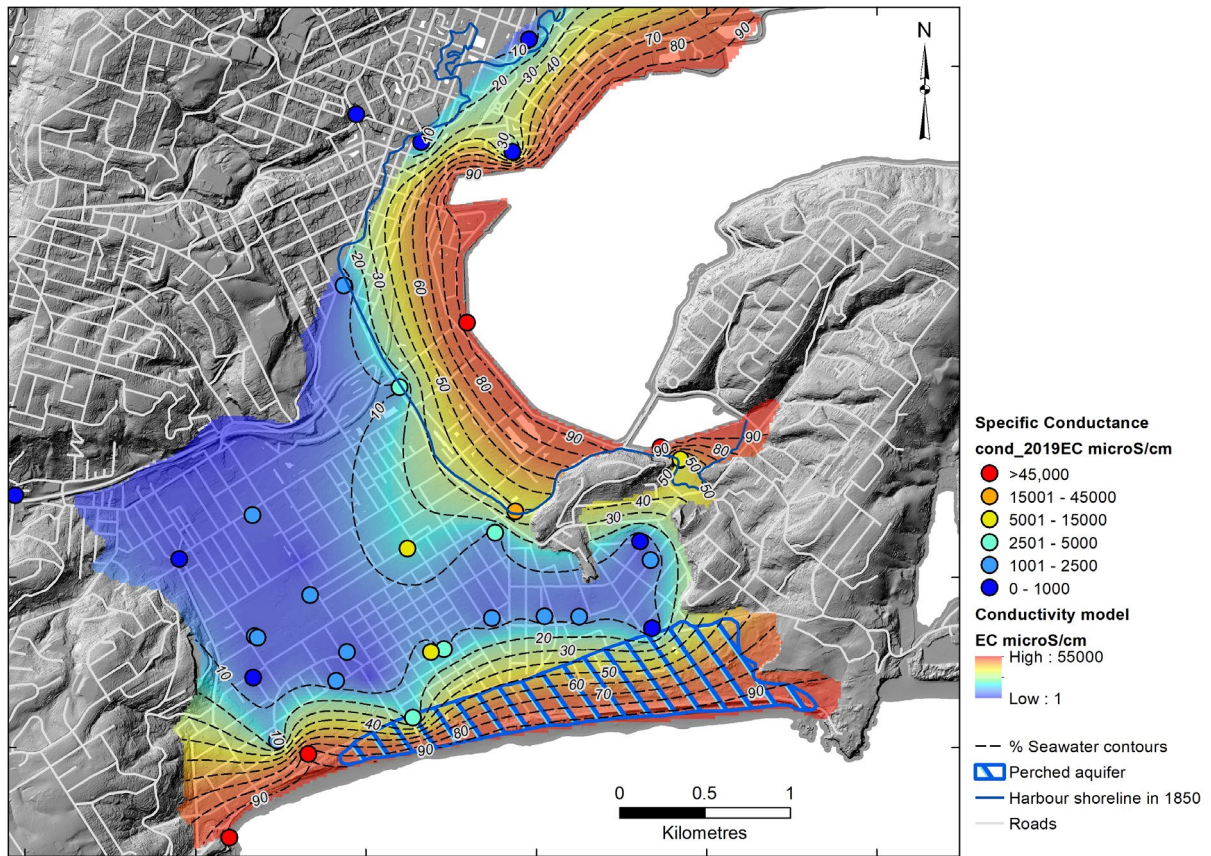


Figure 5.13 Electrical conductance of groundwater ($\mu\text{S}/\text{cm}$) as piezometer spot values and an interpolated grid, overlain by modelled %Seawater contours (at 10% contour intervals), reproduced from Cox et al. (2020). These data are not applicable to the overlying perched aquifer in the St Kilda sand dunes (blue diagonal hatch area), which is relatively fresh and appears not to mix directly with the ocean.

6.0 DISCUSSION AND RESULTS

6.1 Assumptions and Uncertainties

Analyses of climate-change-related flooding hazards and risk are subject to many assumptions and sources of uncertainty. While climate-scenario uncertainties appear to be large at face value and are now becoming more widely understood, they can be locally exceeded by uncertainty caused by a lack of input data or methodological choices in model design (e.g. inundation model and flooding threshold, land elevation model, spatial resolution or damage function) (Cooper et al. 2015; Yunus et al. 2016). We contend that simplistic elevation-based screening models can be quickly improved locally, and uncertainties reduced, once monitoring observations are used to characterise system variability and constrain processes directly responsible for hazards. This enables a shift from general theoretical solutions to models nuanced with spatial and temporal precision. Use of local empirical observations and models may also help where there are multiple hazards to consider, or unclear contribution to hazard.

The need to understand relationships and interplay between ESL during storm surge, coastal inundation, emergence of groundwater and pluvial flooding in Dunedin serves as a good example of a multi-hazard problem. In Dunedin, the acquisition of empirical observations from a network of piezometers has provided a very cost-effective and useful way to enable downscaling from regional elevation-based exposure screening (PCE 2015) to site-specific hazard models nuanced with spatial and temporal precision. Investment of only ~NZ\$100k in the monitoring network enabled definition of the shallow groundwater and spatial variations in water table position, tidal reach and rainfall response. Interpolated statistical surfaces were then used to forecast potential effects of sea-level rise leading to transient or permanent groundwater flooding or to understand relationships between groundwater level, rainfall, sub-surface storage and exposure to pluvial flooding. Understanding these hazards and how uncertainty will evolve over time, for example, due to the non-linear rate of sea-level rise or local land elevation (hypsoetry) profiles, will enable more holistic multi-hazard approaches to investment in mitigation solutions (or otherwise).

But all groundwater models have underlying assumptions that are implicit, yet important, and not always evaluated or stated explicitly. Trade-offs in the capacity to process data, and simulate predictions, are also implicit in the selection of any groundwater model. The empirical-based approach is quite distinct from a fully numerical groundwater model, which may utilise the same observations but lends itself to a different style of data processing, interrogation and solution. Numerical solutions have the advantage of being able to provide flux and volume predictions that are crucial for many engineering solutions (e.g. such as mitigation by pumping). However, numerical models tend to be more time-intensive to set up and develop, as well as constrained in either extent or spatial precision by computational limitation. They also commonly contain simplifications or assumptions on key parameters (in particular, permeability / hydraulic conductivity) and are also strongly dependent on boundary conditions whose evolution is also poorly known (e.g. such as drains). Resultant uncertainties drive the fully numerical models towards calibration over longer (e.g. annual plus) time steps or 'steady-state' solutions. Models that are designed to represent the short-term variability that occurs in shallow groundwater systems and drives flood hazard transience exacerbate the computational burden of these models. The numerical groundwater model for Dunedin (Chambers et al. 2023) is strongly dependent on a drainage function that has yet to be fully tested or calibrated and was, by necessity, assumed to be constant into the future.

By simplifying variables and controlling processes into a single parameter, the empirical geometric models presented in this study also require caveats about the approach and assumptions. At their simplest, the empirical geometric models assume that the absolute position of groundwater will also rise with sea level and that the overall shape of the water table in the future will be, on average, the same as at present. In the present geometric models calculated for Dunedin, land elevation is identified to be constant, and no distinction has been made between relative and absolute sea-level rise that may need to be incorporated in other areas where there is clearer tectonic activity. Spatial precision is controlled by the piezometer distribution in the monitoring network and local heterogeneity, and the sampling rate and longevity enable temporal precision.

Perhaps importantly, it needs to be emphasised that the empirical-based models are approximations of the present statistical condition but do not account for groundwater flow and possible changes in water-budget mass balance. Rainfall duration, intensity and event frequency, or air pressure and storm surge, also have at least some potential to cause short-term changes to the water-table position and its shape. The geometric models assume that (i) these parameters and the magnitude of astronomical tides and harbour amplification effects will not change in the immediate future, (ii) developments of any springs and runoff will not have profound geometric effects on the water table and (iii) interaction with stormwater and/or wastewater networks or imperviousness of urban ground surfaces will not change significantly over time. But, by taking the mapped position and elevation of groundwater into account, the geometric models are a distinct improvement from elevation-based 'bathtub models' that assume a horizontal groundwater surface that is everywhere equilibrated with MSL.

6.2 Application of the Empirical Model

Dunedin is just one example of a city constructed on coastal land underlain by shallow groundwater, where hazards such as liquefaction and flooding vary with seasonal and inter-annual variability in groundwater levels, and potentially with responses over an even shorter time scale. It is exposed to sea-level rise and changes to groundwater driven both from the harbour and ocean. An important conclusion is that the subtle slope and shape of the water table, which has gradient variability at kilometre-scales even in a seemingly very flat low-lying area, interacts with land-surface topography to generate marked differences in the depth to groundwater. These suburb-scale variations in the position of groundwater and availability of subsurface storage are likely important for engineering solutions for habitable land use.

Empirical groundwater-related datasets provide a tool from which inundation- or flood-exposed and/or vulnerable areas can be identified and other hazards such as liquefaction susceptibility modelled. Future needs that can also be informed by such data include real-time integration of groundwater-level data into flood modelling and management, ground-source heat resources, contaminated site plumes and time-varying liquefaction prediction. They also enable monitoring to be targeted on key areas of groundwater-network exchange so that hazard thresholds and any critical tipping points that might lead to infrastructure system collapse can be foreseen.

However, the fluctuations and controlling influences on shallow coastal groundwater can be subtle, so it is critical to minimise uncertainties with fit-for-purpose networks, precise surveying, careful pressure corrections and regular field calibration. The geometric models provide solutions that are site-specific but contain inherent assumptions that result in conservative (potentially over-estimated) impact forecasts, so it is sensible to ensure that any application encompasses a full range of natural variability of processes. Data in the accompanying geodatabases has been generated for an extensive range of groundwater conditions (including conditions of min, p5, median, mean, p95, max, MHWS and calculations based on suite of ESL ARI, rainfall AEP and SLR increments).

6.3 Delineating Hazard and Risk

The negative impacts on people, property and infrastructure from shallow groundwater can occur through either brief episodic events or long-term (permanent) rises (Bosslerelle et al. 2022). While rarely life-threatening, the impacts caused by shallow groundwater occur at a variety of water levels (Figure 6.1). Once shallower than 2 m, it may cause leakage into stormwater and sewage systems, septic tanks and basements. It can lower the bearing capacity of ground, weaken building foundation support, enhance chemical reactions such as oxidation and rust or cause subsidence. In many soils, it will substantially increase vulnerability to liquefaction in an earthquake. At less than half a metre depth, it can lead to rising damp and wet floors and fittings and also begins to impact on people's health. The shallowing of groundwater reduces the pore-space available in the subsurface to store rainfall infiltration, so can also indirectly contribute to pluvial flooding. Once groundwater becomes emergent above the ground, it may pond at nuisance level, impede access to properties, and then eventually cause direct flood damage.

One of the more commonly adopted equations (AGS 2007; Fell et al. 2008) to quantify risk from natural hazards is:

$$Risk = P_H \times P_{S:H} \times P_{T:S} \times V \times E \quad \text{Equation 6.1}$$

where:

- P_H is the annual probability of a hazardous event occurring.
- $P_{S:H}$ is the spatial probability of impact of the hazard on a person or asset.
- $P_{T:S}$ is the temporal spatial probability of a person/asset being present.
- V is the vulnerability or probability of loss of life, or damage, if hazard impacts the asset.
- E is the value of the exposed asset.

However, quantifying hazard and risk from shallow groundwater in this framework can be fraught with difficulty because: (1) the negative impacts occur at such a variety of different groundwater levels, or thresholds; (2) there are few published studies on vulnerability, or probability of damage, once thresholds are attained; (3) it is commonly an indirect, or compounding, contributor to issues that gradually evolve, rather than a distinct, abrupt and clear-cut hazard; (4) negative impacts are strongly perspective dependent, in part because the thresholds at which they occur are quite distinct for city infrastructure managers, roading and building engineers, insurance companies or private property owners.

As an alternative, it is plausible to generate qualitative indicators of exposure, at a site-specific scale, where groundwater-related hazards may have increased or are changing. In turn these can be converted into general measures of risk. Indicators such as the forecast emergence of groundwater, or decrease in subsurface storage capacity for rainfall infiltration, are still very valid and useful proxies for hazard. If defined with confidence to a site-specific scale, the proxies can be combined with information on asset exposure as an indicator of risk. In the general absence of clear information on groundwater depth thresholds and asset vulnerability, this study attempted to provide site-specific analysis of the qualitative exposure to hazardous processes, as opposed to a fully quantified assessment relative to a known hazard threshold.

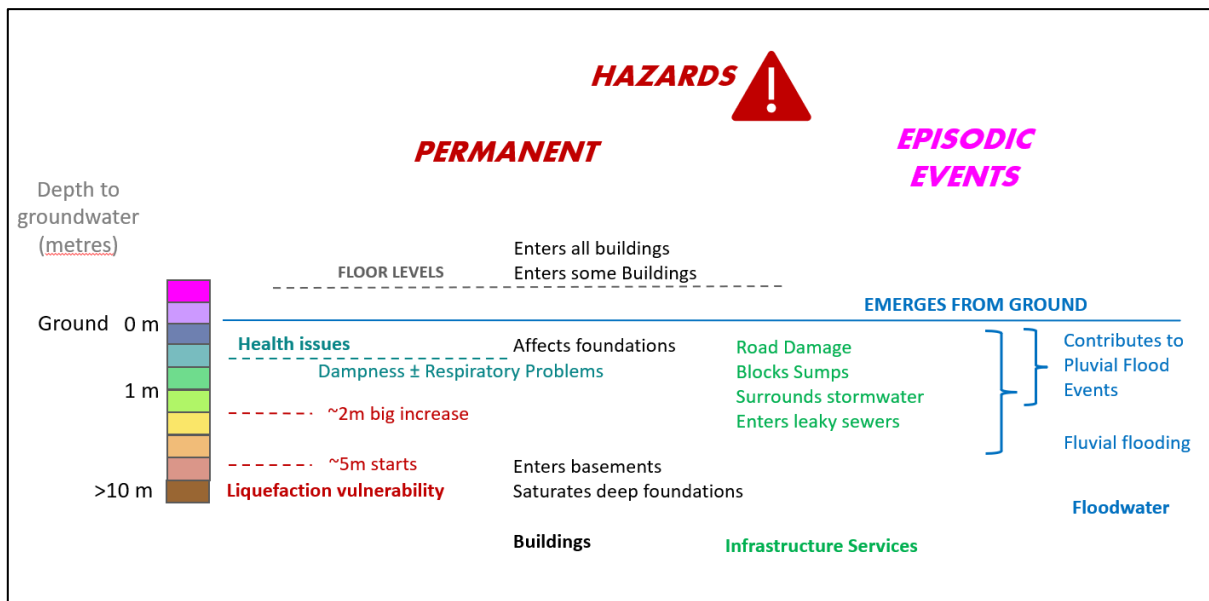


Figure 6.1 Summary of thresholds at which groundwater may become a direct hazard or an indirect contribution to another hazard. The lack of quantification of fragility functions, and poor understanding of tolerance and threshold levels, results in significant uncertainty in the calculation of risk.

6.4 Impact Forecast

The state of present groundwater across Dunedin’s low-lying coastal plain was characterised using data from a groundwater monitoring network and observations during 2019–2023. Grids (8 m cells) were interpolated to represent the median position of the water table, and other elevations, based on site statistics. The influence of rain and effect of tides have been extracted from piezometer observations and also interpolated into grids that characterise changes to groundwater induced by the sea and climate (Section 3). A series of geometric models were then produced to forecast future state of groundwater as might be influenced by sea-level rise (Section 4).

The empirically based geometric models have many inherent assumptions and uncertainties, and variability is captured through the variety of statistics used. As such, it is suggested that the models should be appropriate for suburb-scale work, if not property-scale investigations, but should be considered as a ‘conservative’ (potentially over-predicted) situation. Two key types of derivative data are useful to show how groundwater contributes to hazards, being (1) directly through groundwater levels and the emergence of groundwater; or (2) indirectly through variations in the unsaturated pore-space available to store rainfall infiltration between the water table and the ground surface, potentially contributing to pluvial flood hazard. The conditions are not necessarily hazardous per se but are instead proxies that map evolving contributions to groundwater-related hazard.

Forecasts of spatial reach or exposure to these processes, together with graphs of the percentage of the coastal plain, are combined in Figure 6.2A. Forecasts of land that may potentially be inundated from the coast, as well as ESLs from NIWA models using the same 2023 LiDAR topography, are also shown (Paulik et al. 2023; Stephens and Paulik 2023). This selection of datasets represent conditions that can be expected to occur on annual to decadal time scale, either at a 10-year or lower ARI. The frequency of any episodic-style conditions of groundwater is such that many will be experienced multiple times within every 10 cm increment of sea-level rise. A schematic summary (Figure 6.2B) highlights that the hazards associated with groundwater are likely to be gradual and will precede a step-like increase in exposure to coastal inundation. That ‘flooding from below’ precedes direct

inundation from the sea across the land surface is an important result seen elsewhere (Befus et al. 2020). Likewise, groundwater’s contribution to pluvial flooding may well have been experienced in many places prior to the emergence of groundwater (see also Rahimi et al. [2020]). The impact forecast highlights the need for planning to take a holistic multi-hazard long-term view.

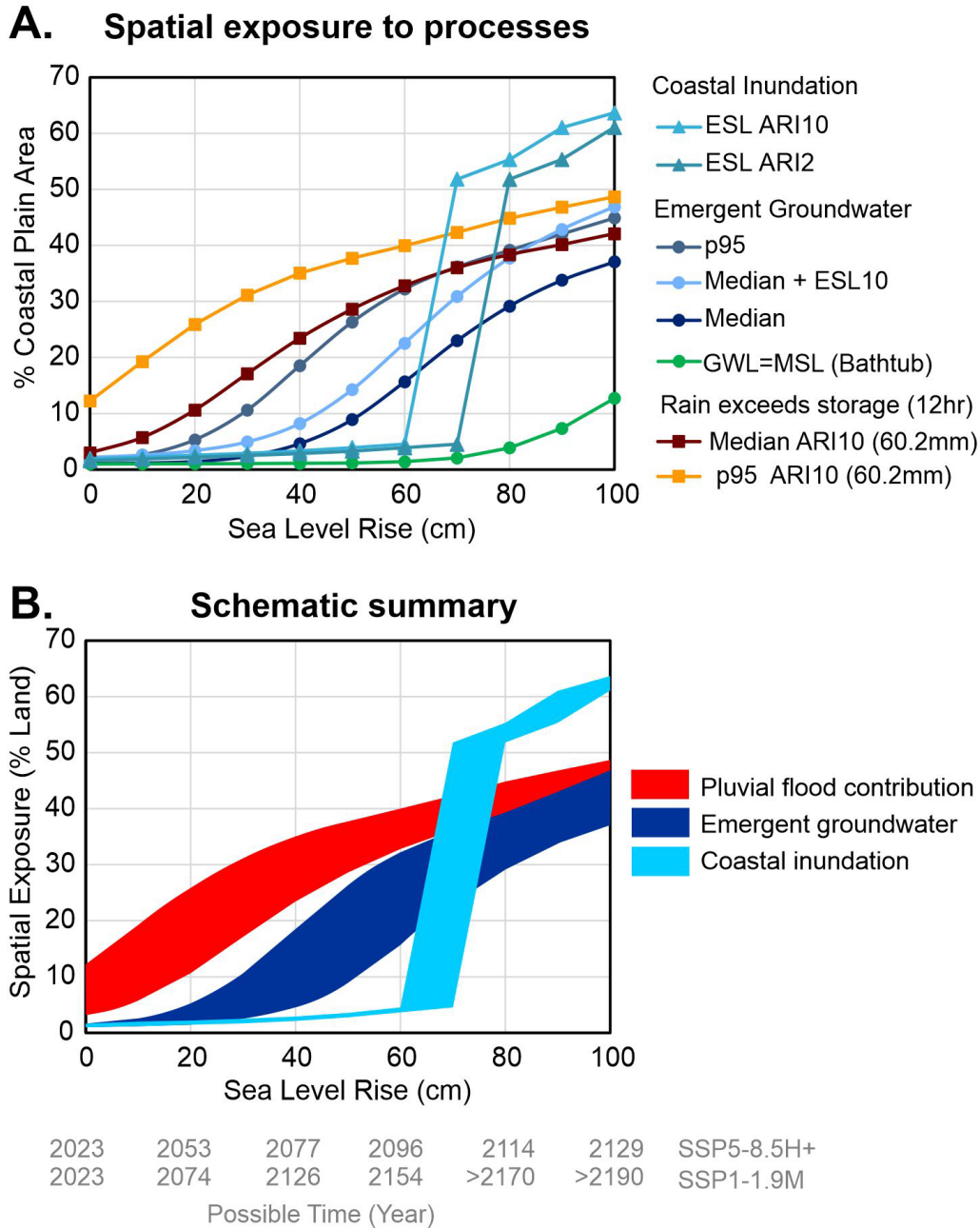


Figure 6.2 Summary of forecasts of the percentage of the 9.2 km² area of Dunedin’s coastal plain exposed to various hazardous or hazard-contributing processes. (A) Comparison of curves for emergent groundwater (circles), rainfall exceedance of available subsurface storage (squares) and coastal inundation (triangles). These data were selected from Figures 4.2, 4.4 and 5.12 to represent processes that can be expected on at least annual to decadal time scale. (B) Summary figure highlighting that annual to decadal hazard associated with groundwater is likely to precede coastal inundation, and groundwater’s contribution to pluvial flooding is likely to be felt/experienced prior to the emergence of groundwater. Possible time ranges of sea-level rise, shown on the bottom axis, have been extracted from local NZ SeaRise data (see Table 2.4).

6.5 Data and its Availability

Data to accompany this report are available for download from Zenodo as zipped archives: <http://doi.org/10.5281/zenodo.10035759>. Files include a timeseries of groundwater levels (Excel file, elevations in NZVD2016) and a series of ArcGIS10.8 geodatabases with feature classes. Data are licenced under Creative Commons Attribution 4.0 (CC-BY-4.0) licence without warranty. They can be used freely with appropriate credit – users are asked to cite both the Cox et al. (2023) data archive reference site (<https://doi.org/10.5281/zenodo.10035758>) and this report (GNS Science report 2023/43: <https://doi.org/10.21420/5799-N894>). In total, there are 646 feature classes, each with metadata that can be viewed either in ArcCatalogue or as an Excel file. Summary information on these geodatabases, and their content, are provided in Table 6.1 and Appendix 4.

Table 6.1 Summary of data that accompanies this report. Zipped geodatabases can be downloaded from Cox et al. (2023) (<http://doi.org/10.5281/zenodo.10035759>). More detail on the content of these files is provided in Appendix 4.

File Summary	Description
<i>metadata_ALL_2023.xlsx</i> 38 Kb Excel file	Excel file describing the content of ArcGIS datasets in detail. These metadata are also held within the ArcGIS datasets and can be seen via ArcCatalog.
<i>monitoring_2019-2023.xlsx</i> 94.2 Mb Excel file	Excel file containing datasheets of site information and groundwater-level observations (in metres NZVD2016 as a time series from 6 March 2019 to 1 May 2023). There are 145,638 rows (representing 15-minute time steps) for each monitoring site (38 columns). 'NA' is used to replace numerical data at times when transducers had been removed from the piezometer for downloading (short spike anomalies) or when there had been drawdown caused by extraction for samples.
<i>sthDunedin_water_table_model2023.gdb</i> 827 Mb ESRI ArcGIS10.8 geodatabase 52 FeatureClasses Vector and Grid file format Geodatabase containing observations and interpolated models of groundwater data for Dunedin derived from observations during the 2019–2023 epoch.	Raw data stored in <i>piezo_data_points</i> and transferred to <i>modelpoints</i> for interpolation. Interpolated grids (8 m) generated for model extent using TopotoRaster function. The watertable elevation is stored as either GWL or <i>watertableRL</i> (metres NZVD2016). Depth to water is stored in DTW, based on the 2021 LiDAR DEM. The extent of the area of interest is stored in <i>modelling_extent</i> . Layers are in NZTM (NZGD2000 EPSG:2193) coordinates and NZVD2016 vertical datum (EPSG:7879)
<i>sthDunedin_water_table_forecasts.gdb</i> 307 Mb ESRI ArcGIS10.8 geodatabase 594 FeatureClasses Vector and Grid file format Geodatabase containing a series of grid datasets that forecast the changing state of groundwater as sea levels rise, as groundwater level (GWL in metres NZVD2016) and depth to groundwater (DTW). Derivative grid and polygon (vector) datasets indicate places where groundwater	Grid and vector (poly) datasets representing a forecast state of groundwater in Dunedin under present (sea-level rise = 000) and future conditions of sea-level rise (= 010, 020, 030 cm, etc., where [OFF] represents increments of changing sea level). Layers are in NZTM (NZGD2000 EPSG:2193) coordinates, named using a convention where: GWL = groundwater level (metres NZVD2016 EPSG:7879), DTW = depth to groundwater (metres relative to ground LiDAR 2021), MED = condition at median level; p95 = condition at a high 95 th percentile level, MHWS = condition at mean high water springs, ESL = condition at storm-tide of particular extreme sea level ARI, RAINstor = maximum possible subsurface storage of rainfall (in mm), [OFF] = an amount of sea-level rise in 10 cm increments,

File Summary	Description
<p>will reach the surface and become emergent, or where amounts of rain exceed the subsurface volume available to store infiltration as groundwater.</p>	<p>[ARI] = average recurrence interval of ESL in years, [AFI] = average recurrence interval of a particular 12-hour rainfall exceedance in years. Polygons define either places where groundwater is emergent (DTW ≤ 0) under a given forecast or places where a rainfall depth at AFI exceeds the available subsurface storage (and any infiltration to groundwater should no longer be possible).</p>
<p><i>DCC_Services_2023.gdb</i> 69 Mb ESRI ArcGIS10.8 geodatabase 24 FeatureClasses Vector and Grid file format Geodatabase of the Dunedin City Council three waters service network, containing data and observations extracted from interpolated models of groundwater data for Dunedin.</p>	<p>Point, line and grid datasets, developed from shapefiles originally supplied by Dunedin City Council, to define the elevation of Wastewater (Foul Sewer) and Stormwater network nodes relative to the water table (statistical position) in Dunedin during 2019–2023. Elevations of network nodes (points) and pipes (polylines) are provided in both NZVD2016 and Dunedin Drainage Datum (= NZVD2016 + 100.376). Attributes show how far the wastewater or stormwater network is locally above (+ve) or below (-ve) the water table. Datasets have been assigned with <NULL> and -9999 values where data are missing or outside the model.</p>

7.0 SUMMARY AND CONCLUSIONS

Dunedin City has a large number of assets and critical infrastructure sitting on a low-lying coastal plain that is underlain by a largely unseen and relatively poorly understood hazard. Shallow groundwater in this area limits the unsaturated ground available to store rain and runoff, promotes flooding and creates opportunities for infiltration into stormwater and wastewater networks. Groundwater levels are expected to rise as sea level rises, causing greater frequency of flooding and/or direct inundation once it nears the ground surface.

A shallow groundwater monitoring network has 35 sites where water levels and temperature are measured every 15 minutes by automated transducers. This report incorporates monitoring and observations over the period 6 March 2019 to 1 May 2023, but longer-term data are available from four sites (since 2009). During 2019–2023, groundwater levels appear to be a reasonable proxy (± 0.07 m) of median conditions during the past decade but, locally, some of the extreme values experienced during the 2015 floods were missed. A new LiDAR survey collected in 2021 provides updated information on the elevation of topography at ± 0.05 m (95% confidence interval) vertical accuracy.

Site observations of groundwater statistics from 2019 to 2023 have been spatially interpolated into a series of statistical surfaces (grids with 8 m cells) to represent the present-day (2023) water-table elevation and depth to groundwater, the response to rainfall recharge and tidal forcing and the available subsurface storage of rain infiltration. Shallow groundwater throughout South Dunedin is unconfined, but there is a perched aquifer locally in dune sand at St Kilda and some semi-confined horizons in the Harbourside area.

The position of the water table relative to ground does not necessarily reflect topographic elevation. The lowest lying suburbs do not necessarily coincide with shallowest groundwater. Instead, the water table has changes in elevation and gradients at kilometre scales that are significant from suburb to suburb and important for assessing hazard and risk. Tides and storm surges cause Dunedin groundwater levels to rise and fall, with locally anomalous sites of strong tidal response but amplitude generally decreasing with distance from the harbour or sea. Changes in groundwater level by infiltration from rain are generally larger, varying in sensitivity between sites. Groundwater responses to rainfall depend on factors such as local stormwater drainage, extent of impervious urban surfaces, piezometer construction method and its protection from runoff and subsurface sediment storativity and permeability. A measure of the available subsurface storage, equivalent to the rainfall required to lift groundwater to the ground surface and cause inundation, was calculated as a grid model.

Simple geometric models to depict how sea-level rise will affect groundwater levels have been developed using the present-day statistical surfaces and 10 cm increments of sea-level rise. At their simplest, the models assume that the absolute position of Dunedin groundwater will also rise and that the shape of the water table in the future will be, on average, the same as at present. By taking the mapped position of the water-table elevation into account, the geometric models are quite distinct from ‘bathtub models’, which assume a horizontal water table surface that is everywhere equilibrated with MSL. The geometric models are strongly empirical, with many caveats and implicit assumptions. They simplify many variables and controlling processes into a single parameter and do not account for groundwater flow and possible changes in water-budget mass balance.

Forecast emergence of groundwater on the Dunedin coastal plain shows a steadily increasing area of land affected as sea levels rise. By the time sea-level rise reaches 40 cm, groundwater emergence is expected over quite a large area of South Dunedin, and, by 60 cm, emergence will be widespread even at median groundwater condition, whereas Harbourside should be relatively free of issues. The emergent groundwater datasets are probably more appropriate, being used to understand the relative contributions of groundwater to a complex hazard rather than a 'hazard' mapping per se.

Maps of subsurface storage across the Dunedin coastal plain show places where rainfall may exceed the available capacity to store infiltration and provide a proxy for situations where and when groundwater levels may begin contributing locally to pluvial flooding. The forecast change also shows a steadily increasing area of land with loss of storage as sea levels rise. At present, there is only a relatively small area of land with insufficient storage for a 12 hour rainstorm at ARI of 1, 10 or 100 at MHWS. But, by 40 cm sea-level rise, there appears to be limited ability for any South Dunedin land to absorb even 12 hour rainfall at annual recurrence (<30.8 mm). The exact effects and implications on the performance of the stormwater network need immediate attention as, in theory, the pluvial flood risk should rise dramatically.

Other tools and datasets available to help forecast the future of sea-level-rise-related hazards in Dunedin include a fully numerical groundwater model (Chambers et al. 2023) in which the projected sea-level-rise-driven probability of groundwater reaching the model top, and spatial extent of inundation, is mitigated by a numerical (and poorly constrained) representation of waste/stormwater drainage networks. Comparison of empirical-based geometric and numerical models highlighted a major difference between the emergent groundwater and hazard predicted by geometric models (pessimistic/over-predicted) compared with numerical models (likely optimistic/under-estimated). It reinforces concerns around the importance, yet difficulty, of incorporating drainage flux and efficiency into numerical models of sea-level rise, which would be required for the design of adaptation and mitigation engineering solutions. Unfortunately, with limited data available from the stormwater and wastewater networks, it results in considerable epistemic uncertainty in groundwater-related hazard impact forecasting for Dunedin. Collection of data from stormwater and wastewater networks, and collaborative work to understand interactions between the natural groundwater system (traditionally the role of geoscience) and the human-built system of urban infrastructure (traditionally the role of engineers), is clearly warranted and must now be recognised as a priority.

An extreme coastal flood map dataset has also been calculated by NIWA, providing a range of scenarios for AEP of 39, 18, 10, 5, 2, 1, 0.5, 0.2 and 0.1% (Paulik et al. 2023). Locally, maps have been generated by combining estimates of tide, storm surge, wave set-up and MSL, and compared against the 2021 LiDAR data at 10 cm increments of sea-level rise. A major change is predicted where inundation is suddenly predicted across the low-lying parts of South Dunedin, which could occur from a 1-in-100-year ARI ESL once sea-level rise has reached 60 cm, or from a smaller 1-in-10-year ESL once sea-level rise reaches 70 cm. These scenarios assume that the level of protection is maintained from the sand dunes, which depends strongly on whether recent erosion of the dunes slows or can be managed. Coastal erosion has not been factored at all into this report but none-the-less will be absolutely critical to the future of South Dunedin.

A series of ArcGIS 10.8 datasets accompany this report and are provided freely without warranty under CC-BY4.0 licence, which only requires that the source of data is acknowledged. The groundwater-related datasets provide tools from which inundation- or flood-exposed and/or vulnerable areas can be identified and other hazards, such as liquefaction susceptibility, modelled. The negative impacts on people, property and infrastructure from shallow groundwater can occur through either brief episodic events or long-term (permanent) rises. While rarely life-threatening, the impacts caused by shallow groundwater occur at a variety of water levels, which complicates the definition of both hazard and risk. Although the empirically based geometric models provide solutions that are site-specific, given the number of inherent assumptions, they are likely to be 'conservative' scenarios, and it would be sensible to ensure that their application encompasses a full range of natural variability of processes. As an alternative, it is plausible to generate qualitative indicators of exposure, at a site-specific scale, where groundwater-related hazards may have increased or are changing, which might in turn be converted into general calculations of risk.

The spatial exposure to the loss of subsurface storage capacity, emergent groundwater and coastal inundation are combined in a summary of negative impact from these processes as sea levels rise. The hazards associated with groundwater are likely to be gradual and will precede a step-like increase in the possibility of coastal inundation. Likewise, groundwater's contribution to pluvial flooding may well have been experienced in many places prior to the emergence of groundwater. The impact forecast highlights the need for planning to take a holistic multi-hazard long-term view.

8.0 ACKNOWLEDGMENTS

Dunedin's monitoring has been supported by Otago Regional Council, GNS Science, Toka Tū Ake EQC, Dunedin City Council, QuakeCoRE (University of Canterbury), Oceana Gold, University of Otago, Golders Associates and McNeill Drilling. Monitoring data and drillhole information from the new Dunedin Hospital site geotechnical investigations have also been provided by Te Whatu Ora and Tonkin & Taylor. Coastal inundation data have been supplied by NIWA through contract to Otago Regional Council. Tidal data were supplied by Port Otago through Glen Rowe at the New Zealand Hydrographic Authority (Land Information New Zealand). Data from the NZ SeaRise programme have also been used. Pascal Sirguy, Clare Lewis and Paul Denys (Otago University Surveying School) helped by surveying piezometer elevations and sea-level datum conversions.

The authors also acknowledge support of many colleagues and collaborators, in particular: Jonathan Rowe, Ian Telfer, Jared Oliver, Raphael Krier-Mariani and previously Paul Gebert (Dunedin City Council); Jean-Luc Payan, Simon Robinson and Sharon Hornblow (Otago Regional Council); Emma Fordyce, Sarah Mager, Quyen Nuygen, Ivan Diaz-Rainey and Tony Moore (University of Otago); Greg Bodeker (Bodeker Scientific); Scott Sutherland (Tonkin & Taylor) and Scott Stephens (NIWA); Phil Glassey, David Barrell, John Haines, Richard Levy and Peter Johnson (GNS Science).

We also wish to thank the wider community of Dunedin whose enthusiasm to understand the place where they work and live, and its environment and future, is seemingly insatiable. It has certainly helped drive the direction and quality of this work. While there are too many people to individually thank, notable champions supporting groundwater research have been: Clare Curran (previous Labour Member of Parliament for South Dunedin), Mayor Jules Radich (Dunedin City Council), Gavin Palmer (Otago Regional Council), Eleanor Doig and Robyn McLean (South Dunedin Community Group).

Work for this report has involved contributions from the Urban Groundwater project (GNS Science's Strategic Science Investment Fund), the STRAND Programme (a Royal Society of New Zealand Marsden-funded project led by University of Otago) and the NZ SeaRise Programme (an Endeavour programme funded by the Ministry of Business, Innovation & Employment led by Victoria University of Wellington). The authors acknowledge Richard Levy, Tim Naish, Ivan Diaz-Rainey, Antoni Moore, Conny Tschritter, Frederika Mourot and Rogier Westerhoff for their leadership and management in these programmes. The report was improved by comments and suggestions provided by Otago Regional Council (Simon Robinson, Andrew Welsh, Naveen Kadaba, Tim van Woerden), as well as by internal reviews by Dr Catherine Moore and Dr Malcolm Arnot.

9.0 REFERENCES

- [AGS] Australian Geomechanics Society. 2007. Practice note guidelines for landslide risk management. *Australian Geomechanics*. 42(1):63–114.
- Barrell DJA, Glassey PJ, Cox SC, Smith Lyttle B. 2014. Assessment of liquefaction hazards in the Dunedin City district. Dunedin (NZ): GNS Science. 66 p. + 1 DVD. Consultancy Report 2014/68. Prepared for Otago Regional Council.
- Beca. 2014. Assessment of options for protecting Harbourside and South City from direct impacts of sea level rise. Wellington (NZ): Beca. 19 p. + appendices. Prepared for Dunedin City Council.
- Befus KM, Barnard PL, Hoover DJ, Finzi Hart JA, Voss CI. 2020. Increasing threat of coastal groundwater hazards from sea level rise in California. *Nature Climate Change*. 10:946–952 <https://doi.org/10.1038/s41558-020-0874-1>
- Bell R, Lawrence J, Allan S, Blackett P, Stephens S. 2017. Coastal hazards and climate change: guidance for local government. Wellington (NZ): Ministry for the Environment. 279 p. + appendices. ME 1341.
- Benson WN. 1968. The W.N. Benson geological map of Dunedin district [map]. Wellington (NZ): Department of Scientific and Industrial Research. 1 folded map + 1 booklet, scale 1:50,000. (New Zealand Geological Survey miscellaneous series map; 1).
- Bosserelle AL, Morgan LK, Hughes MW. 2022. Groundwater rise and associated flooding in coastal settlements due to sea level rise: a review of processes and methods. *Earth's Future*, 10(7):e2021EF002580. <https://doi.org/10.1029/2021EF002580>
- Breilh JF, Chaumillon E, Bertin X, Gravelle M. 2013. Assessment of static flood modelling techniques: application to contrasting marshes flooded during Xynthia (western France). *Natural Hazards and Earth System Sciences*. 13(6):1595–1612. <https://doi.org/10.5194/nhess-13-1595-2013>
- Carey-Smith T, Henderson R, Singh S. 2018. High intensity rainfall design system. Version 4. Wellington (NZ): NIWA. Client report 2018022CH. 73 p. Prepared for Envirolink.
- Chambers LA, Hemmings B, Cox SC, Moore C, Knowling MJ, Hayley K, Rekker J, Mourou FM, Glassey P, Levy R. 2023. Quantifying uncertainty in the temporal disposition of groundwater inundation under sea level rise projections. *Frontiers in Earth Science* 11. <https://doi.org/10.3389/feart.2023.1111065>
- Chen Y, Oliver DS. 2013. Levenberg–Marquardt forms of the iterative ensemble smoother for efficient history matching and uncertainty quantification. *Computational Geosciences*. 17(4):689–703. <https://doi.org/10.1007/s10596-013-9351-5>
- Cooper HM, Zhang C, Selch D. 2015. Incorporating uncertainty of groundwater modelling in sea level rise assessment: a case study in South Florida. *Climatic Change*. 129:281–294. <https://doi.org/10.1007/s10584-015-1334-1>
- Cox SC, Ettema MHJ, Mager SM, Glassey PJ, Hornblow S, Yeo S. 2020. Dunedin groundwater monitoring and spatial observations. Lower Hutt (NZ): GNS Science. 86 p. (GNS Science report; 2020/11). <https://doi.org/10.21420/AVAJ-EE81>
- Cox SC, Ettema M, Chambers L, Easterbrook-Clark L, Stevenson N. 2023. Data pertaining to 'Dunedin groundwater monitoring, spatial observations and forecast conditions under sea level rise' [dataset]. Version 2023. Genève (CH): Zenodo. <https://doi.org/10.5281/zenodo.10035759>
- Dunedin City Council. 2015. Infrastructure performance during the June 2015 flood event. [Dunedin] (NZ): Department of Water and Waste Services. 15 p. Prepared for Dunedin City Council.
- Dunedin City Council. 2016. South Dunedin public infrastructure performance during June 2015 flood event follow up. [Dunedin] (NZ): Dunedin City Council Infrastructure Services Committee.

- Denys PH, Beavan RJ, Hannah J, Pearson CF, Palmer N, Denham M, Hreinsdottir S. 2020. Sea level rise in New Zealand: the effect of vertical land motion on century-long tide gauge records in a tectonically active region. *Journal of Geophysical Research: Solid Earth*. 125:e2019JB018055. <https://doi.org/10.1029/2019JB018055>
- Doherty J, Moore C. 2021. Decision support modelling viewed through the lens of model complexity. Adelaide (AU): National Centre for Groundwater Research and Training, Flinders University. <https://doi.org/10.25957/p25g-0f58>
- Emmanouil S, Langousis A, Nikolopoulos EI, Anagnostou EN. 2022. The spatiotemporal evolution of rainfall extremes in a changing climate: a CONUS-wide assessment based on multifractal scaling arguments. *Earth's Future*. 10(2):e2021EF002539. <https://doi.org/10.1029/2021EF002539>
- Erskine AD. 1991. The effect of tidal fluctuation on a coastal aquifer in the UK. *Groundwater*. 29(4):556–562. <https://doi.org/10.1111/j.1745-6584.1991.tb00547.x>
- Fell R, Corominas J, Bonnard C, Cascini L, Leroi E, Savage WZ. 2008. Guidelines for landslide susceptibility, hazard and risk zoning for land use planning. *Engineering Geology*. 102(3–4):85–98. <https://doi.org/10.1016/j.enggeo.2008.03.022>
- Ferris JG. 1952. Cyclic fluctuations of water level as a basis for determining aquifer transmissibility. Washington (DC): US Geological Survey. 17 p. (Groundwater Notes; 1). <https://doi.org/10.3133/70133368>
- Fordyce E. 2014. Groundwater dynamics of a shallow coastal aquifer [MAppSc thesis]. Dunedin (NZ): University of Otago. 155 p. <http://hdl.handle.net/10523/4918>
- Freeze RA, Cherry JA. 1979. Groundwater. Englewood Cliffs (NJ): Prentice-Hall. 604 p.
- Gerstenberger MC, Bora S, Bradley BA, DiCaprio C, Van Dissen RJ, Atkinson GM, Chamberlain C, Christophersen A, Clark KJ, Coffey GL, et al. 2022. New Zealand National Seismic Hazard Model 2022 revision: model, hazard and process overview. Lower Hutt (NZ): GNS Science. 106 p. (GNS Science report; 2022/57). <https://doi.org/10.21420/TB83-7X19>
- Glassey PJ. 2018. How future sea level rise will affect South Dunedin. *International Journal of Environmental Impacts*. 1(1):40–49. <https://doi.org/10.2495/ei-v1-n1-40-49>
- Glassey PJ, Barrell DJA, Smith Lyttle B, Hornblow S, Mackey B. 2021. Geological model of South Dunedin. Lower Hutt (NZ): GNS Science. 70 p. (GNS Science report; 2021/03). <https://doi.org/10.21420/B5E9-GE25>
- Gleeson T, Marklund L, Smith L, Manning AH. 2011. Classifying the water table at regional to continental scales. *Geophysical Research Letters*. 38(5):L05401. <https://doi.org/10.1029/2010GL046427>
- Goldsmith M, Hornblow S. 2016. The natural hazards of South Dunedin. Dunedin (NZ): Otago Regional Council. 69 p. <https://www.orc.govt.nz/media/2217/the-natural-hazards-of-south-dunedin-report-july-2016.pdf>
- Goldsmith M, Payan J-L, Morris R, Valentine C, MacLean S, Xiaofeng L, Vaitapu N, Mackey B. 2015. Coastal Otago flood event 3 June 2015. Dunedin (NZ): Otago Regional Council. 56 p. <https://www.orc.govt.nz/media/1662/coastal-otago-flood-event-3-june-2015.pdf>
- Habel S, Fletcher CH, Rotzoll K, El-Kadi AI. 2017. Development of a model to simulate groundwater inundation induced by sea level rise and high tides in Honolulu, Hawaii. *Water Resources Research*. 114:122–134. <https://doi.org/10.1016/j.watres.2017.02.035>

- Habel S, Fletcher CH, Rotzoll K, El-Kadi AI, Oki DS. 2019. Comparison of a simple hydrostatic and a data-intensive 3D numerical modelling method of simulating sea level rise induced groundwater inundation for Honolulu, Hawai'i, USA. *Environmental Research Communications*. 1(4):041005. <https://doi.org/10.1088/2515-7620/ab21fe>
- Habel S, Fletcher CH, Anderson TF, Thompson PR. 2020. Sea-level rise induced multi-mechanism flooding and contribution to urban infrastructure failure. *Scientific Reports*. 10:3796. <https://doi.org/10.1038/s41598-020-60762-4>
- Hamling IJ, Wright TJ, Hreinsdóttir S, Wallace LM. 2022. A snapshot of New Zealand's dynamic deformation field from Envisat InSAR and GNSS observations between 2003 and 2011. *Geophysical Research Letters*. 49(2):e2021GL096465. <https://doi.org/10.1029/2021GL096465>
- Hoover DJ, Odigie KO, Swarzenski PW, Barnard P. 2017. Sea-level rise and coastal groundwater inundation and shoaling at select sites in California, USA. *Journal of Hydrology: Regional Studies*. 11:234–249. <https://doi.org/10.1029/2021GL096465>
- Hsieh PA, Bredehoeft JD, Farr JM. 1987. Determination of aquifer transmissivity from Earth tide analysis. *Water Resources Research*. 23(10):1824–1832. <https://doi.org/10.1029/WR023i010p01824>
- Hummel MA, Berry MS, Stacey MT. 2018. Sea level rise impacts on wastewater treatment systems along the U.S. coasts. *Earth's Future*. 6(4):622–633. <https://doi.org/10.1002/2017EF000805>
- Hutchinson MF. 1989. A new procedure for gridding elevation and stream line data with automatic removal of spurious pits. *Journal of Hydrology*. 106(3):211–232. [https://doi.org/10.1016/0022-1694\(89\)90073-5](https://doi.org/10.1016/0022-1694(89)90073-5)
- Hutchinson MF, Dowling TI. 1991. A continental hydrological assessment of a new grid-based digital elevation model of Australia. *Hydrological Processes*. 5(1):45–58. <https://doi.org/10.1002/hyp.3360050105>
- Kreibich H, Thieken AH. 2008. Assessment of damage caused by high groundwater inundation. *Water Resources Research*. 44(9). <https://doi.org/10.1029/2007WR006621>
- Knott JF, Daniel JS, Jacobs JM, Kirshen P. 2018. Adaptation planning to mitigate coastal-road pavement damage from groundwater rise caused by sea-level rise. *Transportation Research Record*. 2672(2):11–22. <https://doi.org/10.1177/0361198118757441>
- Koch J, Berger H, Henriksen HJ, Sonnenborg TO. 2019. Modelling of the shallow water table at high spatial resolution using random forests. *Hydrology and Earth System Sciences*. 23(11):4603–4619. <https://doi.org/10.5194/hess-23-4603-2019>
- [LINZ] Toitū Te Whenua Land Information New Zealand. 2022. Otago Coastal catchments LiDAR 1m DEM (2021). Wellington (NZ): LINZ; [updated 2023 Feb 23; accessed 2023 Dec]. <https://data.linz.govt.nz/layer/109627-otago-coastal-catchments-lidar-1m-dem-2021/>
- [LINZ] Toitū Te Whenua Land Information New Zealand. 2023a. Tide prediction guidance. Wellington (NZ): LINZ; [accessed 2023 Dec]. <https://www.linz.govt.nz/guidance/marine-information/tide-prediction-guidance>
- [LINZ] Toitū Te Whenua Land Information New Zealand. 2023b. Vertical datum relationship grids. Wellington (NZ): LINZ; [accessed 2023 Dec]. <https://www.linz.govt.nz/guidance/geodetic-system/coordinate-systems-used-new-zealand/vertical-datums/vertical-datum-relationship-grids>
- Liu T, Su X, Prigiobbe V. 2018. Groundwater-sewer interaction in urban coastal areas. *Water*. 10(12):1774. <https://doi.org/10.3390/w10121774>
- Macfie R. 2016. Flood fiasco: eye of the storm. *New Zealand Listener*. 254(3968):22–29.

- Masterson JP, Garabedian SP. 2007. Effects of sea-level rise on ground water flow in a coastal aquifer system. *Groundwater*. 45(2):209–217. <https://doi.org/10.1111/j.1745-6584.2006.00279.x>
- Michael HA, Russoniello CJ, Byron LA. 2013. Global assessment of vulnerability to sea-level rise in topography-limited and recharge-limited coastal groundwater systems. *Water Resources Research*. 49(4):2228–2240. <https://doi.org/10.1002/wrcr.20213>
- Ministry for the Environment. 2022. Interim guidance on the use of new sea level rise projections. Wellington (NZ): Ministry for the Environment – Manatū Mō Te Taiao. ME 1667. <https://environment.govt.nz/publications/interim-guidance-on-the-use-of-new-sea-level-rise-projections/>
- Mohssen M. 2017. Investigation of a flood forecasting tool for South Dunedin [abstract]. In: *Filling the knowledge reservoir: New Zealand Hydrological Society Annual Conference*; 2017 Nov 28–Dec 1; Napier, New Zealand. Wellington (NZ): NZ Hydrological Society. p. 147. https://www.hydrologynz.org.nz/files/ugd/623971_43cd8b4f96594057969be72b4e96e226.pdf
- Moore CR, Doherty J. 2021. Exploring the adequacy of steady-state-only calibration. *Frontiers in Earth Science*. 9:692671. <https://doi.org/10.3389/feart.2021.692671>
- Nguyen D, Hilton M, Wakes S. 2022a. Wind flow dynamics and sand deposition behind excavated foredune notches on developed coasts. *Earth Surface Processes and Landforms*. 47(7):1698–1719. <https://doi.org/10.1002/esp.5341>
- Nguyen Q, Thorsnes P, Diaz-Rainey I, Moore A, Cox SC, Stirk-Wang L. 2022b. Price recovery after the flood: risk to residential property values from climate change-related flooding. *Australian Journal of Agricultural and Resource Economics*. 66(3):532–560. <https://doi.org/10.1111/1467-8489.12471>
- [NIWA] National Institute of Water & Atmospheric Research. 2023a. Extreme coastal flood maps for Aotearoa New Zealand. Wellington (NZ): NIWA; [accessed 2023 Oct 4]. <https://niwa.co.nz/natural-hazards/our-services/extreme-coastal-flood-maps-for-aotearoa-new-zealand>
- [NIWA] National Institute of Water & Atmospheric Research. 2023b. High Intensity Rainfall Design System (HIRDS). Wellington (NZ): NIWA; [accessed 2023 Oct 4]. <https://niwa.co.nz/information-services/hirds>
- [Opus] Opus International Consultants Ltd; URS New Zealand Ltd. 2011. Integrated Catchment Management Plans 2010–2060: phase 1 wastewater system – final report. 113 p. + 9 appendices. Prepared for Dunedin City Council.
- [ORC] Otago Regional Council; [LINZ] Toitū Te Whenua Land Information New Zealand. 2022. Dunedin and Mosgiel, Otago, New Zealand 2021 [dataset]. [Wellington (NZ)]: LINZ; [accessed 2023 Jun 25]. <https://doi.org/10.5069/G91J97ZM>
- Osborn T, Sinclair L. 2011. An investigation worth its salt: targeting saline intrusion. In: *Water New Zealand Annual Conference*; 2011 Nov 9–11; Rotorua, New Zealand. Wellington (NZ): Water New Zealand. 18 p. https://www.waternz.org.nz/Article?Action=View&Article_id=641
- Otsu N. 1979. A threshold selection method from gray-level histograms. *IEEE Transactions on Systems, Man, and Cybernetics*. 9(1):62–66. <https://doi.org/10.1109/TSMC.1979.4310076>
- Paulik R, Wild A, Stephens S, Welsh R, Wadhwa S. 2023. National assessment of extreme sea level driven inundation under rising sea levels. *Frontiers in Environmental Science*. 10. <https://doi.org/10.3389/fenvs.2022.1045743>

- [PCE] Parliamentary Commissioner for the Environment. 2015. Preparing New Zealand for rising seas: certainty and uncertainty. [Wellington] (NZ): Parliamentary Commissioner for the Environment. 92 p.
- Plane E, Hill K, May C. 2019. A rapid assessment method to identify potential groundwater flooding hotspots as sea levels rise in coastal cities. *Water*. 11:2228. <https://doi.org/10.3390/w11112228>
- Rahimi R, Tavakol-Davani H, Graves C, Gomez A, Valipour MF. 2020. Compound inundation impacts of coastal climate change: sea-level rise, groundwater rise, and coastal precipitation. *Water*. 12(10):2776. <https://doi.org/10.3390/w12102776>
- Rekker J. 2012. The South Dunedin coastal aquifer & effect of sea level fluctuations. Dunedin (NZ): Otago Regional Council. 25 p.
- Rotzoll K, El-Kadi AI. 2008. Estimating hydraulic properties of coastal aquifers using wave setup. *Journal of Hydrology*. 353(1–2):201–213. <https://doi.org/10.1016/j.jhydrol.2008.02.005>
- Rotzoll K, Fletcher CH. 2013. Assessment of groundwater inundation as a consequence of sea-level rise. *Nature Climate Change*. 3:477–481. <https://doi.org/10.1038/nclimate1725>
- Stephens S, Paulik R. 2023. Mapping New Zealand’s exposure to coastal flooding and sea level rise. Wellington (NZ): National Institute of Water & atmospheric Research [NIWA]. NIWA internal report 2023098HN. 39 p. <https://deepsouthchallenge.co.nz/resource/methodology-mapping-new-zealands-exposure-to-coastal-flooding-and-sea-level-rise/>
- Stephens SA, Bell RG, Haigh ID. 2020. Spatial and temporal analysis of extreme storm-tide and skew-surge events around the coastline of New Zealand. *Natural Hazards and Earth System Sciences*. 20:783–796. <https://doi.org/10.5194/nhess-20-783-2020>
- [URS] URS New Zealand Ltd; Opus International Consultants. 2011. Integrated catchment management plans 2010–2060: summary report. 78 p. + appendices. Prepared for Dunedin City Council.
- van Ballegooy S, Cox SC, Thurlow C, Rutter HK, Reynolds T, Harrington G, Fraser J, Smith T. 2014. Median water table elevation in Christchurch and surrounding area after the 4 September 2010 Darfield Earthquake. Version 2. Lower Hutt (NZ): GNS Science. 79 p + 8 appendices. (GNS Science report; 2014/18).
- van Ballegooy S, Wentz F, Boulanger RW. 2015. Evaluation of CPT-based liquefaction procedures at regional scale. *Soil Dynamics and Earthquake Engineering*. 79(B):315–334. <https://doi.org/10.1016/j.soildyn.2015.09.016>
- Werner AD, Simmons CT. 2009. Impact of sea-level rise on sea water intrusion in coastal aquifers. *Groundwater*. 47(2):197–204. <https://doi.org/10.1111/j.1745-6584.2008.00535.x>
- White JT. 2018. A model-independent iterative ensemble smoother for efficient history-matching and uncertainty quantification in very high dimensions. *Environmental Modelling & Software*. 109:191–201. <https://doi.org/10.1016/j.envsoft.2018.06.009>
- Wu S-Y, Yarnal B, Fisher A. 2002. Vulnerability of coastal communities to sea-level rise: a case study of Cape May County, New Jersey, USA. *Climate Research*. 22:255–270. <https://doi.org/10.3354/cr022255>
- Yang J, Graf T, Herold M, Ptak T. 2013. Modelling the effects of tides and storm surges on coastal aquifers using a coupled surface-subsurface approach. *Journal of Contaminant Hydrology*. 149:61–75. <https://doi.org/10.1016/j.jconhyd.2013.03.002>

- Yeo S. 2021. Hydrochemical analysis of shallow groundwater origin in South Dunedin and Harbourside, New Zealand [MSc thesis]. Dunedin (NZ): University of Otago. 145 p. <http://hdl.handle.net/10523/12846>
- Yunus AP, Avtar R, Kraines S, Yamamuro M, Lindberg F, Grimmond CSB. 2016. Uncertainties in tidally adjusted estimates of sea level rise flooding (bathtub model) for the Greater London. *Remote Sensing*. 8(5):366. <https://doi.org/10.3390/rs8050366>

This page left intentionally blank.

APPENDICES

This page left intentionally blank.

APPENDIX 1 MAP OF PLACE NAMES

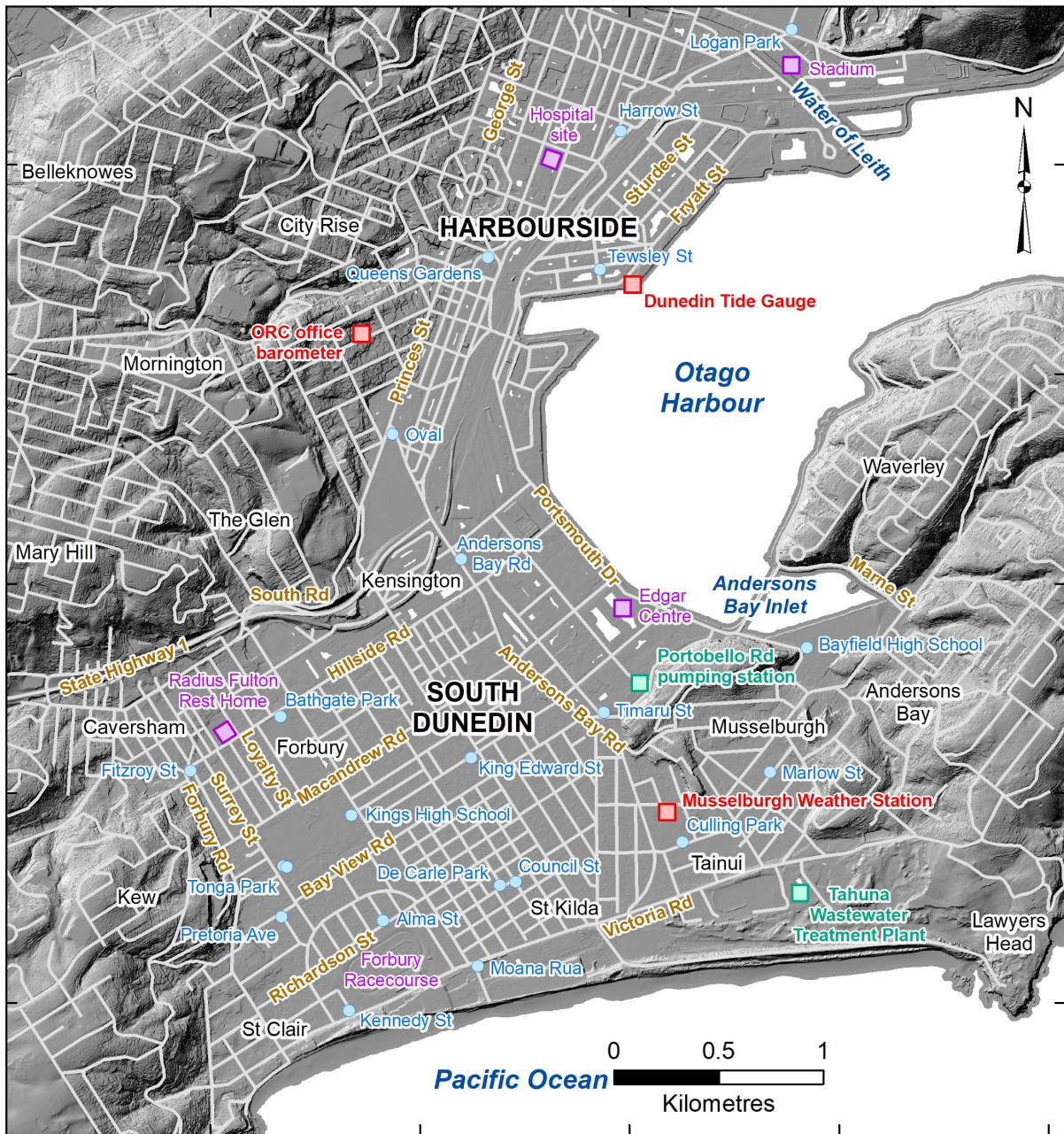


Figure A1.1 Map with key place names that may have been referred to in this study.

APPENDIX 2 GROUNDWATER MONITORING SITES

Table A2.1 Dunedin groundwater monitoring sites that were operational during 2019–2023. GL-MP is a locally measured offset of the measuring point height above or below ground.

Number	Name	Easting (m)	Northing (m)	Total Depth and Lowermost Depth of Screen, if Different (m)	MP Elevation NZVD 2016	GL-MP Offset (m)
I44/0005	Bathgate Park	1405334.7	4914364.8	6.0	1.113	0.050
I44/0006	Tonga Park (shallow)	1405348.5	4913652.2	6.0	1.574	-0.855
I44/0007	Kennedy St	1405662.3	4912961.9	6.0	2.032	-0.855
I44/1094	Culling Park	1407253.0	4913766.7	4.2	0.464	0.065
I44/1105	Kings	1405673.4	4913894.6	3.6	0.735	0.035
I44/1106	Bayfield	1407847.5	4914693.2	3.7	1.767	0.025
I44/1113	Marlow St	1407672.7	4914098.9	5.9	0.693	0.110
I44/1114	Timaru St	1406879.1	4914385.2	5.6	1.232	0.100
I44/1120	Pretoria Ave	1405339.1	4913409.3	5.0	0.739	0.080
I44/1121	Fitzroy St	1404905.8	4914105.3	2.8	4.517	0.095
I44/1122	Andersons Bay Rd	1406198.0	4915115.0	6.0	0.996	0.100
I44/1123	King Edward St	1406244.3	4914166.8	6.1	0.683	0.150
I44/1124	Council St	1406458.7	4913576.9	6.1	0.777	0.115
I44/1125	Alma St	1405825.4	4913390.2	6.0	0.824	0.070
CE17/0100	Oval	1405869.7	4915713.6	14.9 (6.5)	2.746	-0.555
CE17/0101	Queens Gardens	1406325.5	4916556.1	15.9	2.937	-0.575
CE17/0102	Tewsley St	1406860.7	4916498.5	14.7	1.865	0.045
CE17/0103	Harrow St	1406959.1	4917159.3	14.7 (13.5)	2.169	0.055
CE17/0104	Logan Park	1407775.4	4917644.8	14.5 (14.3)	2.753	-0.455
CE17/0105	Tonga Park (deep)	1405365.4	4913645.6	44.5 (19.95)	1.381	-0.650
CE17/0106	De Carle Park	1406382.7	4913559.0	20.7 (19.9)	1.491	-0.660
CE17/0107	Moana Rua (deep)	1406276.7	4913174.4	21.8	3.679	0.055
CE17/0108	Moana Rua (shallow)	1406281.7	4913175.7	6.3	3.744	0.045
CE17/0116	Community Centre	1406142.4	4914447.0	6.0	0.807	0.070
CE17/0117	Holiday Park	1407272.5	4913379.7	3.1	3.673	-0.120
CE17/0118	OMES	1406833.8	4913276.7	2.0	1.971	0.060
CE17/0119	Devon Street	1406948.2	4916820.1	6.1	2.035	0.100
CE17/0120	Oregon St	1409939.5	4913760.6	6.1	3.545	0.105
CE17/0121	Culling Park (new)	1407251.1	4913761.4	6.0	1.088	-0.555
CE17/0122	Turakina Rd	1406620.0	4914986.2	7.3	2.205	0.095
CE17/0123	Surrey St	1405031.3	4914058.3	5.9	1.315	0.110

Number	Name	Easting (m)	Northing (m)	Total Depth and Lowermost Depth of Screen, if Different (m)	MP Elevation NZVD 2016	GL-MP Offset (m)
CE17/0124	Scout Hall (shallow)	1405841.6	4912957.8	10.6	4.475	0.090
CE17/0125	Scout Hall (deep)	1405885.5	4912948.5	61.2 (53.6)	7.356	0.110
CE17/0127	Murrayfield St	1405218.4	4914785.5	10.5	2.410	0.010
CE17/0131	Tahuna Rd	1407683.9	4913697.2	2.7	1.059	-0.075
ASC_BH_101	Cumberland St	1406603.1	4917126.8	6	1.623	0.0
ASB_BH_103	Castle St	1406655.2	4917000.2	10	1.653	0.0
ASB_BH_107	Cadbury	1406614.5	4916922.1	10	2.173	0.0

Table A2.2 Dunedin groundwater level statistics from 2019 to 2023. GWL in metres (NZVD2016).

Number	Name	No. of Observations	Max.	p95	Median (p50)	p5	Min.
I44/0005	Bathgate Park	145419	0.637	0.489	0.386	0.207	0.131
I44/0006	Tonga Park (shallow)	145415	0.418	0.248	0.104	-0.076	-0.152
I44/0007	Kennedy St	145596	0.857	0.487	0.210	-0.040	-0.221
I44/1094	Culling Park	141637	0.490	0.051	-0.366	-0.896	-1.332
I44/1105	Kings	121413	0.645	0.177	-0.003	-0.217	-0.528
I44/1106	Bayfield	79679	1.284	0.520	0.235	0.142	0.119
I44/1113	Marlow St	144953	0.700	0.584	0.482	0.390	0.343
I44/1114	Timaru St	142224	0.189	-0.051	-0.245	-0.369	-0.510
I44/1120	Pretoria Ave	130331	0.610	0.466	0.311	0.159	0.058
I44/1121	Fitzroy St	101550	4.179	3.482	3.192	2.891	2.486
I44/1122	Andersons Bay Rd	142278	0.282	-0.003	-0.265	-0.369	-0.514
I44/1123	King Edward St	140327	0.816	0.561	0.189	-0.293	-0.386
I44/1124	Council St	142478	0.773	0.419	0.123	-0.137	-0.321
I44/1125	Alma St	113063	0.889	0.606	0.373	0.237	-0.250
CE17/0100	Oval	135947	1.884	1.481	1.274	1.084	0.973
CE17/0101	Queens Gardens	130047	1.935	1.874	1.732	1.522	1.197
CE17/0102	Tewsley St	135998	1.004	0.753	0.439	0.136	-0.053
CE17/0103	Harrow St	121786	0.417	0.020	-0.157	-0.260	-0.315
CE17/0104	Logan Park	123707	0.553	0.148	-0.101	-0.176	-0.232
CE17/0105	Tonga Park (deep)	135520	0.530	0.424	0.310	0.160	0.078
CE17/0106	De Carle Park	120269	0.364	0.317	0.246	0.177	0.134
CE17/0107	Moana Rua (deep)	134911	0.511	0.395	0.304	0.217	0.142

Number	Name	No. of Observations	Max.	p95	Median (p50)	p5	Min.
CE17/0108	Moana Rua (shallow)	131495	1.289	1.143	1.003	0.861	0.789
CE17/0116	Community Centre	50155	0.485	0.382	0.221	-0.013	-0.116
CE17/0117	Holiday Park	50160	1.959	1.735	1.384	1.219	1.189
CE17/0118	OMES	50057	1.915	1.437	1.132	0.992	0.966
CE17/0119	Devon Street	50151	0.472	0.258	0.155	0.053	0.012
CE17/0120	Oregon St	50161	2.243	2.008	1.773	1.670	1.651
CE17/0121	Culling Park (new)	50162	0.509	0.058	-0.261	-0.477	-0.684
CE17/0122	Turakina Rd	53959	1.176	0.932	0.815	0.703	0.670
CE17/0123	Surrey St	54013	1.099	0.571	0.395	0.218	0.144
CE17/0124	Scout Hall (shallow)	53972	1.535	1.200	0.886	0.716	0.588
CE17/0125	Scout Hall (deep)	54049	0.647	0.552	0.475	0.313	0.181
CE17/0127	Murrayfield St	2	3.175	3.137	2.798	2.458	2.420
CE17/0131	Tahuna Rd	49973	0.960	0.564	0.305	0.093	-0.034
ASC_BH_101	Cumberland St	53707	0.418	0.090	-0.078	-0.187	-0.254
ASB_BH_103	Castle St	53626	0.574	0.417	0.368	0.278	0.221
ASB_BH_107	Cadbury	53336	2.145	1.266	1.160	1.045	0.974

APPENDIX 3 DUNEDIN GROUNDWATER FORECAST

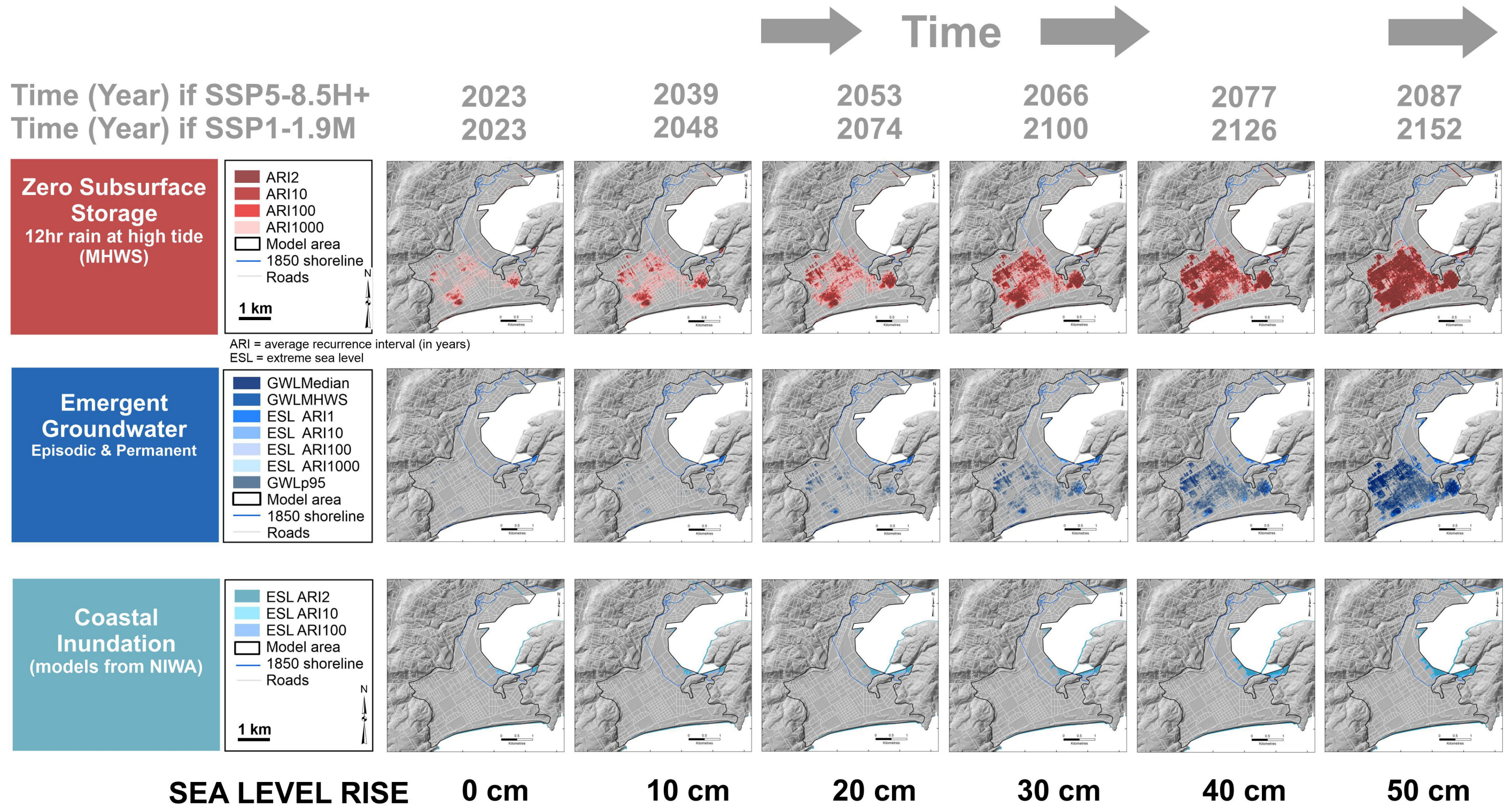


Figure A3.1 Maps showing areas of zero subsurface storage capacity, emergent groundwater and coastal inundation (from NIWA) for various recurrence intervals and increments of sea-level rise. Potential times are extracted from Table 2.4. Figure continued overleaf.

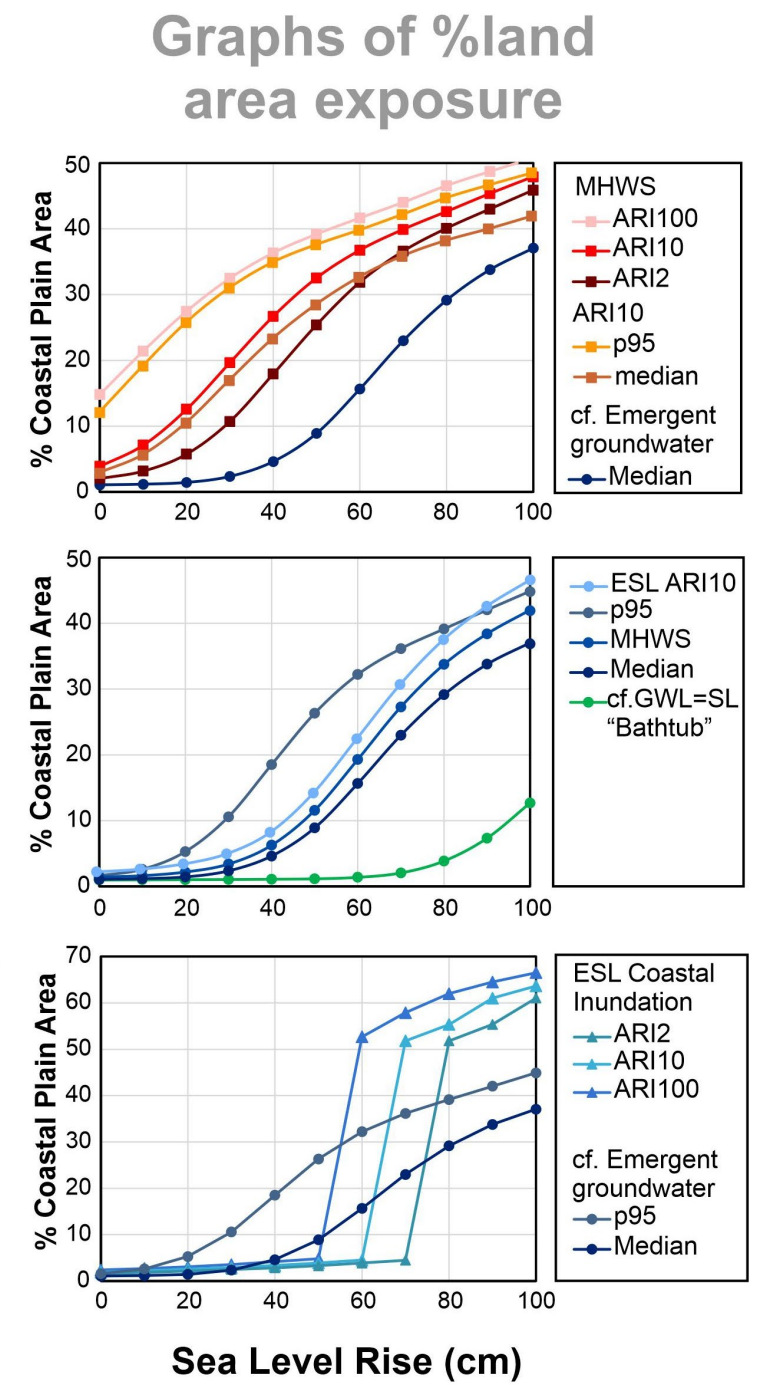
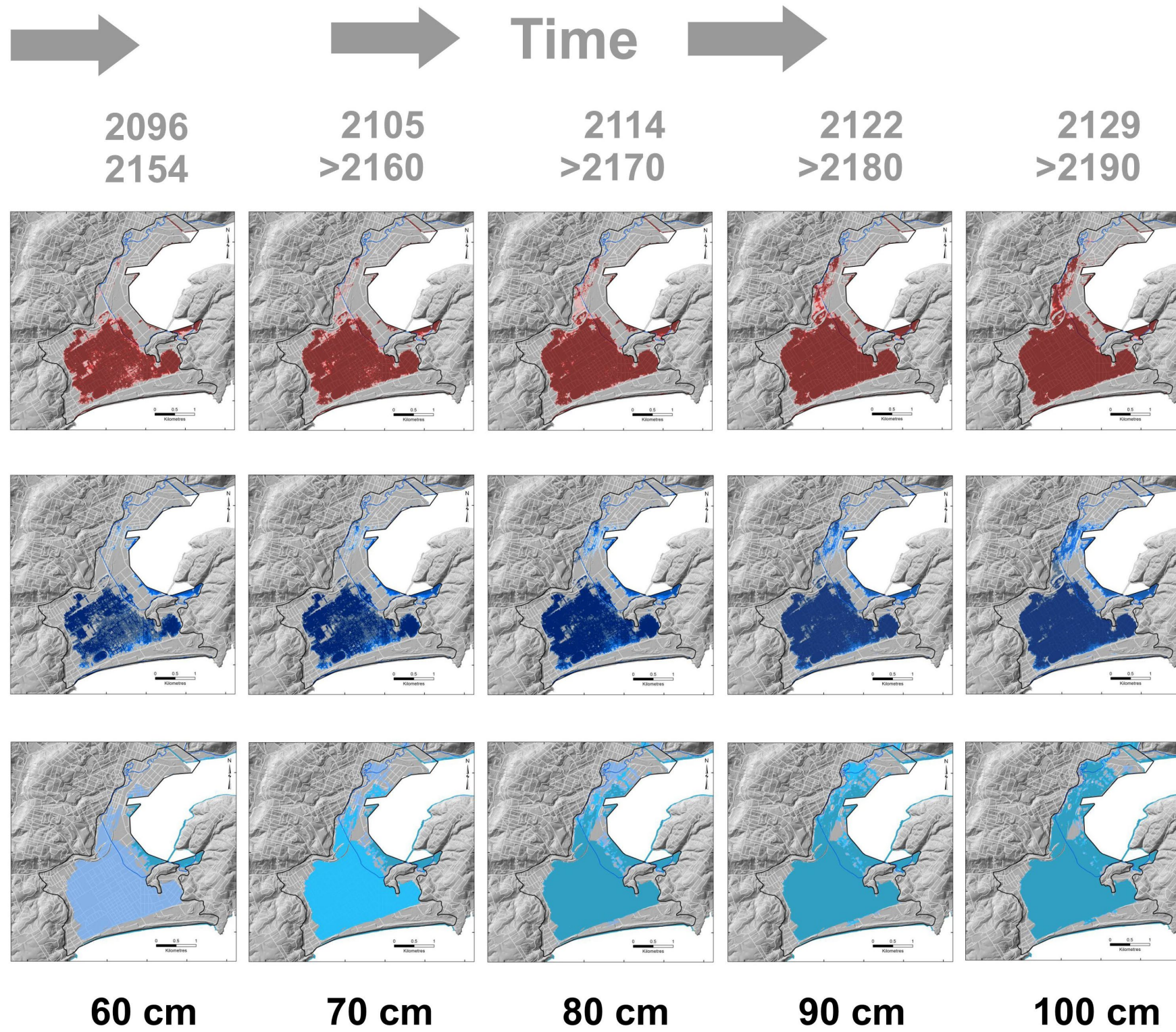


Figure A3.1 Continued from previous page.

APPENDIX 4 METADATA (CONTENT OF GIS DATASETS)

Table A4.1 Detailed description of GIS datasets generated from the 2019–2023 groundwater monitoring and used in this report. Data are found in the geodatabase *sthDunedin_water_table_2023model.gdb*, provided under Creative Commons Attribution 4.0 International licence, that can be downloaded from the Zenodo data archive site <http://doi.org/10.5281/zenodo.10035759>. The geodatabase contains 52 feature classes, listed here in alphabetical order.

File Name	Description
<i>DEM_Dunedin2021_HS</i>	Hillshade of 2021 LiDAR digital elevation model (DEM) of Dunedin land surface (modelled to remove buildings, trees, etc.). Extract from a published dataset. HillShade was created using an azimuth of 315 and elevation of 45 by GNS Science from LiDAR tiles along the coast of Otago Region, covering Milton, Catlins, Palmerston, Dunedin, Mosgiel and Oamaru, captured between 25 June and 1 October 2021. The DEM is available as a layer [Otago Coastal Catchments Lidar 1m DEM (2021): https://data.linz.govt.nz/layer/109627]. These datasets were generated by AAM Ltd and its subcontractors. Data management and distribution is by Toitū Te Whenua Land Information New Zealand. Licence: Creative Commons Attribution 4.0 International.
<i>DEM_Dunedin2021_NZVD2016</i>	2021 LiDAR DEM of Dunedin land surface (modelled to remove buildings, trees, etc.). Extracted from published dataset. Units in metres. 1 m grid. NZTM2000 projection. NZVD2016 vertical datum. This DEM was mosaiced and clipped by GNS Science from LiDAR tiles along the coast of Otago Region, covering Milton, Catlins, Palmerston, Dunedin, Mosgiel and Oamaru, captured between 25 June and 1 October 2021. The DEM is available as a layer [Otago Coastal Catchments Lidar 1m DEM (2021): https://data.linz.govt.nz/layer/109627]. The LAS point cloud and vendor project reports are available from (OpenTopography: https://portal.opentopography.org/datasets?search=new%20zealand). LiDAR was captured for Otago Regional Council by AAM Ltd between 25 June and 1 October 2021. These datasets were generated by AAM Ltd and its subcontractors. Data management and distribution is by Toitū Te Whenua Land Information New Zealand. Licence: Creative Commons Attribution 4.0 International.
<i>DOD_DSMminusDEM_2021</i>	A digital elevation of difference model showing the difference between the digital surface model (DSM) elevation (with buildings, trees, etc.) and the DEM (topographic elevation). Units in metres. 1 m grid. NZTM2000 projection. Generated by GNS Science, using raster calculator in ArcGIS to subtract the DEM of ground elevation from the DSM.
<i>DSM_Dunedin2021_HS</i>	Hillshade of the 2021 LiDAR DSM of Dunedin (includes buildings, trees, etc.). This hillshade was created using an azimuth of 315 and elevation of 45 by GNS Science from LiDAR tiles along the coast of Otago Region, covering Milton, Catlins, Palmerston, Dunedin, Mosgiel and Oamaru, captured between 25 June and 1 October 2021. The DEM is available as a layer [Otago Coastal Catchments Lidar 1m DEM (2021): https://data.linz.govt.nz/layer/109627]. These datasets were generated by AAM Ltd and its subcontractors. Data management and distribution is by Toitū Te Whenua Land Information New Zealand. Licence: Creative Commons Attribution 4.0 International.

File Name	Description
<i>DSM_Dunedin2021_NZVD2016</i>	<p>2021 LiDAR DSM of Dunedin (includes buildings, trees, etc.). Units in metres. 1 m grid. NZTM2000 projection. NZVD2016 vertical datum. This DSM was mosaiced and clipped by GNS Science from LiDAR tiles along the coast of Otago Region, covering Milton, Catlins, Palmerston, Dunedin, Mosgiel and Oamaru, captured between 25 June and 1 October 2021. The DEM is available as a layer [Otago Coastal Catchments LiDAR 1 m DEM (2021): https://data.linz.govt.nz/layer/109627].</p> <p>The LAS point cloud and vendor project reports are available from (OpenTopography: https://portal.opentopography.org/datasets?search=new%20zealand). LiDAR was captured for Otago Regional Council by AAM Ltd between 25 June and 1 October 2021. These datasets were generated by AAM Ltd and its subcontractors. Data management and distribution is by Toitū Te Whenua Land Information New Zealand. Licence: Creative Commons Attribution 4.0 International.</p>
<i>DTWmax_2023</i>	<p>Depth (below ground) of the maximum level of groundwater measured in 2019–2023. An interpolated grid surface (8 m cells) mapping the depth (metres relative to ground) to highest groundwater measured in the period 2019/03/06–2023/05/01. Surface generated using <i>GWLmax_2023</i>, with boundary points in the harbour (set at 1.245 m RL) and coast (1.300 m RL). Values in metres relative to the 2021 LiDAR land surface model.</p>
<i>DTWmean_2023</i>	<p>Depth (below ground) of the average level of groundwater measured in 2019–2023. An interpolated grid surface (8 m cells) mapping the depth (metres relative to ground) to average groundwater measured in the period 2019/03/06–2023/05/01. Surface generated using <i>GWLmean_2023</i>, boundary points in the harbour (set at -0.234 m RL) and coast (-0.075 m RL). Values in metres relative to the 2021 LiDAR land surface model.</p>
<i>DTWmean_2023_ag0</i>	<p>Depth (below ground) of the average level of groundwater measured in 2019–2023, with a re-classification of above-ground values. An interpolated grid surface (8 m cells) mapping the depth (metres relative to ground) to average groundwater measured in the period 2019/03/06–2023/05/01. Surface generated using <i>GWLmean_2023</i>, with boundary points in the harbour (set at -0.225 m RL) and coast (-0.073 m RL). Values in metres relative to the 2021 LiDAR land surface model, with any negative (i.e. above ground) values reset to zero.</p>
<i>DTWmedian_2023</i>	<p>Depth (below ground) of the median level of groundwater measured in 2019–2023. An interpolated grid surface (8 m cells) mapping the depth (metres relative to ground) to median groundwater level measured in the period 2019/03/06–2023/05/01. Surface generated using <i>GWLmedian_2023</i>, with boundary points in the harbour (-0.234 m), Andersons Bay inlet (0.25 m) and coast (-0.075 m). Values in metres relative to the 2021 LiDAR land surface model.</p>
<i>DTWmedian_2023_ag0</i>	<p>Depth (below ground) of the median level of groundwater measured in 2019–2023 with a re-classification of above-ground values. An interpolated grid surface (8 m cells) mapping the depth (metres relative to ground) to median groundwater level measured in the period 2019/03/06–2023/05/01. Surface generated using <i>GWLmedian_2023</i>, with boundary points in the harbour (-0.234 m), Andersons Bay inlet (0.25 m) and coast (-0.075 m). Values in metres relative to the 2021 LiDAR land surface model, with any negative (i.e. above ground) values reset to zero.</p>

File Name	Description
<i>DTWmhws_mean_2023</i>	A modelled depth (below ground) MHWS level of groundwater based on the mean value from <i>GWLmedian_2023</i> . An interpolated grid surface (8 m cells) mapping the depth (metres relative to ground) to MHWS level of groundwater measured in the period 2019/03/06–2023/05/01. Model is based on the present-day difference between MHWS and MSL (0.98 m MHWS7 in ocean at Green Island), multiplied by the tidal efficiency grid of groundwater fluctuations (Note: need to divide tidal efficiency [TE] values in % to a proportion) to get $GWLmhws_mean2023 = GWLmean_2023 + (0.98 \times TE)$. Values are then subtracted from the DEM to give depth in metres relative to the 2021 LiDAR land surface model. Note: negative values in this model suggest areas where groundwater may be above ground, i.e. inundation, but the absolute values are very unlikely to reflect actual pressure or depth of ponding.
<i>DTWmhws_mean_2023_ag0</i>	A modelled depth (below ground) MHWS level of groundwater based on the mean value from <i>GWLmedian_2023</i> , with a re-classification of above-ground values. An interpolated grid surface (8 m cells) mapping the depth (metres relative to ground) to MHWS level of groundwater measured in the period 2019/03/06–2023/05/01. Model is based on the present-day difference between MHWS and MSL (0.98 m MHWS7 in ocean at Green Island), multiplied by the tidal efficiency grid of groundwater fluctuations (Note: need to divide tidal efficiency [TE] values in % to a proportion) to get $GWLmhws_mean2023 = GWLmean_2023 + (0.98 \times TE)$. Values are then subtracted from the DEM to give depth in metres relative to the 2021 LiDAR land surface model, with any above-ground values reset to zero.
<i>DTWmhws_median_2023</i>	A modelled depth (below ground) MHWS level of groundwater based on the median value from <i>GWLmedian_2023</i> . An interpolated grid surface (8 m cells) mapping the depth (metres relative to ground) to MHWS level of groundwater measured in the period 2019/03/06–2023/05/01. Model is based on the present-day difference between MHWS and MSL (0.98 m MHWS7 in ocean at Green Island), multiplied by the tidal efficiency grid of groundwater fluctuations (Note: need to divide tidal efficiency [TE] values in % to a proportion) to get $GWLmhws_median2023 = GWLmedian_2023 + (0.98 \times TE)$. Values are then subtracted from the DEM to give depth in metres relative to the 2021 LiDAR land surface model. Note: negative values in this model suggest areas where groundwater may be above ground, i.e. inundation, but the absolute values are very unlikely to reflect actual pressure or depth of ponding.
<i>DTWmhws_median_2023_ag0</i>	A modelled depth (below ground) MHWS level of groundwater based on the median value from <i>GWLmedian_2023</i> . An interpolated grid surface (8 m cells) mapping the depth (metres relative to ground) to MHWS level of groundwater measured in the period 2019/03/06–2023/05/01. Model is based on the present-day difference between MHWS and MSL (0.98 m MHWS7 in ocean at Green Island), multiplied by the tidal efficiency grid of groundwater fluctuations (Note: need to divide tidal efficiency [TE] values in % to a proportion) to get $GWLmhws_median2023 = GWLmedian_2023 + (0.98 \times TE)$. Values are then subtracted from the DEM to give depth in metres relative to the 2021 LiDAR land surface model, with any above-ground values reset to zero.

File Name	Description
<i>DTWmin_2023</i>	Depth (below ground) of the minimum level of groundwater measured in 2019–2023. An interpolated grid surface (8 m cells) mapping the depth (metres relative to ground) to lowest groundwater measured in the period 2019/03/06–2023/05/01. Surface generated using <i>GWLmin_2023</i> , with boundary points in the harbour (-1.546 m), Andersons Bay inlet (0.19 m) and coast (-1.473 m). Values in metres relative to the 2021 LiDAR land surface model.
<i>DTWp5_2023</i>	Depth (below ground) of the 5 th percentile groundwater level measured in 2019–2023. An interpolated grid surface (8 m cells) mapping the depth (metres relative to ground) to 5 th percentile of groundwater measured in the period 2019/03/06–2023/05/01. Surface generated using <i>GWLp05_2023</i> , with boundary points in the harbour (-1.142 m), Andersons Bay inlet (0.2 m) and coast (-0.913 m). Values in metres relative to the 2021 LiDAR land surface model.
<i>DTWp95_2023</i>	Depth (below ground) of the 95 th percentile groundwater level measured in 2019–2023. An interpolated grid surface (8 m cells) mapping the depth (metres relative to ground) to 95 th percentile of groundwater measured in the period 2019/03/06–2023/05/01. Surface generated using <i>GWLp95_2023</i> , with boundary points in the harbour (0.71502 m), Andersons Bay inlet (0.7 m) and coast (0.775 m). Values in metres relative to the 2021 LiDAR land surface model.
<i>GWLmax_2023</i>	An interpolated grid surface (8 m cells) mapping the maximum elevation (metres NZVD2016) of groundwater monitored in the period 2019/03/06–2023/05/01. Surface generated using boundary points for the Harbour (set at 1.245 m), Andersons Bay (1.182 m RL) and coast (1.300 m RL). Excludes shallow wells in perched aquifer (CE17/0108, 0117, 0118, 0124) and artesian/semi-confined sites (CE17/0127, ASB_BH_107).
<i>GWLmean_2023</i>	An interpolated grid surface (8 m cells) mapping the mean elevation (metres NZVD2016) of groundwater monitored in the period 2019/03/06–2023/05/01. Surface generated using boundary points for the Harbour (set at -0.225 m), Andersons Bay (0.25 m RL) and coast (-0.073 m RL). Excludes shallow wells in perched aquifer (CE17/0108, 0117, 0118, 0124) and artesian/semi-confined sites (CE17/0127, ASB_BH_107). Although 2021–2023 was dry, it appears to be reasonably representative of the long-term mean values (checked against 2010–2018).
<i>GWLmedian_2023</i>	An interpolated grid surface (8 m cells) mapping the median elevation (metres NZVD2016) of groundwater monitored in the period 2019/03/06–2023/05/01. Surface generated using boundary points for the Harbour (set at -0.234 m), Andersons Bay (0.25 m RL) and coast (-0.075 m RL). Excludes shallow wells in perched aquifer (CE17/0108, 0117, 0118, 0124) and artesian/semi-confined sites (CE17/0127, ASB_BH_107). Although 2021–2023 was generally dry, it appears to be reasonably representative of the long-term mean values (checked against 2010–2018).
<i>GWLmedian_2023_25cmContours</i>	Contour lines (at 25 cm intervals, NZVD2016) representing the elevation of the median potentiometric surface height, generated from the interpolated surface <i>GWLmedian_2023</i> .

File Name	Description
<i>GWLmedian_2023_v134</i>	An interpolated grid surface (8 m cells) mapping the median elevation (metres NZVD2016) of groundwater monitored in the period 2019/03/06–2023/05/01. Surface generated using boundary points for the harbour (-0.225 m), Andersons Bay inlet (0.25 m) and coast (-0.073 m) using the same original data points as <i>GWLmedian_2023</i> but including observations of Fordyce (2014) from wells in 2012/07/13–2012/09/17. Excludes shallow wells in perched aquifer (CE17/0108, 0117, 0118, 0124). Note: there are issues with large uncertainty in the survey heights / absolute values of Fordyce piezometers. Provided for comparative purposes only – not to be used as a groundwater surface.
<i>GWLmhwms_mean_2023</i>	A modelled MHWS level of groundwater above the mean elevation. An interpolated grid surface (8 m cells) mapping the groundwater elevation at MHWS. A tidal offset to <i>GWLmean_2023</i> based on the present-day difference between MHWS and MSL (0.98 m MHWS7 in ocean at Green Island), multiplied by the tidal efficiency grid of groundwater fluctuations (Note: need to divide tidal efficiency [TE] values in % to a proportion). $GWLmhwms_mean2023 = GWLmean_2023 + (0.98 \times TE)$.
<i>GWLmhwms_median_2023</i>	A modelled MHWS level of groundwater above the median elevation. An interpolated grid surface (8 m cells) mapping the groundwater elevation at MHWS. A tidal offset to <i>GWLmedian_2023</i> based on the present-day difference between MHWS and MSL (0.98 m MHWS7 in ocean at Green Island), multiplied by the tidal efficiency grid of groundwater fluctuations (Note: need to divide tidal efficiency [TE] values in % to a proportion). $GWLmhwms_median2023 = GWLmedian_2023 + (0.98 \times TE)$.
<i>GWLmin_2023</i>	An interpolated grid surface (8 m cells) mapping the minimum elevation (metres NZVD2016) of groundwater monitored in the period 2019/03/06–2023/05/01. Surface generated using boundary points for the harbour (-1.546 m), Anderson Bay inlet (0.19 m) and coast (-1.473 m). Excludes shallow wells in perched aquifer (CE17/0108, 0117, 0118, 0124) and artesian/semi-confined sites (CE17/0127, ASB_BH_107).
<i>GWLp5_2023</i>	An interpolated grid surface (8 m cells) mapping the 5 th percentile elevation (metres NZVD2016) of groundwater monitored in the period 2019/03/06–2023/05/01. Surface generated using boundary points for the harbour (-1.142 m), Andersons Bay inlet (0.2 m) and coast (-0.913 m). Excludes shallow wells in perched aquifer (CE17/0108, 0117, 0118, 0124) and artesian/semi-confined sites (CE17/0127, ASB_BH_107).
<i>GWLp95_2023</i>	An interpolated grid surface (8 m cells) mapping the 95 th percentile elevation (metres NZVD2016) of groundwater monitored in the period 2019/03/06–2023/05/01. Surface generated using boundary points for the harbour (0.715 m), Andersons Bay inlet (0.7 m) and coast (0.775 m). Excludes shallow wells in perched aquifer (CE17/0108, 0117, 0118, 0124) and artesian/semi-confined sites (CE17/0127, ASB_BH_107).

File Name	Description
<i>GWLrange_2023</i>	An interpolated grid surface (8 m cells) mapping the RANGE of groundwater levels (m) monitored in the period 2019/03/06–2023/05/01. Surface generated by subtracting the maximum and minimum elevations at each site, then interpolating that difference using boundary points for the harbour (2.791 m), Andersons Bay inlet (0.99 m) and coast (2.773 m). Excludes shallow wells in perched aquifer (CE17/0108, 0117, 0118, 0124) and artesian/semi-confined sites (CE17/0127, ASB_BH_107).
<i>GWLstdev_2023</i>	An interpolated grid surface (8 m cells) mapping the standard deviation of groundwater levels (metres) monitored in the period 2019/03/06–2023/05/01. Surface generated using boundary points for the harbour (0.611 m) and coast (0.555 m). Excludes shallow wells in perched aquifer (CE17/0108, 0117, 0118, 0124) and artesian/semi-confined sites (CE17/0127, ASB_BH_107).
<i>modelling_coastline</i>	Polygon defining the onshore land area. Includes Harbourside and South Dunedin.
<i>modelling_extent_full</i>	Polygon defining the area of low-lying land for interpolation of models. Includes Harbourside and South Dunedin.
<i>modelling_extent_SthD</i>	Polygon defining the area of South Dunedin area that is incorporated in the numerical model of Chambers et al. (2023) (https://doi.org/10.3389/feart.2023.1111065).
<i>modelling_region_snap_poly</i>	Polygon defining the wider area around Dunedin for clipping rasters. Includes areas of the hill suburbs. Vertices positioned at X.0 m NZTM precision.
<i>modelpoints_2023_RRI</i>	A point dataset, extracted from <i>piezo_data_202308</i> , used in August 2023 for modelling. Created to minimise definition queries when interpolating the Rainfall Recharge Index (RRI) surface.
<i>modelpoints_2023_TIDES</i>	A point dataset, extracted from <i>piezo_data_202308</i> , used in August 2023 for modelling. Created to minimise definition queries when interpolating tidal efficiency and amplitude surfaces.
<i>modelpoints_v2023_v134</i>	A point dataset, extracted from <i>piezo_data_202308</i> , used in August 2023 for modelling. Created to minimise definition queries when interpolating surfaces. 'v134' refers to the model number: 1 = Otago Regional Council piezometers, 2 = perched aquifer; 3 = Fordyce piezometers; 4 = I44/1121 Fitzroy St; 5 = artesian CE17/0127 and semi-confined ASB_BH_107.
<i>modelpoints_2023_v14</i>	A point dataset, extracted from <i>piezo_data_202308</i> , used in August 2023 for modelling. Created to minimise definition queries when interpolating surfaces. 'v14' refers to the model number: 1 = Otago Regional Council piezometers, 2 = perched aquifer, 3 = Fordyce piezometers, 4 = I44/1121 Fitzroy St, 5 = artesian CE17/0127 and semi-confined ASB_BH_107.
<i>modelpoints_perched_aquifer_2023</i>	Data (metres NZVD2016) around the outer margin of a perched aquifer in coastal dune sand (for modelling groundwater levels). Interpreted and extrapolated values of groundwater level (metres NZVD2016) assigned around the outer margin of a perched aquifer in coastal dune sand. For modelling 'median' groundwater levels.
<i>perched_aquifer_outline</i>	Polygon defining the outer limit of groundwater perched in sand dunes in the St Kilda to Moana Rua area. Defined by monitoring at CE17/0108, 0117, 0118, 0124.

File Name	Description
<i>perched_DTWmedian_2023</i>	An interpolated grid surface (8 m cells) mapping the depth (metres relative to ground) of perched groundwater in dune sand at St Kilda. Median data derived from monitoring at CE17/0108, 0117, 0118, 0124. Surface generated using <i>perched_GWLmedian</i> relative to the 2021 LiDAR land surface model.
<i>perched_GWLmedian_2023</i>	An interpolated grid surface (8 m cells) mapping the elevation (metres NZVD2016) of perched groundwater in dune sand at St Kilda. Median data derived from monitoring at CE17/0108, 0117, 0118, 0124. Surface generated using piezometer data and <i>perched_aquifer_modelpts</i> .
<i>piezo_data_202308</i>	Data for monitoring wells and coastal/harbour points. 'Raw' point dataset used in August 2023 for modelling. Updated from <i>piezo_data_202003</i> – including better locations for Fordyce (2014) wells. Attributes include well XYZ location, measuring point elevation, chemical data, event groundwater levels, groundwater statistical values, etc.
<i>RAIN_pervious_surface_model</i>	Grid model of urban surfaces that are pervious or impervious to rainfall – for the South Dunedin area (does not include all of Harbourside). Model has pervious value = 1 and impervious value = 0 surfaces. Generated by (i) Normalised Vegetation Difference Index (NVDI) classification of 2013 aerial photographs (https://data.linz.govt.nz/layer/52118-dunedin-0125m-urban-aerial-photos-2013/), (ii) binary threshold filtering of the NVDI image (method of Otsu [1979]) and (iii) adding LINZ building outlines (https://data.linz.govt.nz/layer/101290-nz-building-outlines/) as impervious areas so as to remove red roofs and red cars that would otherwise show as pervious. Generated by Frederika Mourou / GNS Science, 2021, using imagery supplied by University of Otago Surveying (P. Sirguey), with additional work by Simon Cox in 2022
<i>RAINstorage_fromGWLmax_2023</i>	Grid model estimate of the rainfall infiltration limit (in millimetres) and/or available storage before groundwater can be expected to reach the ground surface, based on the maximum position of groundwater (<i>GWLmax_2023</i>) and an RRI grid of response site values observed to 10–30 mm rainfall events in 2019–2023 and 2012 (Fordyce [2014] data). Any grid points returning values >1000 mm, reflecting deep groundwater or very low RRI, exceed the limit of any daily (24 hour) rainfall expected for Dunedin.
<i>RAINstorage_fromGWLmedian_2023</i>	Grid model estimate of the rainfall infiltration limit (in millimetres) and/or available storage before groundwater can be expected to reach the ground surface, based on the median position of groundwater (<i>GWLmedian_2023</i>) and an RRI grid of response site values observed to 10–30 mm rainfall events in 2019–2023 and 2012 (Fordyce data). Any grid points returning values >1000 mm, reflecting deep groundwater or very low RRI, exceed the limit of any daily (24 hour) rainfall expected for Dunedin.
<i>RAINstorage_fromGWLmean_2023</i>	Grid model estimate of the rainfall infiltration limit (in millimetres) and/or available storage before groundwater can be expected to reach the ground surface, based on the mean position of groundwater (<i>GWLmean_2023</i>) and an RRI grid of response site values observed to 10–30 mm rainfall events in 2019–2023 and 2012 (Fordyce data). Any grid points returning values >1000 mm, reflecting deep groundwater or very low RRI, exceed the limit of any 24-hour rainfall expected for Dunedin.

File Name	Description
<i>RAINstorage_ fromGWLmin_2023</i>	Grid model estimate of the rainfall infiltration limit (in millimetres) and/or available storage before groundwater can be expected to reach the ground surface, based on the minimum position of groundwater (<i>GWLmin_2023</i>) and an RRI grid of response site values observed to c.30 mm rainfall events in 2019 and 2012 (Fordyce data). Any grid points returning values >1000 mm, reflecting deep groundwater or very low RRI, exceed the limit of any 24 hour rainfall expected for Dunedin.
<i>RRI_2023</i>	An interpolated grid (8 m cells) of the dimensionless RRI. Site values are calculated from observations of change in groundwater level divided by the rainfall amount (dGWL/TotalRain). Sites can be expected to have variable responses depending on local stormwater drainage, extent of 'hard' urban surfaces, piezometers / well completion and subsurface sediment storativity and permeability. Changes in groundwater level have been normalised against rainfall measured at Musselburgh, which assumes that rainfall is constant across the city. Sites in model numbers v1–4 were included in the interpolation: 1 = Otago Regional Council piezometers, 2 = perched aquifer; 3 = Fordyce piezometers; 4 = I44/1121 Fitzroy St (not included was model number 5 = artesian CE17/0127 and semi-confined ASB_BH_107).
<i>RRI_contours</i>	Contours (in values = 1) from an interpolated grid (8 m cells) of the dimensionless RRI. Site values are calculated from observations of rainfall events and representative values selected for interpolation. Sites can be expected to have variable responses depending on local stormwater drainage, extent of 'hard' urban surfaces, piezometers / well completion and subsurface sediment storativity and permeability. Changes in groundwater level have been normalised against rainfall measured at Musselburgh, which assumes that rainfall is constant across the city.
<i>TE_percent</i>	An interpolated grid (8 m cells) of the dimensionless tidal efficiency (in %) derived from the ratio of the tidal change of groundwater level in piezometers to the tidal change in the nearby ocean or harbour (as measured at Green Island and Fryatt St) driving the tidal response. Note: the upper Dunedin Harbour has ~110% TE relative to Green Island due to a geometrical amplification effect; some sites have no tides or have fluctuations that are below detection level (2–3 mm).
<i>TIDE_amplitude</i>	An interpolated grid (8 m cells) of the groundwater 6.2 hour Tidal Amplitude measured in piezometers, interpolated with coastal (0.75 m) and harbour (0.9 m) boundary points. Note: some sites only show tides at certain lower groundwater levels, others show no tides above the lower limit of detection of pressure transducers.
<i>TIDE_range</i>	An interpolated grid (8 m cells) of the groundwater high to low tidal range measured in piezometers, interpolated with coastal (1.5 m) and harbour (1.8 m) boundary points.

Table A4.2 Detailed description of GIS datasets generated to forecast the potential effects of sea-level rise in this report. Data are found in the geodatabase *sthDunedin_water_table_forecasts.gdb* that can be downloaded from the Zenodo data archive site: <http://doi.org/10.5281/zenodo.10035759>. The geodatabase contains 594 feature classes that are provided under Creative Commons Attribution 4.0 International licence. Rather than describing all layers individually, these data are described here using a series of variables where: [OFF] is the offset of sea-level rise as 000, 010, 020, etc., cm; [ARI] is the ESL ARI as 1, 10, 100, 1000 years; and [AFI] the average recurrence interval of 12-hour rainfall as 002, 005, 010, 050, 100 years.

File Name	Description
<i>DTW[OFF]cm_GWLMedian_ESL[ARI]</i>	An interpolated grid surface (8 m cells) mapping the forecast DTW depth to groundwater (in metres relative to ground) after [OFF] cm of sea-level rise, assuming equilibration with a storm-surge tide (as an ESL at an ARI from published NIWA data [Stephens et al. 2020]). A storm-tide effect was calculated from the ocean and harbour ESL at [ARI] year ARI using an interpolation of tidal efficiency observations from boreholes. The storm-tide effect on groundwater was then added to the <i>GWLmedian_2023</i> level, offset by a constant [OFF] cm for the sea-level rise that will have occurred. The resultant <i>SLR[OFF]cm_GWLmedian_ESL[ARI]</i> grid was then subtracted from the ground elevation DEM. Values are provided in metres relative to the 2021 LiDAR land surface model. Negative values represent emergence (i.e. above model inundation) of groundwater.
<i>DTW[OFF]cm_GWLMedian_MED</i>	An interpolated grid surface (8 m cells) mapping the forecast DTW depth to median groundwater (metres relative to ground) after [OFF] cm of sea-level rise. The grid <i>GWLmedian_2023</i> , based on 2019–2023 observations, was offset by a constant [OFF] cm for the sea-level rise that may have occurred. The resultant <i>SLR[OFF]cm_GWLmedian_MED</i> grid was then subtracted from the ground elevation DEM. Values are provided in metres relative to the 2021 LiDAR land surface model. Negative values represent emergence/inundation of groundwater.
<i>DTW[OFF]cm_GWLMedian_MHWS</i>	An interpolated grid surface (8 m cells) mapping the forecast DTW depth to groundwater (metres relative to ground) after [OFF] cm of sea-level rise that can be expected to occur at MHWS. A tide effect was calculated from the ocean and harbour MHWS levels using an interpolation of tidal efficiency observations from boreholes. The tide effect was then added to the <i>GWLmedian_2023</i> level, offset by a constant [OFF] cm for the sea-level rise that will have occurred. The resultant <i>SLR[OFF]cm_GWLmedian_MHWS</i> grid was then subtracted from the ground elevation DEM. Values are provided in metres relative to the 2021 LiDAR land surface model. Negative values represent emergence/inundation of groundwater.
<i>DTW[OFF]cm_GWlp95</i>	An interpolated grid surface (8 m cells) mapping the forecast DTW depth to a HIGH (95 th percentile) level of groundwater (metres relative to ground) after [OFF] cm of sea-level rise. The interpolated grid <i>GWlp95_2023</i> , based on 2019–2023 observations, was offset by a constant [OFF] cm for the sea-level rise that may have occurred. The resultant <i>SLR[OFF]cm_GWlp95</i> grid was then subtracted from the ground elevation DEM. Values are provided in metres relative to the 2021 LiDAR land surface model. Negative values represent emergence/inundation of groundwater.

File Name	Description
<i>poly_DTW[OFF]cm_GWLMedian_ESL [ARI]</i>	Polygon coverage showing areas where emergent groundwater has been forecast. Based on the present-day (2019–2023) geometry of the water table and tidal variability, offset for a storm-surge tide and ESL (at [ARI]-year return interval), plus an amount ([OFF] cm) of sea-level rise. Defined where the 8 x 8 m grid <i>DTW[OFF]cm_GWLMedian_ESL[ARI]</i> ≤ 0 m.
<i>poly_DTW[OFF]cm_GWLMedian_MED</i>	Polygon coverage showing areas where emergent groundwater has been forecast. Based on the present-day (2019–2023) median position of the water table, plus an amount ([OFF] cm) of sea-level rise. Defined where the 8 x 8 m grid <i>DTW[OFF]cm_GWLMedian_MHWS</i> ≤ 0 m.
<i>poly_DTW[OFF]cm_GWLMedian_MHWS</i>	Polygon coverage showing areas where emergent groundwater has been forecast. Based on the present-day (2019–2023) geometry of the water table and tidal variability, plus an amount ([OFF] cm) of sea-level rise. Defined where the 8 x 8 m grid <i>DTW[OFF]cm_GWLMedian_MHWS</i> ≤ 0 m.
<i>poly_DTW[OFF]cm_GWLp95</i>	Polygon coverage showing areas where emergent groundwater has been forecast. Based on the present-day (2019–2023) 95 th percentile position of the water table, plus an amount ([OFF] cm) of sea-level rise. Defined where the 8 x 8 m grid <i>DTW[OFF]cm_GWLp95</i> ≤ 0 m.
<i>poly_RAINstor_12hrEXC_SLR [OFF]cm_ARI[AFI]_MED</i>	Polygons showing places where the predicted depth of 12-hour rainfall at [AFI] year ARI (using NIWA High Intensity Rainfall Design System (HIRDS) predictions for Musselburgh weather station ⁴) exceeds the available subsurface storage of rainfall infiltration in unsaturated pore-space above the water table, referenced by the depth to median groundwater after [OFF] cm of sea-level rise. Derived from an 8 m grid model equivalent <i>RAINstor_12hrEXC_SLR[OFF]cm_ARI[AFI]_MED</i> . May be useful for showing areas that require drainage and/or are exposed to elevated pluvial flood hazard due to influence of groundwater.
<i>poly_RAINstor_12hrEXC_SLR [OFF]cm_ARI[AFI]_MHWS</i>	Polygons showing places where the predicted depth of 12-hour rainfall at [AFI] year ARI (using NIWA HIRDS predictions for Musselburgh weather station) exceeds the available subsurface storage of rainfall infiltration in unsaturated pore-space above the water table, referenced by the depth to MHWS groundwater after [OFF] cm of sea-level rise. Derived from an 8 m grid model equivalent <i>RAINstor_12hrEXC_SLR[OFF]cm_ARI[AFI]_MED</i> . May be useful for showing areas that require drainage and/or are exposed to elevated pluvial flood hazard due to influence of groundwater.
<i>poly_RAINstor_12hrEXC_SLR [OFF]cm_ARI[AFI]_p95</i>	Polygons showing places where the predicted depth of 12-hour rainfall at [AFI] year ARI (using NIWA HIRDS predictions for Musselburgh weather station) exceeds the available subsurface storage of rainfall infiltration in unsaturated pore-space above the water table, referenced by the depth to the (2019–2023) 95 th percentile elevation of groundwater after [OFF] cm of sea-level rise. Derived from an 8m grid model equivalent <i>RAINstor_12hrEXC_SLR[OFF]cm_ARI[AFI]_MED</i> . May be useful for showing areas that require drainage and/or are exposed to elevated pluvial flood hazard due to influence of groundwater.

4 <https://hirds.niwa.co.nz>

File Name	Description
<i>RAINstor_12hrEXC_SLR[OFF]cm_ARI[AFI]_MED</i>	A grid model (8 m cells) showing places where the predicted depth of 12-hour rainfall at [AFI] year ARI (using NIWA HIRDS predictions for Musselburgh weather station) exceeds the available subsurface storage of rainfall infiltration in unsaturated pore-space above the water table, referenced by the depth to median groundwater after [OFF] cm of sea-level rise. May be useful for showing areas that require drainage and/or are exposed to elevated pluvial flood hazard due to influence of groundwater.
<i>RAINstor_12hrEXC_SLR[OFF]cm_ARI[AFI]_MHWS</i>	A grid model (8 m cells) showing places where the predicted depth of 12-hour rainfall at [AFI] year ARI (using NIWA HIRDS predictions for Musselburgh weather station) exceeds the available subsurface storage of rainfall infiltration in unsaturated pore-space above the water table, referenced by the depth to MHWS groundwater after [OFF] cm of sea-level rise. May be useful for showing areas that require drainage and/or are exposed to elevated pluvial flood hazard due to influence of groundwater.
<i>RAINstor_12hrEXC_SLR[OFF]cm_ARI[AFI]_p95</i>	A grid model (8 m cells) showing places where the predicted depth of 12-hour rainfall at [AFI] year ARI (using NIWA HIRDS predictions for Musselburgh weather station) exceeds the available subsurface storage of rainfall infiltration in unsaturated pore-space above the water table, referenced by the depth to the (2019–2023) 95 th percentile elevation of groundwater after [OFF] cm of sea-level rise. May be useful for showing areas that require drainage and/or are exposed to elevated pluvial flood hazard due to influence of groundwater.
<i>RAINstor_mm_SLR[OFF]cm_MED</i>	An estimate of the subsurface storage (in millimetres of rain) and/or limit of infiltration before groundwater can be expected to reach the ground surface and become emergent. Based on the median position of groundwater (<i>GWLMedian_2023</i>) after [OFF] cm of sea-level rise. Derived using the RRI grid of site-response values observed during 10–30 mm rainfall events between 2019–2023 and 2012 (Fordyce data) together with depth to groundwater from 2021 LiDAR. Any grid points returning values >1000 mm reflect deep groundwater or very low RRI, which exceeds the limit of any 24-hour rainfall expected for Dunedin. Any grid points with negative above-ground water levels have been set to zero. The estimate is expected to be useful for understanding the influence of high groundwater on pluvial flooding.
<i>RAINstor_mm_SLR[OFF]cm_MHWS</i>	An estimate of the subsurface storage (in millimetres of rain) and/or limit of infiltration before groundwater can be expected to reach the ground surface and become emergent. Based on the MHWS position of groundwater (<i>GWLMhws_2023</i>) after [OFF] cm of sea-level rise. Derived using the RRI grid of site-response values observed during 10–30 mm rainfall events between 2019–2023 and 2012 (Fordyce data) together with depth to groundwater from 2021 LiDAR. Any grid points returning values >1000 mm reflect deep groundwater or very low RRI, which exceeds the limit of any daily (24 hour) rainfall expected for Dunedin. Any grid points with negative above-ground water levels have been set to zero. The estimate is expected to be useful for understanding the influence of high groundwater on pluvial flooding.

File Name	Description
<i>RAINstor_mm_SLR[OFF]cm_p95</i>	An estimate of the subsurface storage (in millimetres of rain) and/or limit of infiltration before groundwater can be expected to reach the ground surface and become emergent. Based on the high 95 th percentile (p95) position of groundwater (<i>GWLp95_2023</i>) after [OFF] cm of sea-level rise. Derived using the RRI grid of response site values observed during 10–30 mm rainfall events between 2019–2023 and 2012 (Fordyce data) together with depth to groundwater from 2021 LiDAR. Any grid points returning values >1000 mm reflects deep groundwater or very low RRI, which exceeds the limit of any daily (24 hour) rainfall expected for Dunedin. Any grid points with negative above-ground water levels have been set to zero. The estimate is expected to be useful for understanding the influence of high groundwater on pluvial flooding.
<i>SLR[OFF]cm_GWLMedian_ESL[ARI]</i>	An interpolated grid surface (8 m cells) mapping the elevation (metres NZVD2016) of groundwater equilibrated with [RI] year ARI ESL storm-surge conditions and [OFF] cm sea-level rise. An offset of [OFF] cm was added to the <i>GWLmedian_2023</i> to create <i>SLR[OFF]cm_GWLmedian</i> , then a storm-tide component added to lift the groundwater from median to an assumed condition of equilibration with ESL. The tidal component was based on published ESL at [ARI] year ARI (NIWA data: Stephens et al. [2020]), multiplied by the local tidal efficiency of groundwater fluctuations that decay near-exponentially with distance from the harbour and ocean.
<i>SLR[OFF]cm_GWLMedian_MED</i>	An interpolated grid surface (8 m cells) mapping the elevation (metres NZVD2016) of median groundwater equilibrated with the ocean and harbour after [OFF] cm sea-level rise. A simple [OFF] cm offset was added to the interpolated <i>GWLmedian_2023</i> surface.
<i>SLR[OFF]cm_GWLMedian_MHWS</i>	An interpolated grid surface (8 m cells) mapping the elevation (metres NZVD2016) of groundwater at MHWS equilibrated with the ocean and harbour after [OFF] cm sea-level rise. An offset of [OFF] cm was added to the <i>GWLmedian_2023</i> to create <i>SLR[OFF]cm_GWLmedian</i> , then a tidal component added to lift the median to a MHWS level. The tidal offset was based on the present-day difference between MHWS7 and MLOS (0.98 m at Green Island), multiplied by the observed local tidal efficiency of groundwater fluctuations. The harbour tidal efficiency is 110% relative to the ocean (100%) due to amplification.
<i>SLR[OFF]cm_GWLp95</i>	An interpolated grid surface (8 m cells) mapping the elevation (metres NZVD2016) of high (p95) groundwater and its equilibration with the ocean and harbour after [OFF] cm sea-level rise. A simple [OFF] cm offset was added to the interpolated <i>GWLp95_2023</i> surface.

File Name	Description
<i>DTW[OFF]cm_GWLMedian_ESL[ARI]</i>	An interpolated grid surface (8 m cells) mapping the forecast DTW depth to groundwater (in metres relative to ground) after [OFF] cm of sea-level rise, assuming equilibration with a storm-surge tide (as an ESL at an ARI from published NIWA data [Stephens et al. 2020]). A storm-tide effect was calculated from the ocean and harbour ESL at [ARI] year ARI using an interpolation of tidal efficiency observations from boreholes. The storm-tide effect on groundwater was then added to the <i>GWLmedian_2023</i> level, offset by a constant [OFF] cm for the sea-level rise that will have occurred. The resultant <i>SLR[OFF]cm_GWLmedian_ESL[ARI]</i> grid was then subtracted from the ground elevation DEM. Values are provided in metres relative to the 2021 LiDAR land surface model. Negative values represent emergence (i.e. above model inundation) of groundwater.
<i>DTW[OFF]cm_GWLMedian_MED</i>	An interpolated grid surface (8 m cells) mapping the forecast DTW depth to median groundwater (metres relative to ground) after [OFF] cm of sea-level rise. The grid <i>GWLmedian_2023</i> , based on 2019–2023 observations, was offset by a constant [OFF] cm for the sea-level rise that may have occurred. The resultant <i>SLROFFcm_GWLmedian_MED</i> grid was then subtracted from the ground elevation DEM. Values are provided in metres relative to the 2021 LiDAR land surface model. Negative values represent emergence/inundation of groundwater.
<i>DTW[OFF]cm_GWLMedian_MHWS</i>	An interpolated grid surface (8 m cells) mapping the forecast DTW depth to groundwater (metres relative to ground) after [OFF] cm of sea-level rise that can be expected to occur at MHWS. A tide effect was calculated from the ocean and harbour MHWS levels using an interpolation of tidal efficiency observations from boreholes. The tide effect was then added to the <i>GWLmedian_2023</i> level, offset by a constant [OFF] cm for the sea-level rise that will have occurred. The resultant <i>SLR[OFF]cm_GWLmedian_MHWS</i> grid was then subtracted from the ground elevation DEM. Values are provided in metres relative to the 2021 LiDAR land surface model. Negative values represent emergence/inundation of groundwater.

Table A4.3 Detailed description of GIS datasets generated for the Dunedin City Council three waters service network, containing data and observations extracted from interpolated models of groundwater data for Dunedin. Data are found in the geodatabase *DCC_Services_2023.gdb*, which can be downloaded from the Zenodo data archive site <http://doi.org/10.5281/zenodo.10035759>. The geodatabase contains 24 feature classes that are provided under Creative Commons Attribution 4.0 International licence.

File Name	Description
<i>DCC_Foul_Sewer_catchments_withGWdata</i>	Dunedin City Council foul sewer (wastewater) sub-catchment polygons, exported from Infoworks and with geometry repaired, then assigned with mean values within the polygon areas extracted from interpolated 8 m grid models of groundwater. Includes a series of different attributes of present-day position of groundwater and local rain storage.
<i>DCC_Foul_Sewer_modelpoints_v2023</i>	A point dataset selection of Dunedin City Council foul sewer network nodes on the coastal plain (groundwater model area) that have surveyed elevation data available. Groundwater data from the interpolated surfaces have been extracted to these points (e.g. <i>LIDAR_VD16</i> , <i>GWL_median</i> , <i>GWL_max</i> , etc.). Used to model <i>DCC_Foul_SewerRL_VD2016</i> .
<i>DCC_Foul_Sewer_Node_Inverts</i>	Point dataset, originally supplied by Dunedin City Council, of wastewater (foul sewer) network nodes and their elevation (ILEV) in Dunedin Drainage Datum (= NZVD2016 + 100.376). At each point, the various models of water-table elevation are derived as attributes for that site: <ul style="list-style-type: none"> • <i>GWLmedian_2023</i> = median groundwater level model from 2019–2023 • <i>GWLmax_2023</i> = maximum groundwater level for 2019–2023 • <i>GWLmin_2023</i> = minimum water-table elevation • <i>GWLmhws_median2023</i> = groundwater level at MHWS based on the 2019–2023 median. The node elevation is compared relative to the water table by subtracting the water-table elevation from <i>minILEV</i> to give a series of elevation difference attributes of how much the network node is locally above or below the water table (values in metres): <i>ILEV_WTEVmedian</i> , <i>ILEV_WTEVmax</i> , <i>ILEV_WTEVmin</i> , <i>ILEV_WTEVmhws</i> . There are <NULL> and -9999 values where data are missing or outside the model.
<i>DCC_Foul_Sewer_Pipe</i>	A line dataset presenting Dunedin’s foul sewer pipes. Groundwater data (e.g. <i>GWL_median</i> , <i>GWL_max</i> , etc.) from the low-end (downstream) node of each line have been extracted to these nodes and subtracted from the DWNEL. DWNEL-WTEV calculated at each node assigned back to each pipe as a measure of the position of the lowest portion of the pipe relative to the water table (in metres).
<i>DCC_Foul_Sewer_Pipe_Lowend</i>	Line dataset, originally supplied by Dunedin City Council, of wastewater (foul sewer) pipes in Dunedin Drainage Datum (= NZVD2016 + 100.376). The Down Elevation (DWNEV) lowest point of each pipe is compared against various models of water-table elevation by subtracting the water-table elevation at the down-end of the pipe from DWNEL. This gives a series of elevation difference attributes of how much the low-end of the pipe is locally above or below the water table (values in metres): <i>DWNEV_WTEVmedian</i> , <i>DWNEV_WTEVmax</i> , <i>DWNEV_WTEVmin</i> , <i>DWNEV_WTEVmhws</i> . There are <NULL> and -9999 values where data are missing or outside the model.

File Name	Description
<i>DCC_Foul_SewerRL_VD2016</i>	Interpolated grid model (8 m cells) of the foul sewer (wastewater) network elevation (NZVD2016), interpolated over the flat-lying part of Dunedin using the point data <i>DCC_Foul_Sewer_modelpoints_v2023</i> (minILEV).
<i>DCC_FSminusGWLmax_2023</i>	Grid model (8 m cells) of the elevation of the wastewater (foul sewer) network relative to a grid of the maximum groundwater level during 2019–2023, derived using the equation [<i>DCC_WastewaterRL_VD2016</i>] – [<i>GWLmax_2023</i>] in a raster calculator. Negative values mean that the foul sewer infrastructure/invert levels are lower than the water table; positive values mean it is higher.
<i>DCC_FSminusGWLmedian_2023</i>	Grid model (8 m cells) of the elevation of the wastewater (foul sewer) network relative to a grid of the median groundwater level during 2019–2023, derived using the equation [<i>DCC_WastewaterRL_VD2016</i>] – [<i>GWLmedian_2023</i>] in a raster calculator. Negative values mean that the foul sewer infrastructure/invert levels are lower than the water table; positive values mean it is higher.
<i>DCC_FSminusGWLmhws2023</i>	Grid model (8 m cells) of the elevation of the wastewater (foul sewer) network relative to a grid of the MHWS groundwater level during 2019–2023, derived using the equation [<i>DCC_WastewaterRL_VD2016</i>] – [<i>GWLmhws_2023</i>] in a raster calculator. Negative values mean that the foul sewer infrastructure/invert levels are lower than the water table; positive values mean it is higher.
<i>DCC_FSminusGWLmin_2023</i>	Grid model (8 m cells) of the elevation of the Wastewater (foul sewer) network relative to a grid of the minimum groundwater level during 2019–2023, derived using the equation [<i>DCC_WastewaterRL_VD2016</i>] – [<i>GWLmin_2023</i>] in a raster calculator. Negative values mean that the foul sewer infrastructure/invert levels are lower than the water table; positive values mean it is higher.
<i>DCC_Stormwater_modelpoints_v2023</i>	A point dataset selection of Dunedin City Council stormwater network nodes on the coastal plain (groundwater model area) that have surveyed elevation data available. Groundwater data from the interpolated surfaces have been extracted to these points (e.g. <i>LIDAR_VD16</i> , <i>GWL_median</i> , <i>GWL_max</i> , etc.). Used to model <i>DCC_StormwaterRL_VD2016</i> .
<i>DCC_Stormwater_Node_Inverts</i>	Point dataset, originally supplied by Dunedin City Council, of stormwater network nodes and their elevation (ILEV) in Dunedin Drainage Datum (= NZVD2016 + 100.376). At each point, the various models of water-table elevation are derived as attributes for that site: <ul style="list-style-type: none"> • <i>GWLmedian_2023</i> = median groundwater level model from 2019–2023 • <i>GWLmax_2023</i> = maximum groundwater level for 2019–2023 • <i>GWLmin_2023</i> = minimum water-table elevation • <i>GWLmhws_median2023</i> = groundwater level at MHWS based on the 2019 median. <p>The node elevation is compared relative to the water table by subtracting the water-table elevation from minILEV to give a series of elevation difference attributes of how much the network node is locally above or below the water table (values in metres): <i>ILEV_WTEVmedian</i>, <i>ILEV_WTEVmax</i>, <i>ILEV_WTEVmin</i>, <i>ILEV_WTEVmhws</i>. There are <NULL> and -9999 values where data are missing or outside the model.</p>

File Name	Description
<i>DCC_Stormwater_Pipe</i>	Line dataset, originally supplied by Dunedin City Council, of stormwater pipes in Dunedin Drainage Datum (= NZVD2016 + 100.376). The Down Elevation (DWNEV) lowest point of each pipe is compared against various models of water-table elevation by subtracting the water-table elevation at the down-end of the pipe from DWNEV. This gives a series of elevation difference attributes of how much the low-end of the pipe is locally above or below the water table (values in metres): <i>DWNEV_WTEVmedian</i> , <i>DWNEV_WTEVmax</i> , <i>DWNEV_WTEVmin</i> , <i>DWNEV_WTEVmhws</i> . There are <NULL> and -9999 values where data are missing or outside the model.
<i>DCC_Stormwater_Pipe_Lowend</i>	An interim point dataset used for defining the elevation of the down end of stormwater pipes and their position relative to the water table. Derived by distinguishing FROM and TO ends of <i>DCC_Stormwater_Pipe</i> lines, then converting lines to points and assigning water-table values to this point. The points are then re-joined to the pipe lines using the unique ID.
<i>DCC_Stormwater_subcatchments_withGWdata</i>	Dunedin City Council stormwater sub-catchment polygons, exported from Infoworks and with geometry repaired, then assigned with mean values within the polygon areas extracted from interpolated 8 m grid models of groundwater. Includes a series of different attributes of present-day position of groundwater and local rain storage.
<i>DCC_StormwaterRL_VD2016</i>	Grid (8 m) cells of the stormwater network elevation (NZVD2016), interpolated from the point data <i>DCC_Foul_Sewer_modelpoints_v2023</i> (minLEV).
<i>DCC_SWminusGWLmax_2023</i>	Grid model (8 m cells) of the elevation of the stormwater network relative to a grid of the maximum groundwater level during 2019–2023, derived using the equation [<i>DCC_StormwaterRL_VD2016</i>] – [<i>GWLmax_2023</i>] in a raster calculator. Negative values mean that the foul sewer infrastructure/invert levels are lower than the water table; positive values mean it is higher.
<i>DCC_SWminusGWLmedian_2023</i>	Grid model (8 m cells) of the elevation of the stormwater network relative to a grid of the median groundwater level during 2019–2023, derived using the equation [<i>DCC_StormwaterRL_VD2016</i>] – [<i>GWLmedian_2023</i>] in a raster calculator. Negative values mean that the foul sewer infrastructure/invert levels are lower than the water table; positive values mean it is higher.
<i>DCC_SWminusGWLmhws2023</i>	Grid model (8 m cells) of the elevation of the stormwater network relative to a grid of the MHWS groundwater level during 2019–2023, derived using the equation [<i>DCC_StormwaterRL_VD2016</i>] – [<i>GWLmhws_2023</i>] in a raster calculator. Negative values mean that the foul sewer infrastructure/invert levels are lower than the water table; positive values mean it is higher.
<i>DCC_SWminusGWLmin_2023</i>	Grid model (8 m cells) of the elevation of the stormwater network relative to a grid of the minimum groundwater level during 2019–2023, derived using the equation [<i>DCC_StormwaterRL_VD2016</i>] – [<i>GWLmin_2023</i>] in a raster calculator. Negative values mean that the foul sewer infrastructure/invert levels are lower than the water table, positive values mean it is higher.
<i>DCC_Water_Depth_of_Cover</i>	Point dataset of Dunedin City drinking water network nodes. Translated directly from shapefile provided by Dunedin City Council.
<i>DCC_Water_Pipe</i>	Line dataset of Dunedin City drinking water supply. Translated directly from shapefile provided by Dunedin City Council.

File Name	Description
<i>DoD_SWminusFS</i>	Grid model (8 m cells) of the difference in elevation (DoD = DEM of difference) between the Stormwater RL model minus the Wastewater RL. Generated using raster calculator using [<i>DCC_StormwaterRL_VD2016</i>] – [<i>DCC_WastewaterRL_VD2016</i>]. Note that stormwater pipes and nodes should generally sit higher than wastewater, so values (in metres) should be positive for the most part.
<i>RAIN_pervious_surface_model</i>	A grid model of pervious value = 1 and impervious value = 1 surfaces in South Dunedin. Generated by (i) NVDI classification of 2013 aerial photographs (https://data.linz.govt.nz/layer/52118-dunedin-0125m-urban-aerial-photos-2013/), (ii) binary threshold filtering of the NVDI image (method of Otsu [1979]) and (iii) adding LINZ building outlines (https://data.linz.govt.nz/layer/101290-nz-building-outlines/) as impervious areas so as to remove red roofs and red cars that would otherwise show as pervious.

APPENDIX 5 GLOSSARY OF TERMS

AEP	Annual Exceedance Probability. The probability of a flood, or inundation event, of a certain size or greater occurring in any year. Mostly used here to describe the chance of an event reaching or exceeding a certain groundwater level, storm surge or rainfall depth-duration in any given year.
ArcGIS	A programme for working with maps and geographic information. Used for creating and using maps, compiling geographic data, analysing mapped information and sharing and discovering geographic information.
Artesian	Referring to an aquifer or underground layer containing groundwater that is under positive pressure. If a well is sunk into the ground, the water will rise and equilibrate at a point that is above ground level.
ARI	Average Recurrence Interval. Also known as ‘annual return period’. It is the average time interval between events of a specified magnitude (or larger) when averaged over many occurrences, i.e. a long time; number of years that are predicted to pass before an event of a given magnitude occurs. ARI (or its often-used surrogate ‘return period’) can be misinterpreted on the assumption that, because one large event has just occurred, then the ARI will pass before another such event. The term ‘AEP’ is commonly preferred for weather-related hazards, as it conveys the continuous probability that large events could occur at any time.
Aquifer	An underground layer of water-bearing permeable rock, rock fractures or unconsolidated materials from which groundwater can be extracted.
Aquitard	An impermeable layer of sediment, or barrier of rock, that acts as a barrier to the flow of groundwater.
Climate	Climate in a narrow sense is usually defined as the average weather or, more rigorously, as the statistical description in terms of the mean and variability of relevant quantities over a period of time, ranging from months to thousands of years.
Confined groundwater	Groundwater that is separated from atmospheric pressure by a layer of relatively impermeable material.
Drawdown	The reduction of the pressure head in an aquifer as the result of the withdrawal of free water.
Electrical conductivity	A measure of the ability of water to conduct electricity that is directly related to the concentration of ions dissolved in the water. Usually measured in micro- or millisiemens per centimetre ($\mu\text{S}/\text{cm}$ or mS/cm).
Empirical	Based on, concerned with, or verifiable by observation or experience rather than system theory or pure logic.
ESL	Extreme sea level, which comes from a combination of mean sea level, any long-term mean sea level anomaly, astronomical tide, storm surge and wave set-up.

Exposure	The presence of people, livelihoods, ecosystems, environmental functions, services and resources; infrastructure; or economic, social or cultural assets in places and settings that could be adversely affected by natural hazards and climate change.
GIS	Geographic Information System. A framework for gathering, managing and analysing data rooted in the science of geography.
Hilltop	Software for storing and analysing time-series environmental data. The software is used in New Zealand by regional councils, electricity companies and consulting engineers. http://www.hilltop.co.nz/
Hydraulic conductivity	For an isotropic porous medium and homogenous fluid, the volume of water that moves in unit time under a unit hydraulic gradient through a unit area measured at right angles to the direction of flow. Commonly, though imprecisely, taken to be synonymous with permeability. Units: m/day.
Hydraulic gradient	Slope of the water table or potentiometric surface. The change in static head per unit of distance in a given direction. If not specified, the direction is generally understood to be that of the maximum rate of decrease in head.
Hydraulic head	The height above a datum plane (such as sea level) of the column of water that can be supported by the hydraulic pressure at a given point in a groundwater system. For a piezometer, the hydraulic head is equal to the distance between the water level in the piezometer and the datum plane.
IPCC	Intergovernmental Panel on Climate Change. A United Nations body for assessing the science related to climate change.
LiDAR	Light Detection and Ranging. Provides high-resolution topography datasets.
Liquefaction	A change in state that occurs when a saturated or partially saturated soil substantially loses strength and stiffness in response to an applied stress, such as shaking during an earthquake or other sudden change in stress condition. Material that is ordinarily a solid behaves like a liquid.
MHWS	Mean High Water Springs. The highest level that spring tides reach on the average over a period of time – usually about 24 hours in each semi-lunation (approximately every 14 days) when the range of the tide is greatest (Spring Range).
MHL	Mean Harbour Level
MLOS	Mean Level of Sea
MSL	Mean Sea level. Average (mean) level of the sea relative to a vertical datum over a defined epoch, usually of several years to decades. Baseline MSL for IPCC sea-level rise projections is the average over the period 1986–2005. MSL is used in a more general context in this report when not referring specifically to the Otago Harbour MHL or Pacific Ocean MLOS.

NZ SeaRise	The NZ SeaRise project was a \$7.1 million, five-year (2018–2023) research programme funded by the Ministry of Business, Innovation & Employment. The overarching goal of the programme, hosted at Victoria University of Wellington, was to improve predictions of sea-level rise in Aotearoa New Zealand to 2100 and beyond. https://www.searise.nz/
Percentile	A percentile is a measure used in statistics indicating the value below which a given percentage of observations in a group of observations or projections fall. The 50 th percentile is the median. Used to measure the spread of numerous sea-level rise projection simulations from various models and inputs for a particular representative concentration pathway.
Perched groundwater	Subsurface water that forms a saturated horizon within porous media at an elevation higher than the local or regional groundwater table.
Permeability	Used in a general sense, it is a measure of how easily water can flow through a rock or unconsolidated sediment and how easy it will be to extract the water. A more strict definition is the measure of the relative ease with which a porous medium can transmit a fluid under a potential gradient. It is the property of the medium only and is independent of the fluid. Commonly, but imprecisely, taken to be synonymous with the term 'hydraulic conductivity' (which implies that the fluid is water).
Piezometer	An open well or standpipe installed into the ground with a slotted or screened casing within a zone where water pressure is being measured.
Porosity	The ratio of the volume of the interstices to the total volume of rock expressed as a fraction. Effective porosity includes only the interconnected pore spaces available for groundwater transmission; measurements of porosity in the laboratory usually exclude any void spaces caused by cracks or joints (secondary porosity).
Potentiometric surface	An imaginary surface representing the elevation and pressure head of groundwater and defined by the level to which water rises in a well or piezometer. The water table is a particular potentiometric surface.
RRI	Rainfall Recharge Index. The ratio of the change in groundwater level during a rainfall event to the total amount of rain during that event.
Specific Conductance	A measurement of electrical conductivity that has been made at, or corrected to, 25°C.
Storativity	The volume of water that an aquifer releases from or takes into storage per unit surface area of the aquifer per unit change in head.
Tidal amplitude	The elevation of tidal high water above MSL (equals half of the tidal range between high tide and low tide).
Tidal efficiency	The ratio of the amplitude (or range) of tidal-related fluctuations in groundwater to the tidal amplitude (or range) in the sea. Expressed herein as a percentage using the nearest water body (harbour or ocean).

Transducer	A measuring device that converts an applied pressure into an electrical signal. Usually consists of two parts, an elastic material that deforms under the application of pressure and an electrical part that detects this deformation. Can be vibrating-wire, pneumatic or strain-gauge in operation. Converts pressure in groundwater or air into an electrical recording.
Unconfined groundwater	Groundwater in an aquifer where upper-water surface (water table) is at atmospheric pressure and thus able to rise and fall.
Unconsolidated	A deposit consisting of loose grains that are not held together by cement. River terrace deposits are a typical example of an unconsolidated aquifer.
Vulnerability	The predisposition to be adversely affected. Vulnerability encompasses a variety of concepts and elements, including exposure, sensitivity or susceptibility to harm or damage, as well as a lack of capacity to cope and adapt (adaptive capacity).
Water table	The surface of a body of unconfined groundwater at which the pressure is equal to that of the atmosphere. The static water level in a well in an unconfined aquifer.



www.gns.cri.nz

Principal Location

1 Fairway Drive, Avalon
Lower Hutt 5010
PO Box 30368
Lower Hutt 5040
New Zealand
T +64-4-570 1444
F +64-4-570 4600

Other Locations

Dunedin Research Centre
764 Cumberland Street
Private Bag 1930
Dunedin 9054
New Zealand
T +64-3-477 4050
F +64-3-477 5232

Wairakei Research Centre
114 Karetoto Road
Private Bag 2000
Taupo 3352
New Zealand
T +64-7-374 8211
F +64-7-374 8199

National Isotope Centre
30 Gracefield Road
PO Box 30368
Lower Hutt 5040
New Zealand
T +64-4-570 1444
F +64-4-570 4657